MEDIMOND - Monduzzi Editore International Proceedings Division

11th European Biological Inorganic Chemistry Conference

EUROBIC 11

September 12-16, 2012
Granada (Spain)

Editors

Josefa María GONZÁLEZ-PÉREZ
Antonio MATILLA-HERNÁNDEZ
Juan NICLÓS-GUTIÉRREZ

MEDIMOND
INTERNATIONAL PROCEEDINGS

EUROBIC11

Via G. Verdi 15/1, 40065 Pianoro (Bologna), Italy
www.medimond.com • info@medimond.com

Printed in April 2013 by Editografica • Bologna (Italy)

ISBN 978-88-7587-658-6

Foreword

The study of metals in biological systems needs to be carried out by a multidisciplinary approach, involving many branches of chemical, physical and biological sciences. The relevance of metals in biology, environment and medicine has been increasing over the last years. For this reason, Biological Inorganic Chemistry is going strong and emerges as a multidisciplinary field which integrates efforts of many researchers, including inorganic chemists, biologists, pathologists, pharmacologists, toxicologists or biochemists, in order to understand the complexity of the living systems.

Knowing that a high percentage of proteins and metabolic reactions need metal ions to be carried out, it is easy to assume the popularity and importance of biological inorganic chemistry, mainly due to their use for resolving major social problems like cancer diseases, neurodegenerative disorders and even environmental and metal toxicity problems.

In this context, European Biological Inorganic Chemistry Conferences, EUROBICs, good standing conferences in which researchers from all over the world meet to exchange different viewpoints on the development of chemistry of metals in biological systems.

The articles published in this book are a token of the quality of the research presented during the EUROBIC11 Conference. These contributions are representative of the scientific community in this research and indicate the relevance of inorganic chemistry in life sciences.

Josefa Mª Gonzalez Pérez,

Antonio Matilla Hernández

Juan Niclós Gutierrez

Index

Poly-His and poly-Gln sequences in bacterial proteins: tempting sites for metal ions to interact with

Chiera N.[1], Guerrini R.[1], Kozłowski H.[2], Remelli M.[1], Rowinska-Zyrek M.[2], Wieczorek R.[2], Witkowska D.[2]

[1] Department of Chemical and Pharmaceutical Sciences, University of Ferrara, via L. Borsari 46, I-44121 Ferrara (Italy)
[2] Faculty of Chemistry, University of Wroclaw, F. Joliot-Curie 14, PL-50383 Wroclaw (Poland)
Corresponding author. E-mail: maurizio.remelli@unife.it

Abstract

Hpn and Hpn-like are *Helicobacter pylori* cytoplasmic proteins involved in the homeostasis of nickel; this metal is required for the enzymes urease and Ni-Fe hydrogenase, essential for the bacterium colonization in the human stomach. While almost half of Hpn sequence consists of polyhistydyl repeats, Hpn-like protein is rich in glutamine residues.

In order to shed light on the role of the consecutive His and Gln residues in metal-ion binding, the present investigation is focused on the N-terminal domain of Hpn-like protein. Cu(II) and Ni(II) complexes of peptide models were studied by means of different thermodynamic and spectroscopic techniques, as well as through molecular modeling computations.

Keywords: Helicobacter pylori, complex-formation equilibria, copper, nickel, model peptides.

Introduction

Helicobacter pylori (*H. pylori*) is a gram-negative bacterium of gastric localization, which widely infects humans and primates. It is related to a variety of gastrointestinal disorders, such as chronic gastritis, peptic ulcer disease, lymphoma, MALT (Mucosa Associated Lymphoid Tissue) and stomach cancer. Two enzymes containing nickel, [Ni-Fe] hydrogenase and urease, have been identified as essential for the survival of the bacterium [1, 2]; for the synthesis and the activity of these enzymes a constant supplying of Ni(II) is required. The completion of the genome sequence of *H. pylori* has revealed the presence of several proteins involved in homeostasis of nickel. Among them, the first to be recognized was Hpn, so termed because I was identified in *H. pylori* and it has affinity for nickel ions [3]; Hpn is a cytoplasmic histidine-rich protein, consisting of 60 amino acids, of which 47% are histidine residues. Most of the histidines are situated in the central part of the protein (from residue 11 to residue 33); two distinct sections, of seven and six consecutive histidine residues, can be identified. Hpn-like protein (Hpnl) is composed of 72 amino acids. The sequence analysis indicates that 25% of the amino acids are histidine residues, including a region of six consecutive residues, while 30 of the 72 amino acids are glutamines (42%) (Fig. 1).

Hpn	MAHHEEQHG----GHHHHHHHTHHHHYHGGEHHHHHHSSHHEEG	40
	CCSTS------DSHHQEEGCCHGHHE--	60
Hpnl	MAHHEQQQQQQANSQHHHHHHAHHHHYYGGEHHHHNAQQHAEQQ	44
	AEQQAQQQQQQQAHQQQQQKAQQQNQQY	72

Fig. 1. Amino acid sequences of the proteins Hpn and Hpn-like [4].

The N-terminal sequence (MAH-) is the same for both proteins, and is similar to the N-terminal sequence human serum albumin (DAH-), also known as ATCUN (amino terminal Cu(II) and Ni(II)-binding) domain. It is the well-known that the presence of a histidine residue in the third position with respect to the N-terminus, to form the general sequence Xaa-Yaa-His-, can very effectively bind metal ions like Ni(II) or Cu(II): this sequence gives to albumin its metal-binding properties. The ATCUN domain can form metal complexes with squared plain geometry; the coordination mode, illustrated in Fig.2, is of type "4N", involving the terminal amine, the imidazole group of histidine and the two intermediate (deprotonated) amide groups of the peptidic chain.

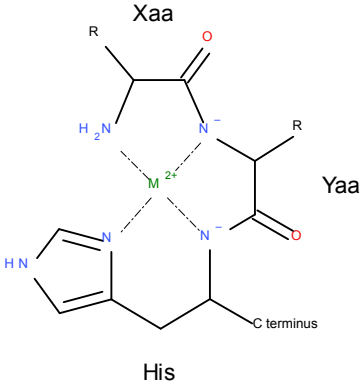

Fig. 2. Planar "4N structure " of metal complexes formed by the sequence Xaa-Yaa-His-

It is interesting to note that a recent study [5] has demonstrated that the hexa-glutaminic sequence (6-11) in Hpnl has a strong impact on the stability of the Ni(II) complexes formed at the N-terminal residue of the protein, although no direct interaction between glutamines and the metal ion has been detected.

The ability to isolate, purify, and characterize the genes has led to a significant advancements in the knowledge of genetic diseases and, in particular, of diseases characterized by polyglutamine (polyQ) repetition, in which some mutant genes produce proteins with glutamine sequences abnormally long. These include the Huntington's disease (HD), the dentatorubral-pallidoluysian atrophy (DRPLA), the Machado-Joseph disease (MJD), the spinal-bulbar muscular atrophy (SBMA) and different types of spinocerebellar ataxia (SCA). The molecular basis for the occurrence of these diseases seem to be related to the conformational changes of the proteins due to the presence and the length of abnormal polyglutamine sequences, leading to protein aggregation and neurotoxicity [6]. Currently, there are no specific therapies against these diseases: drugs having as precise target the proteins containing polyQ sequences and with the ability of inhibiting their aggregation are currently under investigation.

In the present paper, the attention is focused on the N-terminal domain of Hpn and Hpnl proteins, through the study of model peptides of different lengths, corresponding to the N-terminal sequences of the two proteins, protected at their carboxylic terminus (MAHHE-NH_2, MAHHEEQ-NH_2, MAHHEQQ-NH_2 and MAHHEQQHQA-NH_2). Their ability to form complexes with Ni(II) and Cu(II) ions has been deeply investigated by means of potentiometry, Uv-Vis spectrophotometry and some other spectroscopic techniques.

Methodology

Peptides were synthesized according to published methods [7] using Fmoc/t-butyl chemistry with a Syro XP multiple peptide synthesizer (MultiSynTech GmbH, Witten Germany). Crude peptides were purified by preparative reversed-phase HPLC using a Water Delta Prep 4000 system equipped with a Jupiter column C18. Analytical HPLC analyses were performed on a Beckman 116 liquid chromatograph equipped with a Beckman 166 diode array detector. All analogues showed > 90% purity when monitored at 210 nm. Molecular weights of compounds were determined by a mass spectrometer ESI Micromass ZMD-2000.

Stability constants for proton, Cu(II) and Ni(II) complexes were calculated from titration curves carried out over the pH range 3 -11 at 25 °C and ionic strength 0.1 M (KCl). The pH-metric titrations were performed with a MOLSPIN pH-meter system using a Russel CMAW 711 semi-combined electrode calibrated in proton concentrations using HCl. Alkali was added with a 0.500 cm^3 micrometer syringe. The ligand concentration was 1.0×10^{-3} M, the metal-to-ligand ratio was 1 : 1.1. The Hyperquad Suite programs were used for the stability constant calculations [8, 9].

The absorption spectra were recorded on a Cary 300 Bio spectrophotometer. Circular dichroism (CD) spectra were recorded on Jasco J 715 spectropolarimeter in the 800-230 nm range. Electron paramagnetic spectra (EPR) were recorded on a Bruker ESP 300E spectrometer at X-band frequency (9.3 GHz) in liquid nitrogen. The 30% ethylene glycol was used as a cryoprotectant for EPR measurements. Solutions were of similar concentration to those used in the potentiometric studies.

High-resolution mass spectra were obtained on a BrukerQ-FTMS spectrometer Bruker Daltonik, Bremen, Germany), equipped with an Apollo II electrospray ionization source with an ion funnel.

Results and discussion

Preliminary results on the above-described systems will be described below.

All studied ligands form Ni(II) and Cu(II), in the explored pH range. The ESI-MS spectra confirmed that the stoichiometry is always equimolar. The binding mode is invariably that described above for the ATCUN motif of albumin (Fig. 2).

The UV-vis and CD spectra show that nickel forms only complexes of squared planar geometry, variously protonated depending on the pH. All spectroscopic data agree that the Ni(II) ion is surrounded by four nitrogen atoms, starting from pH 6.

Cu(II) complexes begin to form at pH 5. The spectroscopic data confirm, also in this case, the typical bond {NH_2, $2N^-$, N_{im}} with four nitrogen donors bound to the metal at the equatorial plane of an axially distorted octahedron.

In order to compare the global binding ability of two or more ligands forming complexes of different stoichiometries and/or protonation degrees, two parameters are often employed: the dissociation constant K_d [10] and the pM value [11]. The first one refers to the hypothetical equilibrium (at physiological pH): M + L = ML, where the protonation degree of the ligand and the complex are not explicitly considered. The second parameter is the negative logarithm of the concentration of the free metal ion, in the presence of the ligand, under standard experimental conditions, i.e. $[ligand]_{total} = 10^{-5}$ M and $[metal]_{total} = 10^{-6}$ M, at a given pH, normally 7.4 or even different, as shown in Table 1.

Table 1. Derived thermodynamic parameters useful to compare the complexation ability of the various ligands at physiological pH (see text).

Peptide	Ni(II)			Cu(II)		
	K_d (M^{-1})	pM (pH 7.4)	pM (pH 10)	K_d (M^{-1})	pM (pH 7.4)	pM (pH 10)
MAHHE-NH_2	$1.9\cdot10^{-8}$	8.7	13.6	$8.3\cdot10^{-15}$	15.0	21.6
MAHHEEQ-NH_2	$9.9\cdot10^{-9}$	8.9	14.4	$7.7\cdot10^{-15}$	15.1	22.2
MAHHEQQ-NH_2	$2.3\cdot10^{-9}$	9.6	15.2	$6.3\cdot10^{-16}$	16.2	23.1
MAHHEQQHQA-NH_2	$3.4\cdot10^{-9}$	9.4	15.3	$2.1\cdot10^{-15}$	15.6	23.5

From the data of Table 1 it is evident that complexes formed by Cu(II) are highly more stable than those of Ni(II): the difference in K_d is of about six orders of magnitude for the different ligands; the corresponding pM values, at physiological pH, are about six units lower, for copper. Since the coordination mode is the same for all the species, the different stability of each complex should be the result of the influence of residues not directly

involved in complexation. The main difference among the peptides is the number of Gln residues present in the sequence, from 0 to 3. Data reported in Table 1 clearly indicate that the greater the number of glutamines, the more stable is the complex formed. This is especially evident at alkaline pH, where acid or basic side chains belonging to additional amino acids (Asp in MAHHEEQ-NH_2 and His in MAHHEQQHQA-NH_2) are deprotonated and should not influence the stability constant values. Since the side chains of Gln do not directly interact with the metal ion, it can be hypothesized that the observed stabilization depends on the formation of hydrogen bonds involving the side amide-groups of Gln residues. This hypothesis is supported by preliminary studies of molecular dynamics.

Conclusions

The experimental results reported above clearly demonstrate that, in the formation of metal/peptide complexes, also groups not directly involved in the formation of coordination bonds can have a significant impact on the thermodynamic stability of the species formed. Here, the side chains of Gln residues proved capable of stabilizing the complex through the possible creation of a "web" of hydrogen bonds around the metal ion, thus stabilizing and protecting it from dissociation or hydrolysis at basic pH.

Acknowledgements: This work was supported by the Polish Ministry of Science and Higher Education (KBN N N204 146537) and by the University of Ferrara (FAR 2011). M. Rowinska-Zyrek is supported by a scholarship from the Foundation for Polish Science.

References

[1] Bauerfeind, P.; Garner, R.; Dunn, B.E.; Mobley, H.L.T. (1997). Synthesis and activity of Helicobacter pylori urease and catalase at low pH. Gut 40, pp. 25-30.

[2] Olson, J.W.; Maier, R.J. (2002). Molecular hydrogen as an energy source for Helicobacter pylori. Science 298, pp. 1788-1790.

[3] Gilbert, J.V.; Ramakrishna, J.; Sunderman, F.W.; Wright, A.; Plaut, A.G. (1995). Protein Hpn - Cloning and Characterization of a Histidine-Rich Metal-Binding Polypeptide in Helicobacter-Pylori and Helicobacter-Mustelae. Infection and Immunity 63, pp. 2682-2688.

[4] Zeng, Y.B.; Zhang, D.M.; Li, H.Y.; Sun, H.Z. (2008). Binding of Ni^{2+} to a histidine- and glutamine-rich protein, Hpn-like. Journal of Biological Inorganic Chemistry 13, pp. 1121-1131.

[5] Witkowska, D.; Bielinska, S.; Kamysz, W.; Kozlowski, H. (2011). Cu^{2+} and Ni^{2+} interactions with N-terminal fragments of Hpn and Hpn-like proteins from Helicobacter pylori Unusual impact of poly-Gln sequence on the complex stability. Journal of Inorganic Biochemistry 105, pp. 208-214.

[6] Orr, H.T.; Zoghbi, H.Y., Trinucleotide repeat disorders, in: Annual Review of Neuroscience, Annual Reviews, Palo Alto, 2007, pp. 575-621.

[7] Benoiton, N.L. (2005). Chemistry of Peptide Synthesis, Taylor & Francis, London.

[8] Gans, P.; Sabatini, A.; Vacca, A. (1996). Investigation of equilibria in solution. Determination of equilibrium constants with the HYPERQUAD suite of programs. Talanta 43, pp. 1739-1753.

[9] Alderighi, L.; Gans, P.; Ienco, A.; Peters, D.; Sabatini, A.; Vacca, A. (1999). Hyperquad simulation and speciation (HySS): a utility program for the investigation of equilibria involving soluble and partially soluble species. Coord. Chem. Rev. 184, pp. 311-318.

[10] Kozlowski, H.; Luczkowski, M.; Remelli, M. (2010). Prion proteins and copper ions. Biological and chemical controversies. Dalton Trans. 39, pp. 6371-6385.

[11] Crisponi, G.; Remelli, M. (2008). Iron chelating agents for the treatment of iron overload. Coordination Chemistry Reviews 252, pp. 1225-1240.

Nickel Binding Sites in Histone Proteins: Spectroscopic and Structural Characterization

Zoroddu M.A.[a], Peana M.[a], Medici S.[a], Solinas C.[a], Lachowicz J.I.[b], Nurchi V.M.[b]

[a] *University of Sassari, Department of Chemistry and Pharmacy, Via Vienna 2, 07100 Sassari,* zoroddu@uniss.it
[b] *University of Cagliari, Department of Chemical and Geological Sciences, Cittadella Universitaria, SP Monserrato/ Sestu Km 0.700, 09042 Monserrato, Cagliari*

Abstract

Nickel compounds influence carcinogenesis by interfering with a variety of cellular targets. It has been found that nickel is a potent inhibitor in vivo of histone H4 acetylation, in both yeast and mammalian cells. It has preference to specific lysine residues in the H4 N-terminal -S_1GRGK$_5$GGK$_8$GLGK$_{12}$GGAK$_{16}$RH$_{18}$RKVL$_{22}$ tail, in which the sites of acetylation are clustered. About the nature of the structural changes induced by histone acetylation on H4, it has been recently demonstrated that acetylation promotes an increase in a-helical conformation of the acetylated N-terminal tail of H4. This causes a shortening of the tail and such an effect may have an important structural and functional implication as a mechanism of transcriptional regulation. Here we report a study on the conformational changes induced by carcinogenic nickel compounds on the histone H4 protein. From a circular dichroism study we found that nickel is able to induce a secondary structure in the protein. In particular, nickel has the same effect as acetylation: it induces an increase in a-helical conformation of the non-acetylated histone H4. The a-helical increase occurring upon nickel interaction with histone H4 should decrease the ability of histone acetyl transferase to recognize and bind the histone tail, thus affecting the ability of the enzyme to further modify the lysine residues. The shortening of the distance between adjacent amino acids, caused by the translation from an extended to a helical conformation, could disrupt the histone recognition motif; this may eventually compromise the entire "histone code".

Keywords: Histone H4, nickel binding, structural modifications

Introduction

Core histones, the proteins assembled into the beadlike nucleosomes around which the DNA is wrapped up, can be thought of as information modules that acquire coded information based on addition or removal of chemical groups. Their amino-terminal tails protrude from the nucleosome beads [1] and can be modified through the attachment (or removal) of acetyl, phosphate, or methyl groups. The acetylation reaction involves the transfer of an acetyl group from AcCoA onto the e-amino group of specific lysine residues present in the amino-terminal tails of each of the core histones, resulting in the neutralization of a single positive charge [2]. This may allow the termini to be displaced from the nucleosome, causing it to unfold and increase the access to transcription factors [3,5].

The link between alteration in chromatin structure and the development of cancer has been extensively published and both histone hyperacetylation and hypoacetylation appear to be important in the neoplastic process, depending on the target genes involved [6,7]. Certain nickel compounds induce a wide variety of tumors in experimental animals and are implicated in the etiology of human respiratory cancer after inhalation exposure [8]. Humans are exposed to carcinogenic nickel both occupationally and environmentally. The ability of nickel compounds to transform cells has been correlated to properties that increase endocytosis [9]. Such a process is also consistent with the predominance of nasal and lung cancers caused by inhalation of insoluble compounds, particularly Ni_3S_2, a potent human carcinogen [9]. The endocytic vesicles formed may be acidified by fusion with lysosomes, ultimately releasing large quantities of Ni^{2+} ions into the cytoplasm. Further, fusion of vesicles to the nuclear membrane may deliver large quantities of Ni^{2+} ions to the nucleus. After entering the nucleus, nickel ions could promote DNA

hypermethylation, histone deacetylation and chromatin condensation [10-13]. These effects could decrease the transcription of tumor suppressor and senescence genes, and play an important role in the carcinogenic effect of Ni^{2+} ions. Here we report a study on the conformational changes induced by nickel on the histone H4 protein. As shown by CD studies, nickel is able to induce a secondary structure in the protein. In particular, nickel induces an increase in the a-helical conformation of histone H4 in the same manner as acetylation does.

Materials and methods

CD spectra were recorded with a Jasco J710 dichrograph. The Ni(II) effect on the CD spectra of histone H4 was analyzed in water at pH 8.7, and in both 5 mM tetraborate buffer/HCl, pH 8.7, and 50 mM phosphate buffer, pH 7.0.

UV-Vis spectra were recorded on a Jasco-Uvidec 610 instrument using a cuvette with path length of 1 cm and a sample concentration of 1.5 x 10^{-3} mol dm^{-3}.

Histone H4 was from calf thymus (Roche). The purity of the protein was estimated by electrophoresis to be above 97%. The concentration of the protein was calculated using the molar extinction coefficient of 5.4 x 10^3 cm^{-1} mol^{-1} at 275 nm [14,15].

The 22-residue peptide (tail) was synthesized on a solid support with a 9050 Plus Synthesizer by BBM Inc., using a conventional Fmoc (9-fluorenylmethoxycarbonyl) chemistry methodology [16].

Fig. 1 was generated using the UCSF Chimera 1.4 program.

Fig 1

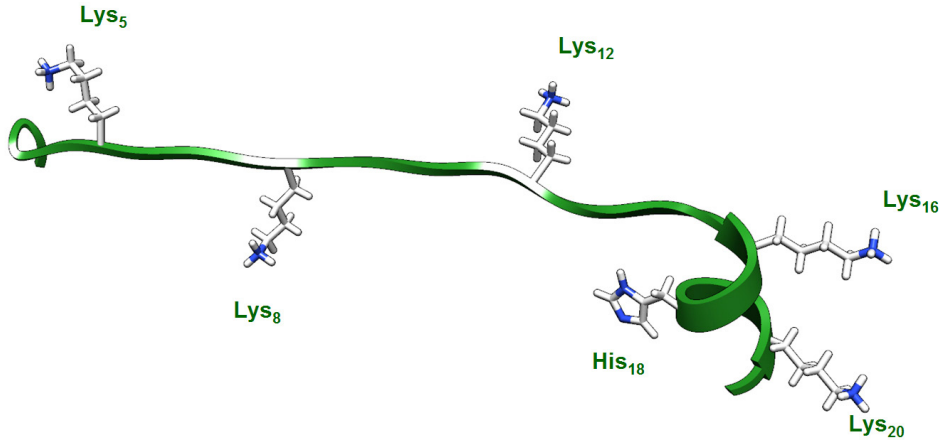

Fig. 1. Molecular-mechanics optimized structure of the helical conformation adopted by the non-acetylated H4 N-terminal tail in the presence of Ni^{2+} ions (only lysine and histidine residues are shown).

Results and discussion

The effect of nickel compounds on transcriptional repression has been previously measured by us as the acetylation status on histone H4 [12]. We found that nickel is a potent inhibitor in vivo of histone H4 acetylation, in both yeast and mammalian cells. This metal exhibits a preference for specific, highly conserved, lysine residues in the H4 N-terminal tail $S_1GRG\mathbf{K}_5$*$GG\mathbf{K}_8$*$GLG\mathbf{K}_{12}$*$GGA\mathbf{K}_{16}$*$RH_{18}RKVL_{22}$ (asterisks indicate the sites of acetylation in the H4 tail sequence), in which the sites of acetylation are clustered. The decrease in the acetylation level differed in extent at position 5, 8, 12 and 16. Lys-12 was the most sensitive residue, and two cell generations with 1 mM $NiCl_2$ were sufficient to inhibit acetylation at this position. Under the same assay conditions histone H3 showed no inhibition of the acetylation reaction by nickel. Interestingly, it has been noted that the spacing between acetylatable lysines is strikingly regular in the amino termini of many histones; lysines occur at positions 5, 8, 12 and 16 in H4 and, curiously, this spacing periodicity is "reminiscent of that of an a–helix" (that is 3.6 residues). This spacing could be part of the histone recognition motif. Regarding the nature of the structural changes induced by histone acetylation on H4, it has been recently demonstrated that acetylation induces an a-helical conformation of the acetylated N-terminal tail [17]. The region in the tail spanning the amino acids from Ala-15 to Val-21 is the most likely candidate for producing the overall H4 a-helical content observed from nucleosome core particle,

histone octamer and from N-terminal H4 tail in 90% TFE (a well known a-helical stabilizer). In the absence of Ni(II) the dominant CD feature of the histone H4 protein is a negative band at 200 nm, indicative of a predominantly random coil conformation.

The effect of nickel on a-helix formation was clearly observed in the CD spectra recorded at pH 8.7 (5 mM tetraborate/HCl aqueous buffer). From these spectra, reported in Fig. 2, an increase in the intensity of the CD bands around 220 nm was observed, indicating a more structured protein. The small but significant and reproducible increase in the negative ellipticity at 222 nm upon addition of Ni(II) indicates an increase of a-helix content; in fact, the random coil has a very low ellipticity at 222 nm.

Fig 2

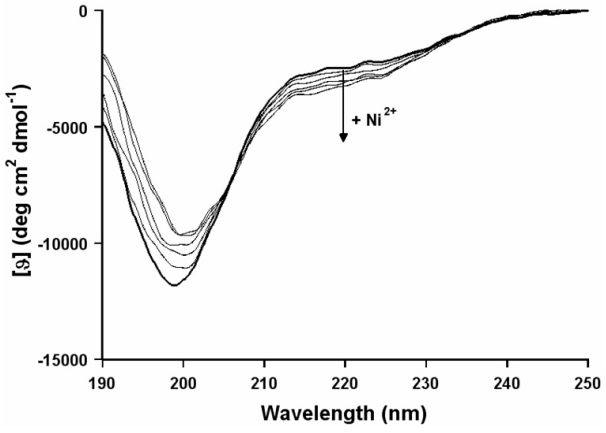

Fig. 2. CD spectra of a solution containing H4 protein and Ni^{2+} ions at pH 8.7 (5 mM tetraborate/HCl buffer) with increasing nickel concentrations (the thick line refers to metal free histone H4).

Evidence for the complexation of Ni(II) with the tail of histone H4 is provided also by UV-Vis experiments using a 22-aminoacids peptide from S1 to L22, the N-terminal tail of histone H4 protein which protrudes out from the nucleosome. From the pH dependence of the spectra in the visible range it is possible to see that coordination of the metal ion to the protein starts above pH 7, although the maximum extent of coordination is reached above pH 8. The blue-shift of the absorption maximum observed on raising the pH indicates a change in Ni(II) coordination state from octahedral (paramagnetic) to square planar (diamagnetic), with four nitrogen donor ligands. The position of l_{max} at 437 nm (e = 199 M^{-1} cm^{-1}), with a shoulder at 485 nm (e = 134 M^{-1} cm^{-1}), is indicative of the involvement of the imidazole nitrogen of histidine residue in the Ni(II) coordination sphere and, as the pH is raised, of the subsequent binding of deprotonated amidic groups from the peptide backbone.

All these data have been confirmed by a series of NMR experiments, both mono- and bidimensional, carried out on different peptide models of histone H4 tail, and reported in our previous papers [18,20].

Although under our experimental conditions the complexation of Ni(II) at physiological pH is not very effective, the hydrophobic environment in the histone octamer or in the entire nucleosome core particle is expected to greatly enhance metal binding capabilities, due to the multiple nonbonding interactions available there. If nickel binding to the histone affects the acetylation process, the a-helical content would be expected to increase with increasing nickel concentration, as it is indeed observed.

Conclusions

Nickel inhibited H4 acetylation in vitro when incubated with the histone substrate and the recombinant yeast Hat enzyme. A comparison with the behavior of histone H3 under the same conditions showed no inhibition of the acetylation status by nickel. These results strengthen the assumption that nickel, by binding to histidine of H4 in vivo, prevents the addition of the acetyl group to the nearby lysines and establishes a repressed chromatin state.

References

[1] Luger, K.; Mader, A. W.; Richmond, R. K.; Sargent D. F.; Richmond, T. J. (1997). Crystal structure of the nucleosome core particle at 2.8 A resolution. Nature, 389, pp 251–260

[2] Jenuwein T.; Allis, C. D. (2001). Translating the histone code. Science, 293, pp 1074–1080

[3] Grunstein, M. (1997). Histone acetylation in chromatin structure and transcription. Nature, 389, pp 349–352

[4] Morales, V.; Richard-Foy, H. (2000). Role of histone N-terminal tails and their acetylation in nucleosome dynamics. Mol. Cell. Biol., 20, pp 7230–7237

[5] Roth, S. Y.; Allis, C. D. (1996). Histone acetylation and chromatin assembly: a single escort, multiple dances? Cell, 87, pp 5–8

[6] Johnson, L. M.; Fisher-Adams, G.; Grunstein, M. (1992). Identification of a non-basic domain in the histone H4 N-terminus required for repression of the yeast silent mating loci. EMBO J., 11, pp 2201–2209

[7] Archer, S.Y.; Hodin, R.A. (1999). Histone acetylation and cancer. Curr. Opin. Genet. Dev., 9, pp 171–174

[8] IARC, Chromium, Nickel and Welding. Monogr. Eval. Carcinog. Risk Chem. Hum, 1990, 49.

[9] Costa, M.; Mollenhauer, H. M. (1980). Carcinogenic activity of particulate nickel compounds is proportional to their cellular uptake. Science, 209, pp 515–517

[10] Lee, Y. W.; Klein, C. B.; Kargacin, B.; Salnikow, K.; Kitahara, J.; Dowjat, K.; Zhitkovich, A.; Costa, M. (1995). Carcinogenic nickel silences gene expression by chromatin condensation and DNA methylation: a new model for epigenetic carcinogens. Mol. Cell. Biol., 15, pp 2547–2557

[11] Klein, C. B.; Conway, K.; Wang, X. W.; Bhamra, R. K.; Lin, X.; Cohen, M. D.; Annab, L.; Barret, J.C.; Costa, M. (1991). Senescence of nickel-transformed cells by an X chromosome: possible epigenetic control. Science, 251, pp 796– 799

[12] Broday, L.; Peng, W.; Min-Hao, K.; Salnikow, K.; Zoroddu, M. A.; Costa, M. (2000). Nickel compounds are novel inhibitors of histone H4 acetylation. Cancer Res., 60, pp 238–241

[13] Zetter, B. R.; Banyard, J. (2002). Cancer. The silence of the genes. Nature, 419, pp 572–573

[14] Moss, T.; Cary, P. D.; Crane-Robinson, C.; Bradbury, E. M. (1976). Physical studies on the H3/H4 histone tetramer. Biochemistry, 15, pp 2261–2267

[15] Creighton, T. E.; Proteins 2nd Ed. 1996, W. H. Freeman and Co., New York

[16] Meienhofer, M.; Waki, M.; Heimer, E. P.; Lambros, T. J.; Makofske, C. D.; Chang, C. D. (1979). Solid phase synthesis without repetitive acidolysis. Preparation of leucyl-alanyl-glycyl-valine using 9-fluorenylmethyloxycarbonylamino acids. Int. J. Pept. Protein Res., 13, pp 35–42

[17] Wang, X.; Moore, S. C.; Laszckzak, M.; Ausio, J. (2000). Acetylation increases the alpha-helical content of the histone tails of the nucleosome. J. Biol. Chem., 275, pp 35013–35020

[18] Zoroddu, M. A.; Peana, M.; Kowalik-Jankowska, T.; Kozlowski, H.; Costa, M. (2002). The binding of Ni(II) and Cu(II) with the N-terminal tail of the histone H4. J. Chem. Soc., Dalton Trans., pp 458–465

[19] Zoroddu, M. A.; Medici, S.; Peana, M. (2007). Multidimensional NMR spectroscopy for the study of histone H4-Ni(II) interaction. Dalton Trans., pp 379–384

[20] Zoroddu, M. A.; Peana, M.; Medici, S.; Casella, L.; Monzani, E.; Costa, M. (2010). Nickel binding to histone H4, Dalton Trans., 39, pp 787–793

Harnessing the flexibility of peptidic scaffolds to control their copper(II) coordination properties

Fragoso A., Lamosa P., Delgado R., Iranzo O.

Instituto de Tecnologia Química e Biológica, Universidade Nova de Lisboa, Av. da República, 2780-157 Oeiras, Portugal
oiranzo@itqb.unl.pt

Abstract

Two decapeptides, C-Asp (cyclic) and O-Asp (linear), containing three His and one Asp have been synthesized. Potentiometric studies in aqueous solution revealed the formation of a major species, $[CuHL]^{2+}$, at 1:1 Cu^{2+}:peptide ratio and in the pH range 5.0–7.5. A detailed spectroscopic study, including UV-Vis, CD, EPR and NMR, showed that the $[CuHL]^{2+}$ species is very similar for both peptides and that Cu^{2+} is coordinated by the amino acid side chain functionalities . Nonetheless, as a result of the cyclization, different behaviours were observed as revealed by CD and NMR data. Namely, a more rigid structure and slower Cu^{2+} exchange rate for $[CuH(C\text{-}Asp)]^{2+}$ compared to $[CuH(O\text{-}Asp)]^{2+}$.

Keywords: metallopeptides, copper, cyclic peptides, acid-base reactions, stability constants

Introduction

Copper(II) complexes of short histidine-containing peptides have been the focus of numerous studies to investigate biologically relevant copper(II) species related to neurodegenerative diseases, to generate metalloenzyme mimics as well as to develop artificial metalloenzymes. In the last two cases, peptidic ligands that can favor the coordination of Cu^{2+} to the amino acid side chains vs. the amide nitrogen in the neutral pH range are important. Nonetheless, few examples are reported in the literature where the formation of single species of this type is observed [1,2]. In this context, cyclic peptides are an attractive approach as cyclization leads to a restricted mobility of the peptide backbone and can allow a better control in the spatial distribution of functional groups. These properties play a crucial role in determining metal ion binding and subsequently, coordination geometries and speciation. Using the RAFTs templates [3], a cyclic peptide containing three His and one Asp residues was designed and its Cu^{2+} coordination properties studied using potentiometric and different spectroscopic methods. Its linear counterpart was also prepared and the comparative analysis revealed that although both scaffolds form a similar major species, they present different behaviour.

Experimental

Peptide synthesis

The Ac-GlyAspTrpHisProGlyHisLysHisGly-NH_2 (O-Asp) and cyclo(GlyAspTrpHisProGlyHisLysHisPro) (C-Asp) peptides were synthesized on a CEM Liberty microwave-assisted automated peptide synthesizer using Fmoc Chemistry [4]. Purification was carried out by preparative reverse-phase HPLC and ESI-MS was used to determine their identity. Purity was always > 95% as determined by analytical reverse-phase HPLC.

Stock solutions

Fresh solutions of the peptides were prepared for each experiment using MQ-water and concentration was determined by UV-Vis spectroscopy using the extinction coefficient of Trp [5]. The $Cu(NO_3)_2$ stock solution was prepared from analytical grade metal salt and the concentration determined by titration with K_2H_2EDTA [6].

Potentiometric studies

Experiments were carried out under inert atmosphere in aqueous solutions at 25.0 °C and ionic strength 0.10 M KNO_3 following published protocols [7]. The calculation of overall equilibrium constants β_i^H (being $\beta_i^H = [H_hL_l]/[H]^h[L]^l$) and β_{MmHhLl} (being $\beta_{MmHhLl} = [M_mH_hL_l]/[M]^m[H]^h[L]^l$) was done by fitting the potentiometric data with the HYPERQUAD program [8]. Species distribution diagrams were plotted from the calculated constants with the HYSS program [9].

Spectroscopic Studies

UV-Vis and CD spectra were recorded in aqueous solution at 0.5 – 1.0 mM peptide and $Cu(NO_3)_2$ concentration, I = 0.10 M KNO_3 and 25.0 °C. The final pH (6.0–6.3) was adjusted by addition of KOH or HNO_3. UV-Vis spectra were collected on a Varian Cary 100 Bio UV-Vis spectrophotometer and the CD spectra on a Jasco J-715 spectropolarimeter. The far-UV CD spectra of the peptides were collected at 5.0 μM peptide concentration. The molar circular dichroism (Δε, $M^{-1}\,cm^{-1}$) and the molar ellipticities (θ, deg $cm^2\,dmol^{-1}$) are reported referenced to the total peptide concentration. The X-band EPR spectra were recorded on a Bruker ESP 380 spectrometer at 92.2 – 93.5 K, pH 6.0 and 1.1 mM peptide and $Cu(NO_3)_2$ concentration. The experimental EPR spectra were simulated using the SpinCount software [10]. NMR spectra were acquired on a Bruker AVANCE III 800 spectrometer working at a proton operating frequency of 800.33 MHz. Spectra were run in D_2O:H_2O (10:90) at 25.0 °C using standard Bruker pulse programs. For resonance assignment 2D COSY, NOESY and TOCSY spectra were acquired at pH 4.0.

Results and discussion

Protonation constants of the peptides and formation constants of their copper(II) complexes

The calculated stepwise protonation constants of the C-Asp and O-Asp peptides are presented in Table 1. In agreement with their primary sequences (see Experimental), five protonation constants were determined. The first protonation constant can be assigned to the protonation of Lys, the following three values in the range 5.56–7.22 to the protonation of imidazole groups of the His residues, and the low log K value to the protonation of the Asp residue.

Table 1. Stepwise protonation (K_i^H) of C-Asp and O-Asp and stability ($K_{Cu_mH_hL_l}$) constants of their copper(II) complexes in aqueous solution (25.0 °C and I = 0.10 M KNO_3).

Equilibrium reaction[a]	log K_i^H		Equilibrium reaction	log $K_{Cu_mH_hL_l}$	
	C-Asp	O-Asp		C-Asp	O-Asp
$L^- + H^+ \rightleftarrows HL$	10.11	10.04	$[CuHL]^{2+} + H^+ \rightleftarrows [CuH_2L]^{3+}$	3.76	4.37
$HL + H^+ \rightleftarrows H_2L^+$	7.22	6.86	$[CuL]^+ + H^+ \rightleftarrows [CuHL]^{2+}$	8.69	7.93
$H_2L^+ + H^+ \rightleftarrows H_3L^{2+}$	6.40	6.29	$Cu^{2+} + L^- \rightleftarrows [CuL]^+$	12.20	11.39
$H_3L^{2+} + H^+ \rightleftarrows H_4L^{3+}$	5.61	5.56	$[CuH_{-1}L] + H^+ \rightleftarrows [CuL]^+$	8.53	7.84
$H_4L^{3+} + H^+ \rightleftarrows H_5L^{4+}$	2.87	3.46	$[CuH_{-2}L]^- + H^+ \rightleftarrows [CuH_{-1}L]$	9.87	9.97
			$[CuH_{-3}L]^{2-} + H^+ \rightleftarrows [CuH_{-2}L]^-$	10.1	10.68
			$[CuL]^+ + Cu^{2+} \rightleftarrows [Cu_2L]^{3+}$	5.0	–
			$[Cu_2H_{-2}L]^+ + H^+ \rightleftarrows [Cu_2H_{-1}L]^{2+}$	–	6.3
			$[Cu_2H_{-3}L] + H^+ \rightleftarrows [Cu_2H_{-2}L]^+$	6.73	7
			$[Cu_2H_{-4}L]^- + H^+ \rightleftarrows [Cu_2H_{-3}L]$	9.22	9.35
			$[Cu_2H_{-5}L]^{2-} + H^+ \rightleftarrows [Cu_2H_{-4}L]^-$	10.0	10.04
			$[Cu_2H_{-6}L]^{3-} + H^+ \rightleftarrows [Cu_2H_{-5}L]^{2-}$	10.3	10.81
			$[Cu_3H_{-5}L] + H^+ \rightleftarrows [Cu_3H_{-4}L]^+$	–	6.12
			$[Cu_3H_{-6}L]^- + H^+ \rightleftarrows [Cu_3H_{-5}L]$	–	9.93
			$[Cu_3H_{-7}L]^{2-} + H^+ \rightleftarrows [Cu_3H_{-6}L]^-$	–	10.55
			$[Cu_3H_{-8}L]^{3-} + H^+ \rightleftarrows [Cu_3H_{-7}L]^{2-}$	–	10.99

[a] L^- is the completely deprotonated form of the peptides.

The stability constants for the formation of the copper(II) complexes with the peptides were determined by potentiometric titrations using different Cu^{2+}:peptide ratios (0.5:1, 1:1, 2:1 and 3:1). For the O-Asp peptide precipitation was not observed for the Cu^{2+}:peptide ratios studied indicating the binding to one, two and three Cu^{2+} ions. For the C-Asp peptide, precipitation occurred at the 3:1 Cu^{2+}:peptide ratio at pH values higher than 6.94 and only titration data of Cu^{2+}:peptide ratios up to 2:1 were considered in the fitting model. This drastically limited the evaluation of the presence of trinuclear complexes with this peptide. The calculated stepwise formation constants are collected in Table 1 and the speciation diagrams for the copper(II) complexes of these peptides at 1:1 Cu^{2+}:peptide ratio are shown in Fig. 1.

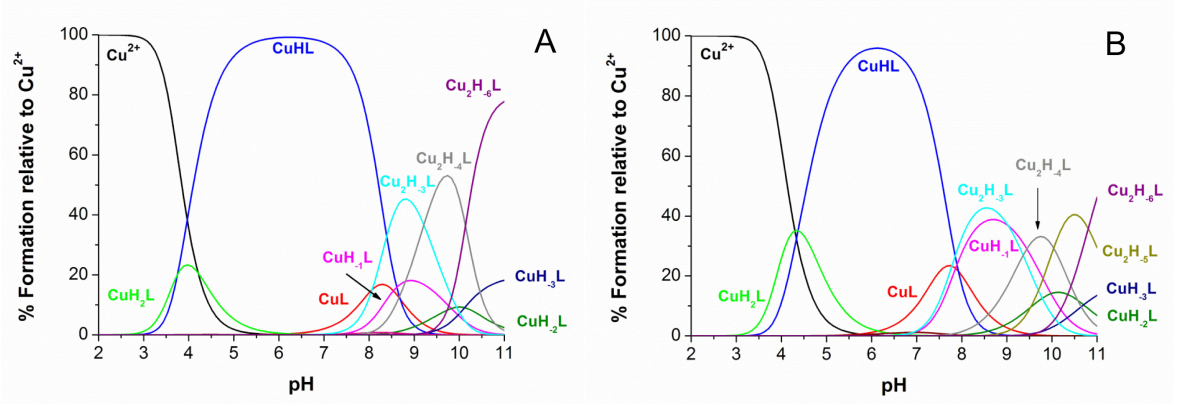

Fig. 1. Species distribution diagrams for the copper(II) complexes of C-Asp (**A**) and O-Asp (**B**) at 25.0 °C, *I* = 0.1 M KNO_3 and [L = peptide] = [$Cu(NO_3)_2$] = 1.0 mM. Charges are omitted for simplicity.

Free Cu^{2+} ion is not present in solution at pH > 5.5 and $[CuHL]^{2+}$ is the main species between pH 5.0 to 7.5 and 5.5 to 7.0 for the C-Asp and O-Asp peptides, respectively (see the speciation diagrams). The stepwise constant values indicate that $[CuHL]^{2+}$ is a complex where the carboxylate oxygen (Asp) and three deprotonated imidazoles are coordinated to the metal centre. This coordination environment is corroborated by the spectroscopic studies shown below. The $[Cu_mH_{-h}L]^{2m-h-1}$ species are those corresponding to the deprotonation of the amide centers and these species correspond indeed to $Cu_mH_{-h-1}(HL)$ (i.e. $CuH_{-3}L = CuH_{-4}(HL) = 4$ deprotonated amides and 1 protonated Lys). In Fig. 1 is shown that coordination to amide nitrogens occurs at pH > 6.0 and 7.0 for the O-Asp and C-Asp peptides, respectively. This indicates that the species $[CuHL]^{2+}$ is more stable for C-Asp requiring higher pH value to displace the imidazole ring in favor of the stronger amide binding donors ($\log K_{CuH(C\text{-}Asp)} = 8.69$ vs $\log K_{CuH(O\text{-}Asp)} = 7.93$). The K_{eff} (effective or apparent constant) for both peptides was calculated at each pH value using the potentiometric data and HySS program [9]. The data indicate stronger binding of Cu^{2+} to the C-Asp compared to the O-Asp, not only at 1:1 ratio but even at 2:1 ratio (data not shown).

Spectroscopic studies

The spectroscopic parameters corresponding to the UV-Vis and CD spectra of $[CuH(O\text{-}Asp)]^{2+}$ and $[CuH(C\text{-}Asp)]^{2+}$ complexes are reported in Table 2. The data for both complexes are similar and consistent with the coordination of Cu^{2+} to the imidazole ring of the His residues [1,2,11]. The wavelengths of the maximum absorbance in the UV-Vis spectra are in agreement with the predicted value for the λ_{max} of a [3 His, 1 carboxylate] equatorial coordination environment [12]. When the pH is increased, changes in the CD and UV-Vis spectra are observed that indicate the binding of Cu^{2+} to amide nitrogens and thus, a change in coordination geometry (data not shown). These changes are consistent with the speciation diagrams (Fig. 1) and the formation of the species $[Cu_mH_{-h}L]^{2m-h-1}$ at pH > 6.0 and 7.0 for the O-Asp and C-Asp peptides, respectively. However, these deprotonations occur simultaneously and thus, different species are present in solution in measurable concentration precluding the individual spectroscopic analysis. The EPR parameters corresponding to the $[CuH(O\text{-}Asp)]^{2+}$ and $[CuH(C\text{-}Asp)]^{2+}$ complexes are presented in Table 2. The three different principal values of g, $g_z > (g_x + g_y)/2$ and the lowest $g \geq 2.04$, are characteristic of mononuclear copper(II) complexes in rhombic symmetry with elongation of the axial bonds and a d_{x2-y2} ground state. A square planar geometry or square pyramidal, in case of one water molecule directly coordinates to the Cu^{2+} in the axial position, would be consistent with these data. The binding of Cu^{2+} to the peptides was also followed by ^{1}H-NMR spectroscopy and the data indicate coordination of Cu^{2+} to the His residues and a different Cu^{2+} exchange

rate which, in the NMR timescale, it is slower for C-Asp and faster for O-Asp. This different behaviour can be the result of the higher affinity of C-Asp for Cu^{2+} and its more constrained scaffold.

The effect of Cu^{2+} coordination in the structure of the two peptides was evaluated by CD spectroscopy (Fig. 2A). While the O-Asp peptide is unstructured in solution, the C-Asp peptide adopts a type II β-turn folding. However, upon Cu^{2+} binding, conformational changes are observed for both peptides and the final copper(II) complexes display a very similar CD spectrum (more intense for $[CuH(C\text{-}Asp)]^{2+}$ as expected for its constrained scaffold).

Table 2. Spectroscopic data for the copper(II) complexes.

Spectroscopy	CuH(C-Asp)	CuH(O-Asp)
UV-Vis		
$\Delta\lambda_{max}$(nm), Δε ($M^{-1}cm^{-1}$)	603, 56[a]	609, 60[a]
CD		
$\Delta\lambda_{max}$(nm), Δε ($M^{-1}cm^{-1}$)	248, + 7.050[b]	247, +4.205[b]
	557, -0.538[a]	558, - 0.309[a]
EPR		
A_z (× 10^{-4} cm^{-1})	177.82	181.66
A_x (× 10^{-4} cm^{-1})	3.92	6.39
A_y (× 10^{-4} cm^{-1})	21.82	21.57
g_z	2.277	2.271
g_y	2.069	2.074
g_x	2.045	2.042

[a] Cu^{2+} d-d transitions. [b] $N_{imidazole}$-His → Cu^{2+} CT / Intramolecular transition.

The data obtained by the set of experiments used led us to propose the structures presented in Fig. 2B. Both peptides will coordinate Cu^{2+} solely by the His and the Asp side chains that are located on the same face of the peptidic scaffold. The coordination of one water molecule in the axial position cannot be ruled out based on the spectroscopic data.

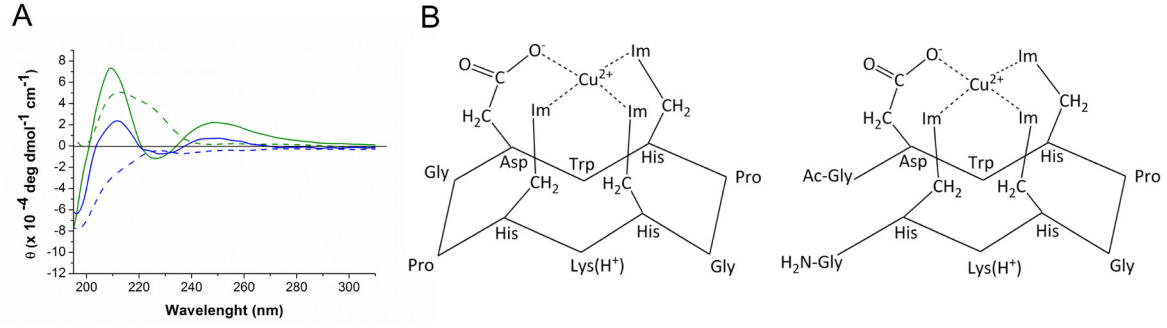

Fig. 2. (**A**) Far-UV CD spectra of the O-Asp (blue) and C-Asp (green) peptides (5.0 μM) in the absence (dash line) and in the presence (solid line) of 1 equiv of Cu^{2+} at 25.0 °C and pH 6.0. (**B**) Proposed structure for $[CuH(C\text{-}Asp)]^{2+}$ (right) and $[CuH(O\text{-}Asp)]^{2+}$ (left). Im = Imidazole.

Conclusion

In summary, two decapeptides, O-Asp and C-Asp, containing three His and one Asp residues but backbones with different degree of flexibility were prepared. The detailed potentiometric and spectroscopic study carried out showed that both scaffolds are well-tuned for Cu^{2+} binding forming a very similar major $[CuHL]^{2+}$ species at 1:1 Cu^{2+}:peptide ratio. Nonetheless, cyclization has remarkable effects on the Cu^{2+} coordination properties of the C-Asp peptide that has a higher affinity for Cu^{2+} at all pH values, a lower Cu^{2+} exchange rate and different copper(II) complexes speciation.

Acknowledgments: This work has been carried out with financial support from Fundação para a Ciência e a Tecnologia with co-participation of the European Community funds FEDER, POCI, QREN and COMPETE (PTDC/QUI-BIQ/098406/2008, PTDC/QUI/67175/2006, REDE/1517/RMN/2005, REDE/1504/REM/2005) and from the European Commission (Marie Curie FP7-IRG-230896).

References

1. Jakab I.N., Lőrincz O., Jancsó A., Gajda T., Gyurcsik B. (2008). Dalton Trans., pp. 6987-6995.
2. Czapor H., Bielińska S., Kamysz W., Szyrwiel Ł., Brasuń J. (2011). J. Inorg. Biochem. 105, pp. 297-302.
3. Boturyn D., Defrancq E., Dolphin G.T., Garcia J., Labbe P., Renaudet O., Dumy P. (2008). J. Pept. Sci. 14, pp. 224-240.
4. Chan WC, White PD (2000) Fmoc solid phase peptide synthesis: a practical approach: Oxford University Press.
5. Creighton T.E. (1997) Protein structure: a practical approach: IRL Press at Oxford University.
6. Schwarzenbach G., Flaschka W. (1969) Complexometric Titrations. London: Methuen
7. Lima L.M.P., Esteban-Gómez D., Delgado R., Platas-Iglesias C., Tripier R. (2012). Inorg. Chem. 51, pp. 6916-6927.
8. Gans P., Sabatini A., Vacca A. (1996). Talanta 43, pp. 1739-1753.
9. Alderighi L., Gans P., Ienco A., Peters D., Sabatini A., Vacca A. (1999). Coord. Chem. Rev. 184, pp. 311-318.
10. Hendrich M.P. SpinCount software; Carnegie Mellon University: Pittsburgh, PA; SpinCount is available at http://www.chem.cmu.edu/groups/hendrich/.
11. Jancsó A., Paksi Z., Jakab N., Gyurcsik B., Rockenbauer A., Gajda T. (2005). Dalton Trans., pp. 3187-3194; Valensin D., Mancini F.M., Łuczkowski M., Janicka A., Wiśniewska K., Gaggelli E., Valensin G., Łankiewicz L., Kozłowski H. (2004). Dalton Trans., pp. 16-22; Jakab N.I., Jancsó A., Gajda T., Gyurcsik B., Rockenbauer A. (2008). J. Inorg. Biochem. 102, pp. 1438-1448; Stańczak P., Juszczyk P., Grzonka Z., Kozłowski H. (2007). FEBS Letters 581, pp. 4544-4548; Ősz K., Nagy Z., Pappalardo G., Di Natale G., Sanna D., Micera G., Rizzarelli E., Sóvágó I. (2007). Chem. Eur. J. 13, pp. 7129-7143; Kowalik-Jankowska T., Biega Ł., Kuczer M., Konopińska D. (2009). J. Inorg. Biochem. 103, pp. 135-142.
12. Prenesti E., Daniele P.G., Prencipe M., Ostacoli G. (1999). Polyhedron 18, pp. 3233-3241.

Self-assembled Mn(III)-salen type complexes as catalysts for degradation of lignin analogues

González-Riopedre G.[1], Bermejo M.R.[2], Fernández-García M.I.[1], González-Noya A.M.[1], Maneiro M.[1]

[1] University of Santiago de Compostela, Department of Inorganic Chemistry, Facultade de Ciencias, E-27002 Lugo (SPAIN)
[2] University of Santiago de Compostela, Centro Investigación en Química Biolóxica e Materiais Moleculares, CIQUS (SPAIN)
gustavo.gonzalez@usc.es, misabel.fernandez.garcia@usc.es, marcelino.maneiro@usc.es

Abstract

Mn(III) complexes **1**-**3**, incorporating dianionic hexadentate Schiff base ligands and different anions (perchlorate for **1**, acetylacetonate for **2** and dicyanamide for **3**) have been synthesized and characterized by elemental analysis, ESI mass spectrometry, IR spectroscopy, room temperature magnetic and molar conductivity measurements. Complex **3** was also crystallographically characterized. The catalytic studies for the use of these complexes as oxygen activators for the selective oxidation of the lignin model compound veratrylalcohol (VA) have been studied. H_2O_2 and O_2 have been alternatively tested as oxidants. Yields up to 30% of VA conversion to veratrylaldehyde have been achieved at room temperature in presence of air flow using 0.5% of catalyst.

Keywords: Peroxidase, Manganese, Schiff bases, supramolecular structure, veratrylalcohol.

Introduction

The objective of pulping and bleaching of wood is the selective removal of lignin without degrading the polysaccharoses, and the removal of colored structures which are originally present in the wood pulp or have been formed during the pulping process [1]. Manganese Peroxidase is able to degrade lignin in Nature. In search of biomimetic models for peroxidase, we have reported active manganese complexes involving tetradentate ONNO Schiff bases, and the influence of the geometry around the manganese ion on peroxidase activity has also been studied by us [2-4].

The dimeric nature of the complexes is decisive on their peroxidase activity since the oxidation of the hydroperoxide to generate dioxygen involves an intramolecular two-electron transfer reaction which is forbidden for a monomeric Mn(III) complex [5]. Dimeric complexes can be achieved using the appropriate ligands, for instance polydentate Schiff bases with both inner and outer compartments. Herein we report three Mn(III) complexes obtained from the reaction between different manganese salts and the Schiff base ligands N,N'-bis(3-methoxy-5-bromo-salicylidene) propane-1,2-diamine (H_2L^1) and N,N'-bis(3-methoxysalicylidene)ethylenediamine (H_2L^2). Peroxidase-like activity of the complexes was followed by the oxidation of the of the diammonium salt of 2,2'-azinobis(3-ethylbenzothiazoline)-6-sulfonic acid (ABTS) at pH 6.8 in aqueous solution. The possibility of evaluating catalyst properties of **1**-**3** for pulp-bleaching purposes has been studied using veratrylalcohol (VA), which can be considered as a model compound for lignin substructures [6].

Methodology

Physical measurements

Elemental analyses were performed on a Carlo Erba Model 1108 CHNS-O elemental analyzer. The IR spectra were recorded as KBr pellets on a Bio-Rad FTS 135 spectrophotometer in the range of 4000-400 cm^{-1}. ^1H NMR spectra were recorded on a Bruker AC-300 spectrometer using CD_3OD (296 K) as solvent and $SiMe_4$ as an internal

reference. The electro-spray mass spectra of the compounds were obtained on a Hewlett-Packard model LC-MSD 1100 instrument. Room-temperature magnetic susceptibilities were measured using a digital measurement system MSB-MKI, calibrated using mercury tetrakis(isothiocyanato)cobaltate(II) $Hg[Co(NCS)_4]$ as a susceptibility standard. Conductivities of 10^{-3} M solutions in DMF were measured on a Crison microCM 2200 conductivity meter.

Synthesis of the complexes

$Mn_2L^1_2(H_2O)_4(ClO_4)_2$ (1), This compound has been synthesized by a method previously reported by us [3]. Anal. Calc. for $C_{38}H_{44}Br_4Cl_2Mn_2N_4O_{16}$ (1312.4): C, 34.7; H, 3.4; N, 4.3. Found: C, 34.0; H, 3.4; N, 4.0 %. MS ES (*m/z*): 553 $[MnL]^+$. IR (KBr, cm^{-1}): ν(O-H) 3438 (m), ν(C=N) 1625 (vs), ν(C-O) 1295 (s), $\nu_3(ClO_4^-)$ 1120 (vs). μ = 4.7 BM. Conductivity (in DMF) Λ_M = 82 µS.

$Mn_2L^1_2(H_2O)_2$(AcAc) (2), This compound has been synthesized by a method previously reported by us [7]. Anal. Calc. for $C_{43}H_{47}Mn_2Br_4N_4O_{12}$ (1240.5): C, 41.6; H, 3.8; N, 4.5. Found: C, 40.4; H, 3.9; N, 4.3 %. MS ES (*m/z*): 553 $[MnL]^+$. IR (KBr, cm^{-1}): ν(O-H) 3432 (m), ν(C=N) 1626 (vs), ν(C-O) 1298 (s), $\nu_{asym}(CO_2)$ 1546 (s), $\nu_{sym}(CO_2)$ 1438 (m). μ = 5.0 BM. Conductivity (in DMF) Λ_M = 10 µS.

$Mn_2L^2_2(H_2O)_2(DCA)_2$ (3), 0.46 mmol (0.15 g) of H_2L^2 was dissolved in methanol (40 mL) and 0.46 mmol (0.11 g) of $Mn(CH_3COO)_2$ was added to the initial yellow solution which changed to brown. The mixture was gently heated and stirred for 30 min, and then 0.46 mmol (0.04 g) of $NaN(CN)_2$ in 10 mL of methanol was added. Anal. Calc. for $C_{40}H_{40}Mn_2N_{10}O_{10}$ (930.8): C, 51.6; H, 4.3; N, 15.0. Found: C, 50.8; H, 4.4; N, 14.8 %. MS ES (*m/z*): 381 $[MnL]^+$; 828 $[MnL(DCA)]^+$. IR (KBr, cm^{-1}): ν(O-H) 3421 (m), ν(C=N) 1624 (vs), ν(C-O) 1259 (s), ν_{sym}(C≡N) 2148 (vs), ν_{asym}(C≡N) 2250 (m). μ = 5.0 BM. Conductivity (in MeOH) Λ_M = 63 µS.

Peroxidase probes

An aqueous solution of ABTS (50 µL; 0.009 M; 4.5 x 10^{-7} mol) and a methanolic solution of the complex (10 µL; 10^{-3} M; 10^{-8} mol) were added to water (3 mL). The **intensity** of the UV **absorption** bands of **ABTS** started to increase immediately after addition of an aqueous solution of H_2O_2 (50 µL; 10 M; 5 x 10^{-4} mol).

Oxidation of veratrylalcohol

VA (200 mmol, 0.29 mL), previously dissolved in 20 mL of dihydrogenfosfate/NaOH buffer pH 8, was mixed with a methanolic solution (15 mL) of the catalytic complex (0.5 mmol, *ca.* 6 mg). The oxidant (600 mmol) was added in three portions at 20 min intervals. The reaction mixture was stirred for 10 hours at 22 ºC with an air flow bubbling through the solution and then filtered through a short silica gel plug to remove the catalyst and excess oxidant. The reaction mixture was extracted in CH_2Cl_2 in the presence of saturated aqueous NaCl solution. The organic layer was dried over $MgSO_4$ and evaporated under reduced pressure. The mixture was then purified by column cromatography using a 1:1 mixture of ethyl acetate:hexane as eluent. The veratrylaldehyde fraction was characterized by ^{1}H NMR spectrometry:: 9.62 (s, 1H); 7.44 (d, 1H); 7.33 (s, 1H); 7.18 (d, 1H); 3.83 (s, 6H).

Results and discussion

Synthesis and characterization of the complexes

Complexes **1-3** were prepared in high yield as detailed in the Section 2.3. Elemental analyses establish the formula $Mn_2L^1_2(H_2O)_4(ClO_4)_2$ for **1**, $Mn_2L^1_2(H_2O)_2$(AcAc) for **2** and $Mn_2L^2_2(H_2O)_2(DCA)_2$ for **3**. Molar conductivity measurements in 10^{-3} M dimethylformamide solutions, in the range 63-82 show the electrolyte behaviour for **1** and **3**, while **2** shows non-electrolyte behaviour. ESI mass spectra registered in methanol show peaks corresponding to the fragment $[MnL]^+$ for all the complexes, indicating the coordination of the Schiff base ligand to the metal centre. Other minor signals could be assigned to $[Mn_2L_2(X)]^+$ units (being X the anion), which could be attributed to the presence of dimeric species. Values for the magnetic moments at room temperature are very close to the spin-only value of 4.9 B.M., as expected for a high-spin magnetically diluted d^4 manganese(III) ion. Infrared spectroscopy verifies the coordination of the Schiff base ligand to the manganese ion. Some other IR spectroscopical features allow understanding how the former manganese salt anions are bound to the central ion [7].

Crystal structure of 3

Single crystals of complex **3**, suitable for X-ray diffraction studies, were obtained by slow evaporation of the methanolic solution at room temperature. Intensity data were collected on a Bruker X8 APEXII diffractometer employing graphite-monochromated *Mo-Kα* radiation (λ = 0.71073 Å) at 100 K. An ORTEP view of **3** with the atomic numbering scheme is shown in Fig. 1.

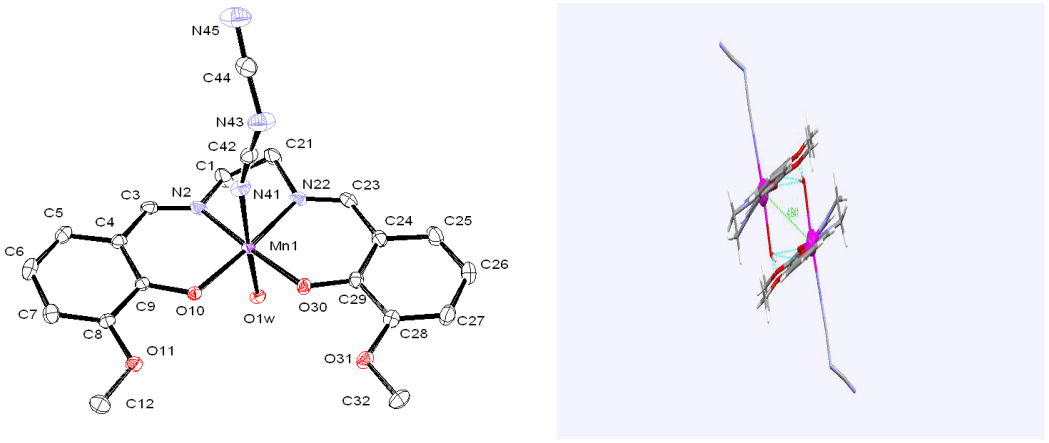

Fig. 1. ORTEP view of the environment around the manganese ion in **3** (left) and mercury drawing of the resulting μ-aquo dimer (right).

The coordination sphere around each manganese centre comprises the planar Schiff base ligand, tightly bound to the metal ion through the inner N_2O_2 compartment by the N_{imine} and O_{phenol} atoms (Mn–N_{imine} bond lengths of 1.98–1.99 Å and Mn–O_{phenol} of 1.88 Å which are typical of such complexes and corroborate the bisdeprotonation of the ligands), The axial positions of the octahedron are occupied by a capping water molecule and a dicyanamide molecule. The superstructure of **3** involves associations *via* a combination of π-aryl offset interactions [8] and hydrogen bonds between capping water molecules and both phenoxy and methoxy oxygen atoms of the neighbouring Schiff base ligand, forming μ-aquo dimeric units. As result of these supramolecular interactions, the Mn•••Mn distances of about 4.84 Å are short for monomeric compounds.

Peroxidase studies

ABTS reacts readily with H_2O_2 in the presence of a peroxidase catalyst to yield a stable green colored radical cation $ABTS^{\cdot+}$ [9]. The reaction of ABTS with H_2O_2 in the presence of **1**–**3** generates $ABTS^{\cdot+}$ and the characteristic absorption bands of this species could be established. The rate of formation of $ABTS^{\cdot+}$ of about 40-62% indicates a relevant peroxidase activity by complexes **1-3.** The rate of conversion of ABTS increases to 70-76 % using a larger amount of the oxidant (250 μL 10 M). However the higher turnovers numbers (TON) of catalytic cycles is achieved reducing the concentration of the catalyst in solution (Fig. 2); the percentages of conversions in these conditions are ranging from 53 to 61 %. The dimeric nature of the complexes is decisive on their peroxidase activity. The X-ray crystallographic studies reveal dimeric μ-aquo entities for **3**, which are able to perform a two one-electron redox process [Mn^{III}, Mn^{III}] ® [Mn^{II}, Mn^{II}]. The self-assembly of the manganese complexes through hydrogen bonding arises as a key issue to enhance the peroxidase activity for this type of complex [4].

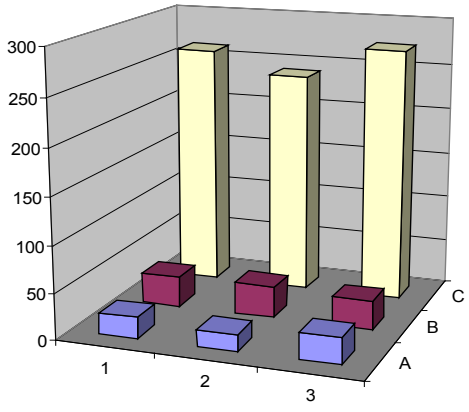

Fig. 2. TONs of catalytic cycles for **1**, **2** and **3** using the standard conditions detailed in section 2.3 (A); increasing the [H_2O_2] adding 250 μL 10 M (B); reducing the [complex] adding 1 μL 10^{-3} M.

Oxidation of lignin analogues

The results of the oxidation of VA to veratrylaldehyde are shown in Fig. 3. Conversions up to 30% were obtained at 22 ºC with an air flow bubbling for 10 h. These are mild conditions compared with the experimental setup of other authors [10], where high temperatures and pressures are needed to reach similar yields with different catalysts. No conversion has been shown in absence of catalyst or in absence of hydrogen peroxide. Air flow providing oxygen as oxidant is crucial to increase the yield, but the presence both catalyst and H_2O_2 are obliged to find some degradation of VA. This behaviour suggests that H_2O_2 could induce the oxidation of the catalyst to a more catalytically active species which subsequently would degrade the VA using dioxygen as oxidant.

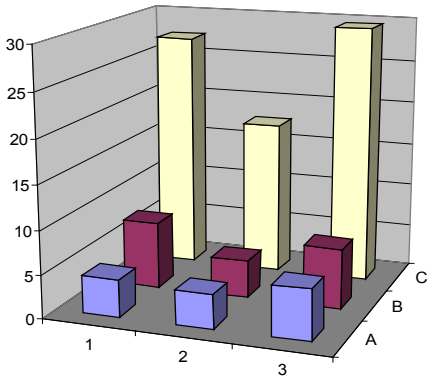

Fig. 3. Conversions of VA to veratrylaldehyde catalyzed by **1**, **2** and **3**:
A) in absence of air flow; B) reducing reaction time to 3 h; C) standard reaction conditions as detailed in section 2.4.

Conclusions

The X-ray structure of **3** shows the self-assembly of the Mn(III)-Schiff base complexes through μ-aquo bridges. This type of structures is crucial to obtain peroxidase-like activity for these complexes. **1-3** behave as efficient peroxidase mimics achieving TON close to 300 catalytic cycles, and they are also able to decompose VA in very mild conditions.

Acknowledgments. We thank Xunta de Galicia (09DPI004291PR) for financial support.

References

[1] Sixta, H. (2006). Handbook of Pulp, Ed. Wiley-VCH, Weinheim (Germany).

[2] Bermejo, M.R.; Fernández, M.I.; González-Noya, A.; Maneiro, M.; Pedrido, R.; Rodríguez, M.J.; García-Monteagudo, J.C.; Donnadieu, B. (2006). J. Inorg. Biochem. 100, pp. 1470-1478.

[3] Bermejo, M.R.; Fernández, M.I.; Gómez-Fórneas, E.; González-Noya, A.M.; Maneiro, M.; Pedrido, R.; Rodríguez, M.J. (2007). Eur. J. Inorg. Chem., pp. 3789-3797.

[4] Vázquez-Fernández, M.A.; Bermejo, M.R.; Fernández-García, M.I.; González-Riopedre, G.; Rodríguez-Doutón, M.J.; Maneiro, M. (2011). J. Inorg. Biochem. 105, pp. 1538-1547.

[5] Maneiro, M.; Bermejo, M.R.; Fernández, M.I.; Gómez-Fórneas, E.; González-Noya, A.M., Tyryshkin, A.M. (2003). New J. Chem. 27, 727-733.

[6] Zucca, P.; Sollai, F.; Garau, A.; Rescigno, A.; Sanjust, E. (2009). J. Mol. Catal. A. 306, 89-96.

[7] Bermejo, M.R.; Fondo, M.; Garcia-Deibe, A.; González, A.; Sousa, A.; Sanmartín, J.; McAuliffe, C.A.; Pritchard, R.G.; Watkinson, M.; Lukov, V. (1999). Inorg. Chim. Acta 293, 210-217.

[8] Constable, E.C.; Housecroft, C.E.; Kopecky, P.; Schonhofer, E.; Zampese, J.A. (2011). CrystEngComm 13, 2742-2752.

[9] Eulering, B.; Schmidt, M.; Pinkernell, V.; Karst, U.; Krebs, B. (1996). Angew. Chem. Int. Ed. Engl. 35, 1973-1974.

[10]Kervinen, K.; Allmending, M.; Leskelä, M.; Repo, T.; Rieger, B. (2003). Phys. Chem. Chem. Phys. 5, 4450-4454.

Coordination of Divalent Cations to a Multihistidinic Domain in Cap43 Protein

Zoroddu M.A.[a], Peana M.[a], Medici S.[a], Juliano C.[a], Solinas C.[a], Anedda R.[b], Nurchi V.M.[c]

[a] *University of Sassari, Department of Chemistry and Pharmacy, Via Vienna 2, 07100 Sassari, zoroddu@uniss.it*
[b] *Porto Conte Ricerche S.r.l., SP 55 Porto Conte/Capo Caccia Km 8.400, Loc. Tramariglio, 07041 Alghero*
[c] *University of Cagliari, Department of Chemical and Geological Sciences, Cittadella Universitaria, SP Monserrato/Sestu Km 0.700, 09042 Monserrato, Cagliari*

Abstract

Multi-histidinic peptides have been investigated for Ni(II) and Cu(II) binding. We present spectroscopic evidence that, at low pH and from sub-stoichiometric to stoichiometric amounts of metals, macrochelate and multi-histidinic Ni(II) and Cu(II) complexes are formed; but, from neutral pH and above, both nickel and copper bind to individual histidine residues. NMR, EPR, UV–Visible and UV–Visible CD spectroscopy were used to understand about the variety of complexes obtained at low pHs, where amide deprotonation and coordination is unfavoured. A structural transition between two coordination geometries, as the pH is raised, was observed. From EPR a distortion from planarity has been evidenced for the Cu(II) multi-histidinic macrochelate systems, which may be relevant to biological activity. The behaviour of our peptides was comparable to the pH-dependent effect on Cu(II) coordination observed in octapeptide repeat domain in prion proteins and in amyloid precursor peptides involved in Alzheimer's disease. Changes in pH and levels of metal affect coordination mode and can have implications for the affinity, folding and redox properties of proteins and peptide fragments.

Keywords: multihistidinic proteins, pH-dependent behaviour, coordination geometries

Introduction

Histidine containing peptides have drawn considerable attention as the models for studying molecular phenomena associated with metal ion binding in proteins involved in fatal neurodegenerative disorders, such as Alzheimer's and prion diseases, or involved in metal detoxification mechanisms, thus protecting against deleterious redox activity by sequestering excess metal ions [1–6]. Despite an increasing body of evidence linking copper to neurodegenerative diseases, the precise coordination geometry, the affinity and stoichiometry of binding, as well as what triggers multi-histidinic amyloid-β peptide to convert from its soluble form to an amyloidogenic form, are yet to be established [7].

We have used two peptides, the two and the three repeats Ac-$(T_1R_2S_3R_4S_5H_6T_7S_8E_9G_{10})_n$–$NH_2$ sequence (n = 2, 20aa; n = 3, 30aa), as the models to further investigate the role of multi-histidine sites in metal coordination. It has been suggested that the three histidines coordination mode of amyloid-β peptide controls the redox activity of copper ions [8]. The presence of His-rich domains in our peptides, similar to those in prion protein, can contribute to the understanding of the crucial role of poly-imidazole centres in the protein coordination process.

In the present paper we report data for the interaction of Ni(II) and Cu(II) with the peptide fragments obtained by NMR, EPR, UV–Vis and UV–Vis CD spectroscopy study. Our results reinforce the suggestion that the change in coordination with pH could be the key to the pH-dependence of biological activities, such as the conformational changes observed in the presence of copper which only induced aggregation of multi-histidinic amyloid-β peptides as the pH was lowered from physiological to 6.8 [9].

Materials and methods

NMR experiments were performed on Bruker Avance 600 MHz spectrometers with 5 mM solutions and different metal to ligand molar ratios over a pH range 3.0–11.0 at steps of 0.5 units by addition of NaOH.

X-band EPR spectra were obtained at different concentrations (from 1 to 3 mM) and different metal to ligand molar ratios at room temperature and at 120 K on a Varian E-9 spectrometer.

Absorption and Visible CD spectra were recorded using concentrations from 2 mM to 0.7 mM on a Varian Cary 50 Scan spectrophotometer and J-810 Jasco (Jasco Inc., Eaton, MD) equipped with a temperature controller at 25°C.

Molecular mechanics geometry optimisation was carried out by using AMBER force field method which was implemented in HyperChemTM 8.0.3 (Hypercube, Inc., Gainesville, FL, 2007) molecular modeling software.

Models of the most likely coordination spheres of Cu(II) '"low pH" multi-histidinic species, Fig. 1, were generated with YASARA (YASARA Biosciences) program.

Fig. 1

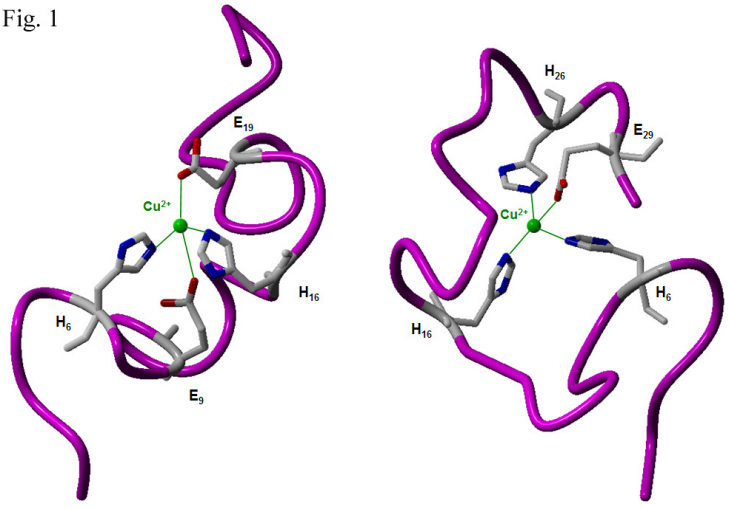

Fig. 1 Models of the most likely coordination spheres of "low pH" Cu(II) multi-histidinic species.

Results and discussion

The coordination features of Ni(II) and Cu(II) towards the two peptides were studied through a series of spectroscopic measurements (CD, NMR, EPR and UV-vis) which gave a clear evidence that two different binding modes are possible at low and high pH values, respectively.

3.1 Ni(II) binding

Comparison of visible CD for Ni(II) at 1 mol equiv added onto the 20aa and 2 and 3 mol equiv added onto the 30aa fragment at pH 10–11, is reported in Fig. 2.

Fig. 2

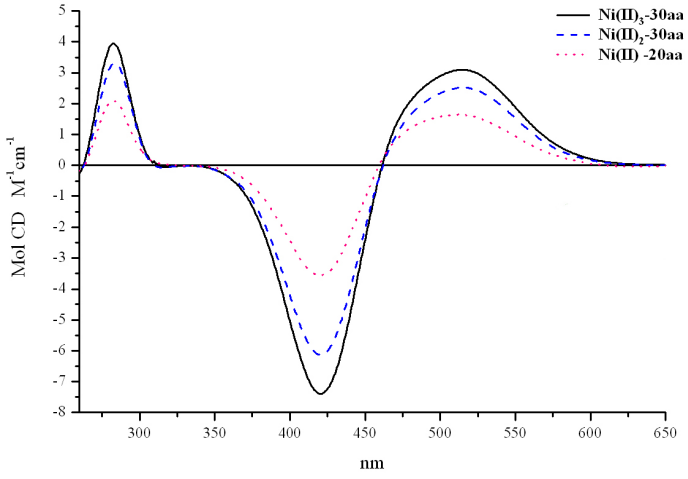

Fig. 2 Comparison of visible CD for Ni(II)–20aa 1:1 and Ni(II)–30aa 2:1 and 3:1, pH10–11.

The shape of the spectrum is the same with the two and three Ni(II) bound-30aa, showing that Ni(II) ions bind independently to either His_6, His_{16} or His_{26}. From UV–Vis spectra obtained for 1:1, 1:2 and 1:3 ligand to metal molar ratios the abs at 438 nm, λ_{max} characteristic of 4N–Ni species, increases as a function of the nickel added at pH 10. This behaviour shows that the three Ni atoms bind tightly to the three histine residues by forming Ni–30aa, Ni_2–30aa and Ni_3–30aa at the three histidine anchoring sites His_6, His_{16} and His_{26}. No significant CD activity was measured for Ni(II)–20aa at low pH. A visible CD is not apparent until pH is raised up to 8, but some species have clearly been potentiometrically evidenced. The lack of appreciable d–d transition CD bands suggests minimal vicinal effects [10] implying that there is no main-chain coordination at physiological pH and below, thus suggesting the involvement of imidazol donor atoms in macrochelate systems. At pH 8 the profound change in the visible CD spectra suggests the change in coordinating ligands around the nickel atom. This was confirmed also by NMR studies. At low pH values, from the differential broadening of the NMR resonances the direction of the coordination occurs towards the C-terminus in the form of less stable macrocycles. They are favoured also because of the possible metal interaction with side chain residues as carboxylate group from glutammic acid in the 9th position, two residues following the histidine anchoring site towards the C-terminus. This is also in agreement with the deprotonation of glutammic acid at low pH (pKa in the range 4–4.7 or 4–4.9 for the 20aa and the 30aa ligand, respectively) [11]. At high pH, when amide main-chain coordination with the formation of one 6- and two 5-membered rings is a favoured process, N_δ of histidine is involved in nickel coordination, as we previously found by NMR studies [12]. From NMR spectra obtained at low pH and for sub-stoichiometric amount of nickel, though the overlap of aromatic signals makes the interpretation difficult, His $H_{\varepsilon 1}$ and His $H_{\delta 2}$ signals simultaneously disappeared upon nickel addition, pointing to N_ε as the anchoring site. Thus, we can suggest that a tautomeric effect, i.e. binding either by His N_δ or N_ε as a function of the pH, could be possible for nickel binding.

3.2 *Cu(II) binding*

Visible CD spectra for the 20aa and for the 30aa–Cu interaction have, at pH 10, a positive band at about 640 nm which appears to longer wavelengths than that of the absorption maximum (λ_{max} = 540 nm for Cu-bound) and a negative one at 510 nm to shorter wavelengths than that of the absorption maximum. The band at about 310 nm, which appears above pH 8, is attributed to the N^-_{amide}–Cu(II) and at 360 nm to the $N_{imidazol}$–Cu(II) charge transfer transition [13]. The shape of the spectra is the same for the 20aa and for the 30aa, showing that, also for copper, the mode of coordination has not changed at high pH for the larger fragment. The shapes of CD spectra obtained are similar to those reported for copper and nickel bound to prion protein fragments containing a single histidine residue at position 111 or 96, for copper and nickel bound to model peptides at high pH in order to ensure a 4N coordination [10,14]. Due to this similarity, we can suggest that the shape could be indicative of 4N square planar species with the involvement of His as the anchoring site and amide main-chain coordination with the formation of one 6- and two 5-membered rings. From UV–Vis spectra obtained for 1:1, 1:2 and 1:3 ligand to metal molar ratios the abs at 540 nm, λ_{max} characteristic of 4N–Cu species, proportionally increases as a function of the copper added at pH 11. This behaviour shows that the three Cu atoms bind tightly to the three histidine residues by forming Cu–30aa, Cu_2–30aa and Cu_3–30aa at the three histidine anchoring sites His_6, His_{16} and His_{26}. The increase in the abs, at 540 nm for copper and at 438 nm for nickel by adding 1, 2 or 3 mol equiv, suggests that the longer fragment is loaded with 3 mol equiv of metal at pH 11 and 10. There is a clear transition in the visible CD spectra at pH 7.7 suggesting that at this pH a change in the coordinating ligands around the copper ion occurs.

For the 20aa and the 30aa fragments with Cu at 1:1, 1:2 and 1:3 molar ratios below pH 6, no significant visible CD activity was measured, although several species have clearly been potentiometrically evidenced, thus providing a suggestion for the involvement of imidazole atoms in macrochelate system, Fig. 3.

Fig. 3

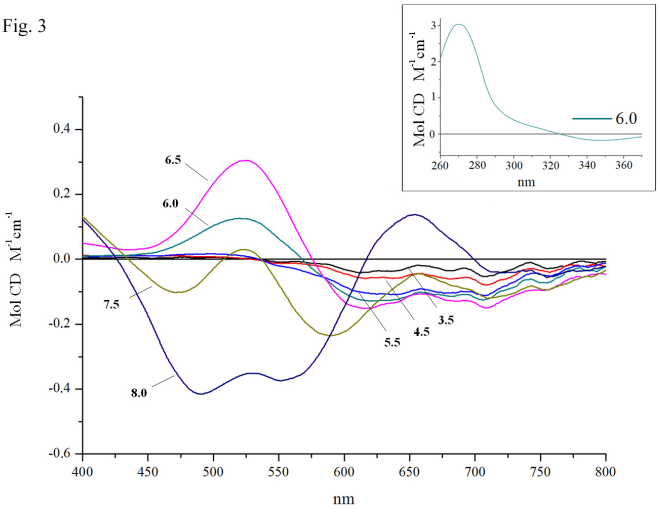

Fig. 3 Visible CD for Cu–20aa 1:1, pH range 3.5–8.

20aa–Cu 1:1 visible CD measurements at pH 6.5 result in a spectrum having a sigmoidal shape which hints the presence of species where multiple histidine residues coordinate a single copper ion [2].

EPR spectroscopy has been used to investigate about the Cu-site transition between the two coordination geometries evidenced going from mildly acidic condition to high pH. For all the spectra, at both 120 K and room temperature, axial or nearly axial parameters are obtained with $g_{\|} > g_{\perp} > 2.040$, suggesting a d_{x2-y2} or, less commonly, a d_{xy} ground state in a square planar, square pyramidal or tetragonal elongated octahedral stereochemistry [15,16]. Addition of the second and the third equivalent of copper does not modify EPR spectrum of the first copper atom. Thus, the three sites can be considered independent (Fig. 4).

Fig. 4

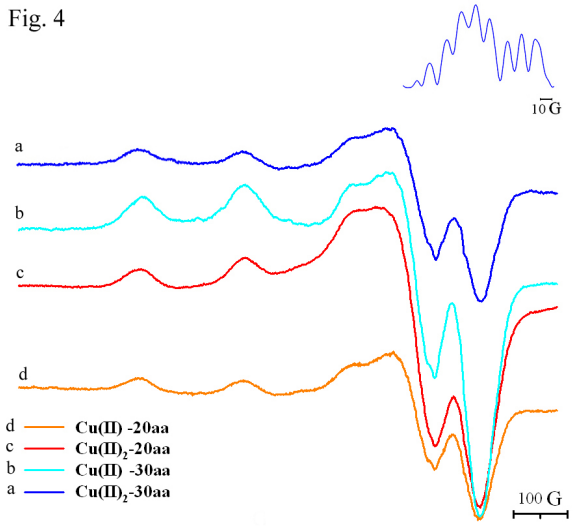

Fig. 4 EPR spectra of Cu–30aa, Cu–20aa 1:1 and 2:1 metal to ligand molar ratio, at pH 10.5; inset 2nd derivative on the perpendicular region.

In addition, in the pH range 10–11 and at 1:1, 1:2 and 1:3 ligand to metal molar ratios, no free copper has been evidenced and the only bound 4N–30aa species is present, thus indicating the formation of Cu_3–30aa species.

In basic solution deprotonation of amide groups leads to a square planar four coordination as previous observed [17], $A_{\|}$ (Cu–30aa, 3N) = 172.7 x 10^{-4} cm^{-1} and $g_{\|}$ = 2.232, $A_{\|}$ (Cu–30aa, 4N) = 196.7 x 10^{-4} cm^{-1} and $g_{\|}$ = 2.195 and $A_{\|}$ (Cu–20aa, 4N) = 190.3 x 10^{-4} cm^{-1} and $g_{\|}$ = 2.203. Careful inspection of the 2nd derivative spectra and other parameters points to a geometrical distortion of the planar moiety towards a tetrahedral arrangement.

In accordance with the results collected for the Ni(II) study, also paramagnetic Cu(II) broadens ^{1}H NMR signals when in close proximity to metal or on donor atoms directly coordinated to metal [18,19]. A selective and simultaneous disappearance of both $H_{\delta 2}$ and $H_{\varepsilon 1}$ can be clearly observed. This result strongly points to N_{ε} as the anchoring site and to its involvement in poly-imidazole macrocycles complexes formation at low pH. The almost complete lack of significant broadening of all the other resonances, but only a drop in intensity of His_6 $H_{\beta 1}$, Glu_9 H_{γ}, $H_{\beta 2}$ and Thr_7 NH indicates the direction of coordination towards the C-terminus, in agreement with the formation of macrochelate systems.

Conclusions

We have demonstrated for our systems a dynamic pH-dependent behaviour of their coordination mode, switching from the macrochelate to the square planar or distorted complexes while going from acidic to basic pH values. The transition between the two coordination geometries could be the critical point for a dual mechanism operating in multi-histidine proteins, e.g. metal transport in a redox-inactive state through individual multiple anchoring sites, protecting against deleterious effects, plus antioxidant activity from macrochelate and multi-histidinic metal coordination. In fact, it has been reported that multiimidazole coordination mode might be critical for the biological implications, in particular for the redox activity [20,21]. From EPR parameters, obtained at room and low temperature, a distortion from planar to tetrahedral arrangement was clearly evidenced, particularly for the Cu–20aa macrochelate systems. As reported in the literature [22,23], SOD activity is better developed for complexes in a distorted environment. In fact, in this case, the molecular orbital scheme has a Cu-d_{xy} atomic orbital, which is better suited to allow $d_{\pi-\pi\pi}$ overlap with O^-_2 anion. Otherwise, in the case of planar complexes, interaction is

not allowed by the symmetry of the HMSOs of the two species. The multi-histidinic coordination mode facilitates Cu^{+}–Cu^{2+} redox cycle and dismutation of superoxide radical becomes active. In conclusion, the copper transport and the antioxidant activity could be the major biological function of this kind of sites in proteins.

References

[1] Sigel, A.; Sigel, H.;.Sigel, R.K.O (Eds), Neurodegenerative Diseases and Metal Ions in Life Sciences, Wiley, Chichester, 2006, Vol. 1

[2] Syme, C.D.; Nadal, R.C.; Rigby, S.E.J.; Viles, J.H. (2004). Copper binding to the amyloid-beta (Abeta) peptide associated with Alzheimer's disease: folding, coordination geometry, pH dependence, stoichiometry, and affinity of Abeta-(1-28): insights from a range of complementary spectroscopic techniques. J. Biol. Chem., 279, pp 18169–18177

[3] Jackson, G.S.; Murray, I.; Hosszu, L.L.P.; Gibbs, N.; Waltho, J.P.; Clarke, A.R.; Collinge, J. (2001). Location and properties of metal-binding sites on the human prion protein. Proc. Natl. Acad. Sci. USA 98, pp 8531-8535

[4] Millhauser, G.L. (2007). Copper and the prion protein: methods, structures, function, and disease. Ann. Rev. Phys. Chem., 58, pp 299-320

[5] Gaggelli, E.; Kozlowski, H.; Valensin, D.; Valensin, G. (2006). Copper homeostasis and neurodegenerative disorders (Alzheimer's, prion, and Parkinson's diseases and amyotrophic lateral sclerosis). Chem. Rev., 106, pp 1995-2044

[6] Bonomo, R.P.; Impellizzeri, G.; Pappalardo, G.; Rizzarelli, E.; Tabbì, G. (2000). Copper(II) binding modes in the prion octapeptide PHGGGWGQ: a spectroscopic and voltammetric study. Chem. Eur. J., 6, pp 4195-4202

[7] Faller, P.; Hureau, C. (2009). Bioinorganic chemistry of copper and zinc ions coordinated to amyloid-beta peptide. Dalton Trans., 7, pp 1080-1094

[8] Nakamura, M.; Shishido, N.; Nunomura, A.; Smith, M.A.; Perry, G.; Hayashi, Y.; Nukayama, K.; Hayashi, T. (2007). Three histidine residues of amyloid-beta peptide control the redox activity of copper and iron. Biochemistry, 46, pp 12737-12743

[9] Atwood, C.S.; Moir, R.D.; Huang, X.; Scarpa, R.C.; Bacarra, N.M.E.; Romano, D.M.; Artshorn, M.A.; Tanzi, R.E.; Bush, A.I. (1998). Dramatic aggregation of Alzheimer abeta by Cu(II) is induced by conditions representing physiological acidosis. J. Biol. Chem., 273, pp 12817-12826

[10] Klewpatinond, M.; Viles, J.H. (2007). Empirical rules for rationalising visible circular dichroism of Cu^{2+} and Ni^{2+} histidine complexes: applications to the prion protein. FEBS, 58, pp 1430-1434

[11] Zoroddu, M.A.; Peana, M.; Kowalik-Jankowska, T.; Kozlowski, H.; Costa, M. (2004). Nickel(II) binding to Cap43 protein fragments. J. Inorg. Biochem., 98, pp 931-939

[12] Zoroddu, M.A.; Peana, M.; Medici, S.; Anedda, R. (2009). An NMR study on nickel binding sites in Cap43 protein fragments. Dalton Trans., 28, pp 5523-5534

[13] Fawcett, T.G.; Bernarducci, E.E.; Jespersen, K.K.; Schugar, H.J. (1980). Charge-transfer absorptions of copper(II)-imidazole and copper(II)-imidazolate chromophores. J. Amer. Chem. Soc., 102, pp 1998-2003

[14] Klewpatinond, M.; Viles, J.H. (2007). Fragment length influences affinity for Cu^{2+} and Ni^{2+} binding to His96 or His111 of the prion protein and spectroscopic evidence for a multiple histidine binding only at low pH. Biochem. J., 404, pp 393–402

[15] Hathaway, B.J.; Billing, D.E. (1970). Electronic Properties and Stereochemistry of Mononuclear Complexes of the Copper (II) Ion. Coord. Chem. Rev., 5, pp 143-207

[16] Hathaway, B.J.; Tomlinson, A.A.G. (1970). Copper(II) ammonia complexes. Coord. Chem. Rev., 5, pp 1- 43

[17] Zoroddu, M.A.; Peana, M.; Kowalik-Jankowska, T.; Kozlowski, H. (2008). Copper(II) binding to Cap43 protein fragments. Dalton Trans., 44, pp 6127–6134

[18] Bertini I.; Luchinat, C. (1998); NMR of paramagnetic substances. Coord. Chem. Rev., 150, pp 1-296

[19] Gaggeli, E.; D'Amelio, N.; Valensin, D.; Valensin, G. (2003). 1H NMR studies of copper binding by histidine-containing peptides. Magn. Reson. Chem. 41, pp 877-883

[20] Stanczak, P.; Kozlowski, H. (2007). Can chicken and human PrPs possess SOD-like activity after beta-cleavage? Biochim. Biophys. Res. Commun. 352, pp 198-202

[21] Multhaup, G.; Schlicksupp, A.; Hesse, L.; Beher, D.; Ruppert, T.H.; Masters, C.L.; Beyreuter, K. (1996). The amyloid precursor protein of Alzheimer's disease in the reduction of copper(II) to copper(I). Science, 271, pp 1406-1409

[22] Tainer, J.A.; Getzoff, E.D.; Richardson, J.S. (1983). Structure and mechanism of copper, zinc superoxide dismutase. Nature, 306, pp 284-287

[23] Hathaway, B.J. in: G. Wilkinson (Eds), Comprehensive Coordination Chemistry, Pergamon, Oxford, 1987, Vol.5, p. 134.

Nano-Sized Carriers for Carbon Monoxide Releasing Molecules

Kunz P.C.[1]*, Meyer H.[1], Schmidt A.[2]*, Janiak C.[1]*

[1] *Heinrich-Heine-Universität, Institut für Anorganische Chemie und Strukturchemie, Universitätsstr. 1, D-40225 Düsseldorf (Germany)*
[2] *Universität zu Köln, Institut für Physikalische Chemie, Luxemburger Str. 116, D-50939 Köln (Germany)*
peter.kunz@hhu.de, annette.schmidt@uni-koeln.de, janiak@hhu.de

Abstract

Nanoparticles (NPs) can not only act as scaffolds, but also can be used to trigger carbon monoxide (CO) release. The very elegant light-induced CO release can so far only be used in treatment of surface tissues as the light used does not penetrate deeply into tissues. Here we report on our on-going work to modify the CO release characteristics by incorporation into nano-scale composites. Different biocompatible nanoparticles were decorated by CO-releasing molecules (CORMs). For efficient decoration we developed a L-DOPA (Levodopa, L-3,4-dihydroxyphenylalanine) derived CORM-3 analog. The CORM-functionalized NPs show temperature and pH-dependent CO release.

Keywords: Carbonyl ligands, metal carbonyl, CO release, CORM, nanoparticle, gasotransmitter.

Introduction

The use of nanoparticles (NPs) for biomedical applications is a continuously and rapidly growing research field, with heavy emphasis on imaging and drug delivery. The unique properties of NP-based systems hold strategic advantages over small molecular drugs including, for example, high drug load, conjugation of little soluble drugs to a soluble NP carrier and use of multiple targeting devices on a NP scaffold for targeted drug delivery [1]. Furthermore, drug carrier systems at the nano-scale are ideally suited to target sites of inflammation and distinct cancerous tissues due to their *enhanced permeability and retention* (EPR) effect [2]. Although macromolecular scaffolds are long known in nitrogen oxide (NO) release [3], only a few examples of carbon monoxide (CO) releasing nano-sized scaffolds are known [4].

Cellular role of carbon monoxide

The role of carbon monoxide as a small molecule messenger in cellular processes is now broadly accepted, as it intervenes in the regulation of inflammation processes, cellular proliferation, apoptotic cell death and neural transmission (Fig. 1) [5].

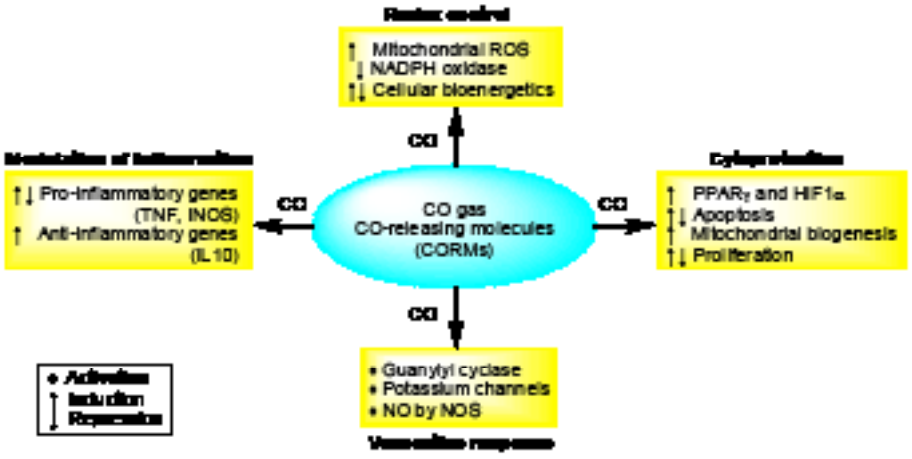

Fig. 1 Potential mechanisms of biological action of carbon monoxide (CO) delivered as gas or CORM in preclinical models (graphics adapted from ref. 7a).

The signal transduction pathway of CO is not fully elucidated, yet carboxylation of the involved proteins in response to oxidative stress seems to play a central role. While on the one hand CO is rated as cytoprotective under these conditions, its general toxicity becomes dominant at higher systemic concentrations of free CO due to inference with heme proteins and thus inhibition of oxygen transport. Both the cytoprotective and cytotoxic properties of CO can be exploited for therapeutic purposes in a locally restricted tissue volume, for example in tumor tissue.

CO releasing molecules (CORMs)

The pharmacological requirement to deliver precise amounts of CO to specific locations under physiological conditions recently triggers an enormous research activity towards solid storage forms for carbon monoxide, which are safe to handle and from which the CO can be released by a specific trigger [6]. Metal carbonyl complexes are a natural choice for such CO releasing molecules (CORMs) (Fig. 2) [5d,7,8].

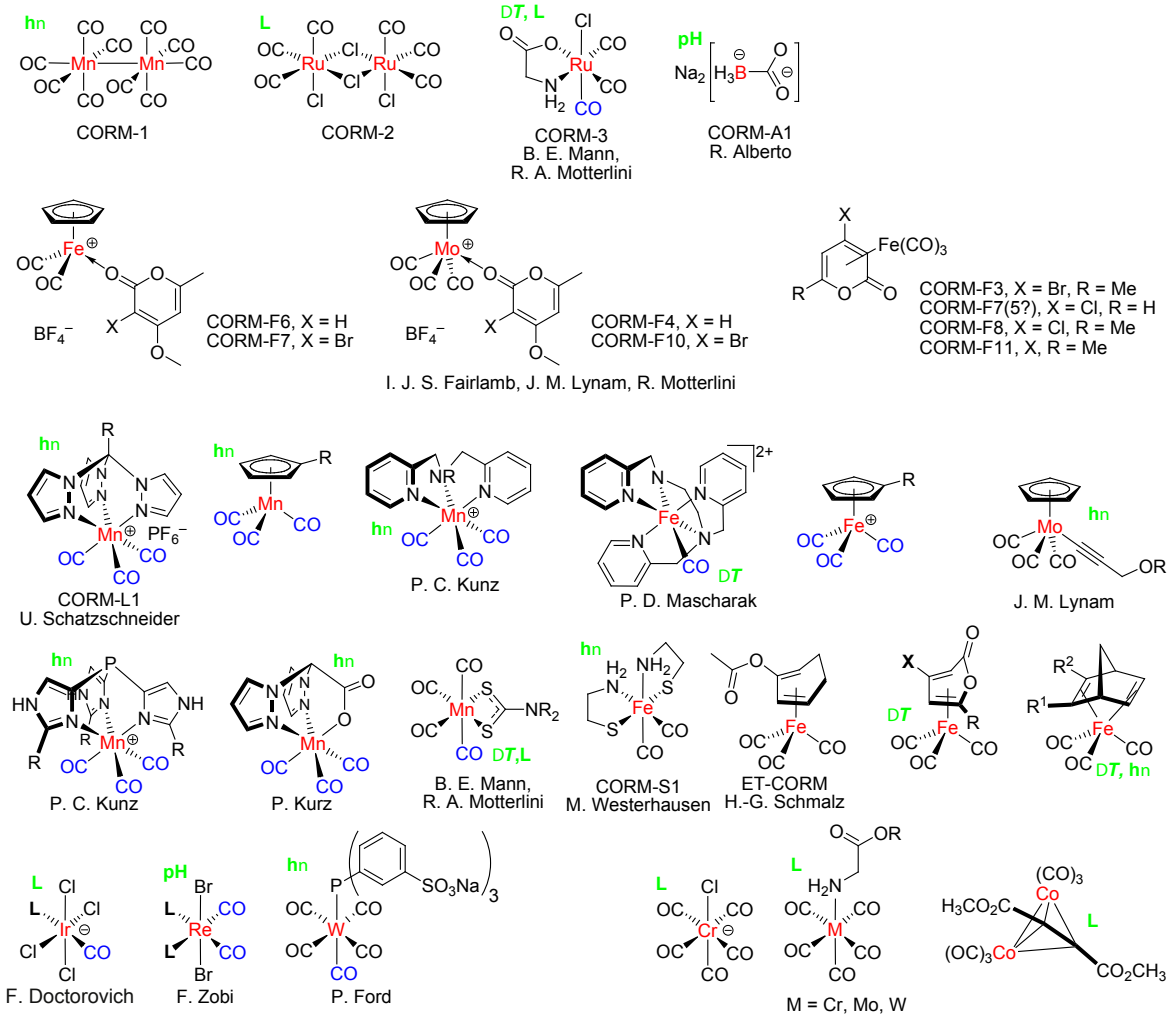

Fig. 2 Present examples for CO-releasing molecules (CORMs) with accepted acronym (CORM-A1, CORM-2 etc.), principal investigator and specific release trigger (in green: hν = photolysis, ΔT = temperature increase, pH change or ligand, L substitution); see also Table 1.

In most CORMs known to date, the release of carbon monoxide is triggered by hydrolytic processes in aqueous environments, and thus their half-life under physiological conditions that determines their potential therapeutic utility is often limited to a few minutes. To overcome such limitations, recent research activities include the development of CORMs that allow the liberation of CO upon the application of an external trigger such as light (photoCORMs) [6b,e] or by specific enzyme activity (ET-CORMs) [6a]. However, the CO release in photoCORMs, so far, relies mostly on UV irradiation and, thus, suffers from limited penetration depth into tissue. Typical CORMs and their CO release characteristics are summarized in Fig. 2 and Table 1.

Table 1. Properties of some CORMs sketched in Fig. 2 [5].

Compound	properties and activation	pharmacological effects
CORM-1	photoinduced, fast release, lipophilic	vasodilatative
CORM-2	fast release after ligand exchange, lipophilic	vasodilatative
CORM-3	fast release after ligand exchange, hydrophilic	cardioprotective, anti-inflammatory
CORM-Fx	fast and spontaneous release, hydrophilic	vasodilatative
CORM-A1	slow, pH depended release, hydrophilic	vasodilatative, antiapoptotic
CORM-L1	photoinduced, slow release, hydrophilic	anticancerogenic

Enhanced permeability and retention (EPR) effect

Many attempts have been made to discover nontoxic cancer therapeutic agents that exclusively act on-site of the malign tissue. However, no truly selective anticancer agent that is clinically satisfactory is yet available. Small molecules, as are many of the drugs being used today for chemotherapy, do not discriminate tumor tissue from normal tissue; they reach most normal tissues and organs as well as tumor tissues by free diffusion-dependent equilibrium. One promising approach though is based on a significant size-exclusion effect of the tumor vascular permeability and is thus concerned with nanoparticular or polymeric drugs. The clearance of macromolecules and lipids from tumor is so impaired that they remain in the tumor interstitium for a long time, while clearance of macromolecules and lipids from the interstitial space of normal and inflammatory tissues proceeds rapidly and steadily via the lymphatic system, even in the inflammatory state after extravasation from blood vessels [9] This phenomenon, termed the tumor-selective enhanced permeability and retention (EPR) effect, is now regarded as a ''gold standard'' in the design of new anticancer agents [9a,b,10]. Consequently, macromolecules and nanoparticles with their wide variety of properties and functionalities are the focus of interest, in particular in cancer chemotherapy and in the treatment of inflammatory diseases. Their unique dimensions allow that they passively target malignant tissue with pathophysiological characteristics like leaky vasculature, and in the case of solid tumours impaired drainage (Fig. 3) [11].

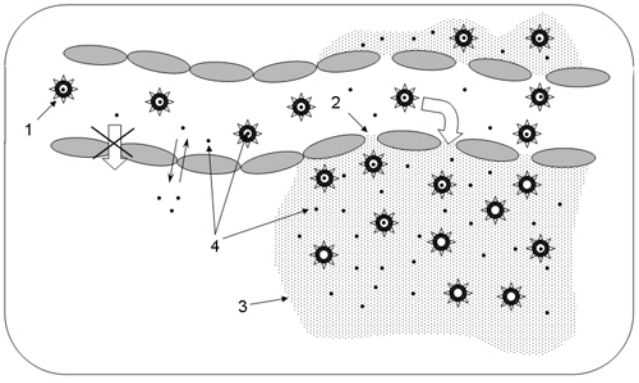

Fig. 3 Enhanced permeability and retention (EPR) effect. Long-circulating drug carriers (1) penetrate through the leaky pathological vasculature (2) into the tumor interstitium (3) and degrade there, releasing a free drug (4) and creating its high local concentration.

Nano-sized carrier systems

The passive EPR-based drug-loaded particle targeting to tumor and inflammatory tissue can be complemented by different mechanisms, like the attachment of tumor-specific peptides or antigens to the surface of NPs [12]. Thus, nanoparticles can improve site-specific drug delivery and reduce systemic exposure, giving rise to reduced side effects of chemotherapies.

While CORMs have already been incorporated into nano-sized carrier systems such as polymers [4a], micelles [4c] or SiO_2 nanoparticles [4b] (Fig. 4), and thus conceptually allow their concentration in malignant tissue, a smart solution is needed to activate the CO release in a controlled manner at the target site within the body.

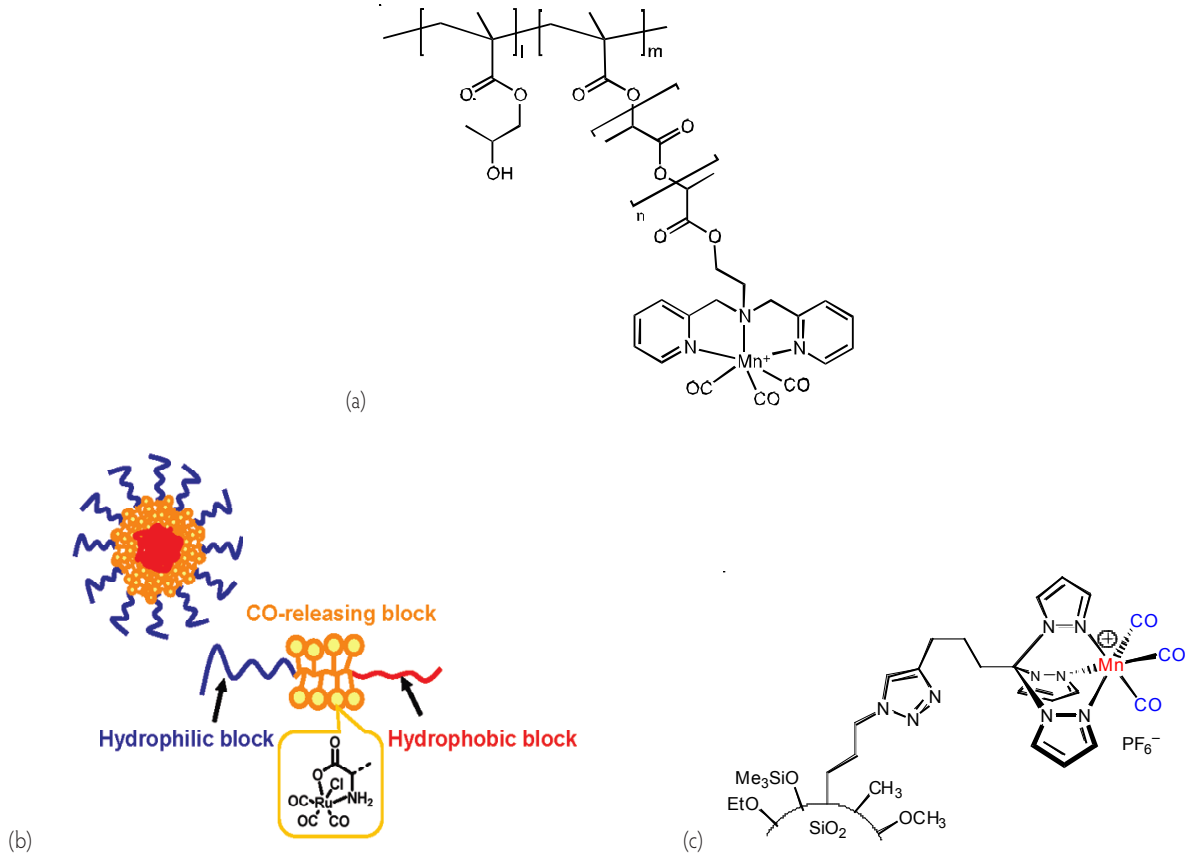

Fig. 4 Nano-sized carrier systems for CO-releasing molecules (a) polymers [4a], (b) micelles [4c] and (c) SiO_2 nano-particles [4b].

The core diameter of NPs can easily be controlled to suit the EPR effect. Furthermore at a diameter of less than 20 nm and overall hydrodynamic diameter of less than 50 nm, NPs are of a size that is comparable to the cell nucleus size (~ 50 nm) and much smaller than a cell (normally 10–100 µm).

The *Kunz* group has developed photoinduced polymer-bound CORMs (polyCORMs) and polymeric vectors labelled by fluorescent $Re(CO)_3$ complexes (Fig. 5 and 6). These fluorescent polymers have been used for the determination of their cellular uptake [13].

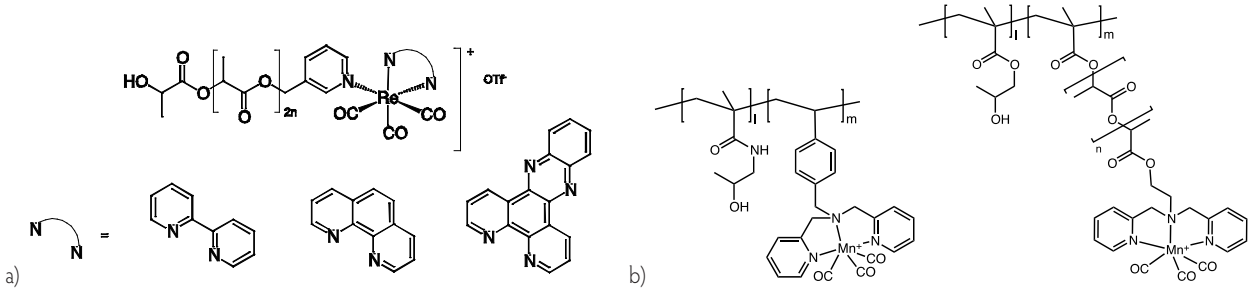

Fig. 5 Polymeric vectors incorporating $Mn(CO)_3$ and $Re(CO)_3$ units. (a) Fluorescent polymers for cell uptake and distribution studies, (b) photoinduced polyCORMs [13].

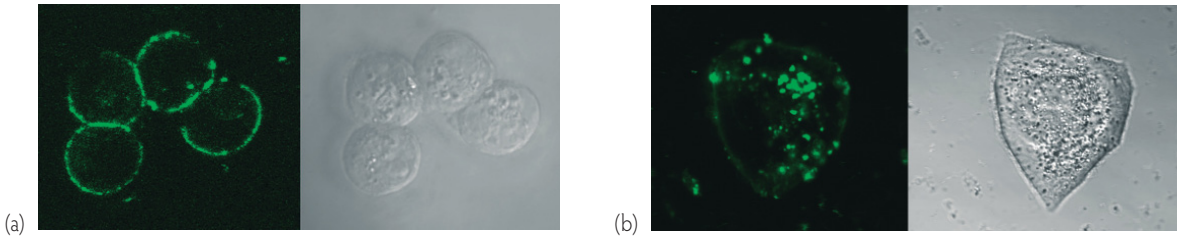

Fig. 6 Cell uptake of an [Re(CO)$_3$(bipy(py)]-labelled polymer.
Confocal fluorescence and bright field images of A2780 cells incubated the labelled polymer for (a) 2 hours and (b) 72 hours. Figures taken from ref. 13.

Different techniques like encapsulation, covalent attachment or adsorption can be used to modify the surface properties of nanoparticles and to immobilize therapeutic agents on these particles [14]. The presence of Lewis acidic atoms and of surface-attached hydroxyl groups, such as in (-OH), on the nanoparticle surfaces provide versatile synthetic handles for the attachment of functionalized molecules. Anchoring groups to attach molecules onto the surface of nanoparticles are catechols, carboxylates, (poly)phosphonates or siloxanes (Fig. 7) [15].

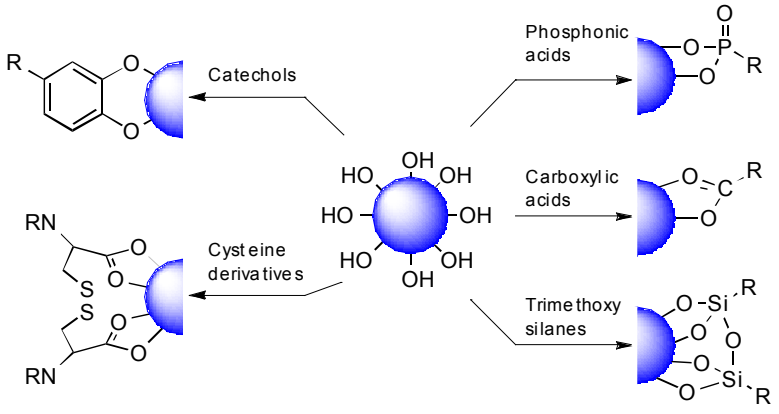

Fig. 7 Groups that can be used to anchor polymers on ferrite nanoparticle surfaces (Figure adapted from Boyer et al. [15]).

References

[1] Doane, T. L.; Burda, C. (2012). Chem. Soc. Rev. 41, pp. 2885-2911.

[2] Maeda, H. (2010). Bioconjugate Chem. 21, pp. 797.

[3] Riccio, D. A.; Schoenfisch, M. H. (2012). Chem. Soc. Rev. 41, pp. 3731-3741.

[4] (a) Brückmann, N. E.; Wahl, M.; Reiß, G. J.; Kohns, M.; Wätjen, W.; Kunz, P. C. (2011). Eur. J. Inorg. Chem. pp. 4571-4577; (b) Dördelmann, G.; Pfeiffer, H.; Birkner, A.; Schatzschneider, U. (2011). Inorg. Chem. 50, pp. 4362-4367; (c) Hasegawa, U.; van der Vlies, A. J.; Simeoni, E.; Wandrey, C.; Hubbell, J. A. (2010). J. Am. Chem. Soc. 132, pp. 18273-18280.

[5] (a) Romão, C. C.; Blättler, W. A.; Seixas, J. D.; Bernardes, G. J. L. (2012). Chem. Soc. Rev., 41, pp. 3571-3583; (b) Mann, B. (2010). Top. Organomet. Chem. 32, pp. 247-285; (c) Alberto, R.; Motterlini, R. (2007). Dalton Trans. pp. 1651-1660; (d) Mann, B.; Motterlini, R. (2007). Chem. Commun. pp. 4197-4208; (e) Motterlini, R. (2007). Biochem. Soc. Trans. 35, pp. 1142-1146; (f) Johnson, T.; Mann, B.; Clark, J.; Foresti, R.; Green, C. (2003) Angew. Chem. Int. Ed. 42, pp. 3722-3729.

[6] (a) Romanski, S.; Kraus, B.; Schatzschneider, U.; Neudörfl, J.-M.; Amslinger, S.; Schmalz, H.-G. (2011). Angew. Chem. 123, pp. 2440-2444; (b) Schatzschneider, U. (2011). Inorg. Chim. Acta 374, pp. 19-23; (c) Zhang, W.-Q.; Whitwood, A. C.; Fairlamb, I. J. S.; Lynam, J. M. (2010). Inorg. Chem. 49, pp. 8941-8952; (d) Pitchumony, T. S.; Spingler, B.; Motterlini, R.; Alberto, R. (2010). Org. Biomol. Chem. 8, pp. 4849-4854; (e) Schatzschneider, U. (2010). Eur. J. Inorg. Chem. 10, pp. 1451-1467; (f) Foresti, R.; Bani-Hani, M. G.; Motterlini, R. (2008). Intensive Care Med. 34, pp. 649-658.

[7] (a) Fairlamb, I. J. S.; Lynam, J. M.; Moulton, B. E.; Tayler, I. E.; Duhme-Klair, A. K.; Sawle, P.; Motterlini, R. (2007). Dalton Trans. pp. 3603-3605; (b) Sawle, P.; Hammad, J.; Fairlamb, I. J. S.; Moulton, B.; O'Brien, C. T.; Lynam, J. M.; Duhme-Klair, A. K.; Foresti, R.; Motterlini, R. (2006). J. Pharmacol. Exp. Ther. 318, pp. 403-410.

[8] (a) Motterlini, R.; Otterbein, L. E. (2010). Nat. Rev. Drug Discovery 9, pp. 728-743; (b) Johnson, T. R.; Mann, B. E.; Clark, J. E.; Foresti, R.; Green, C. J.; Motterlini, R. (2003). Angew. Chem., Int. Ed. 43, pp. 3722-3729; (c) Motterlini, R.; Mann, B. E.; Johnson, T. R.; Clark, J. E.; Foresti, R.; Green, C. J. (2003). Curr. Pharm. Des. 9, pp. 2525-2539; (d) Motterlini, R.; Mann, B. E.; Foresti, R. (2005). Expert Opin. Invest. Drugs 14, pp. 1305-1318; (e) Mann, B. E. (2010). Carbon monoxide: an essential signalling molecule, in: Metzler-Nolte, N.; Jaouen, G. (Eds.), Top. Organomet. Chem., 32, pp. 247-285.

[9] (a) Maeda, H.; Matsumura, Y. (1989). Crit. Rev. Ther. Drug Carrier Sys. 6, pp. 193-210; (b) Maeda, H. (1991) Adv. Drug Deliv. Rev. 6, pp. 181-202; c) Maeda, H. (1994). in Polymer Site Specific Pharmacotherapy (Domb, A. J. ed.), Wiley, New York, USA, pp. 95-116; (d) Maeda, H.; Seymour, L.; Miyamoto, Y. (1992). Bioconjugate Chem. 3, pp. 351-362; (e) Courtice, F. C. (1963) in Lymph and Lymphatic System (Meyersen, H. S. Chairman) Charles C. Thomas, Springfield, IL, USA, pp. 89-126.

[10] Muggia, F. M. (1999). *Clin. Cancer Res*. 5, pp. 7-8.

[11] (a) Maeda, H.; Matsumura, Y. (2011). Adv. Drug Delivery Rev. 63, pp. 129-130; (b) Maeda, H. (2010). Bioconjugate Chem. 21, pp. 797-802; (c) Khemtong, C.; Kessinger, C.; Gao, J. (2009). Chem. Commun. pp. 3497-3510; (d) Maeda, H.; Sawa, T.; Konno, T. (2001). J. Controlled Release 74, pp. 47-61.

[12] (a) Gunn, J.; Park, S. I.; Veiseh, O.; Press, O. W.; Zhang, M. (2011). Mol. Biosyst. 7, pp. 742-748; (b) Singh, R. (2009). Exp. Mol. Pathol. 86, pp. 215-223; (c) Farokhzad, O. C.; Karp, J. M.; Langer, R. (2006). Expert Opin. Drug Deliv. 3, pp. 311-324.

[13] Brückmann, N. E.; Kögel, S.; Hamacher, A.; Kassack, M. U.; Kunz, P. C. (2010). Eur. J. Inorg. Chem. pp. 5063-5068.

[14] (a) Brewer, E.; Coleman, J.; Lowman, A. (2011). J. Nanomater. pp. 1-10; (b) McKinlay, A.; Morris, R.; Horcajada, P.; Férey, G.; Gref, R.; Couvreur, P.; Serre, C. (2010). Angew. Chem. 122, pp. 6400-6406; (c) Vallet-Regí, M.; Balas, F.; Arcos, D. (2007). Angew. Chem. 119, pp. 7692-7703.

[15] Boyer, C.; Whittaker, M. R.; Bulmus, V.; Liu, J.; Davis, T. P. (2010). NPG Asia Mater. pp. 23-30.

Factors Influencing the Formation of Mixed Metal Complexes of Peptide Fragments of Prion Protein and Related Ligands

Sóvágó I., Turi I., Grenács Á.

Department of Inorganic and Analytical Chemistry, University of Debrecen, H-4010 Debrecen, Hungary
sovago@science.unideb.hu

Abstract

Peptide fragments of human prion protein (HuPrP) can effectively bind both copper(II) and nickel(II) ions. In the case of copper(II), the species bonded at His111 were found to be the most abundant coordination isomers, while His96 was the major binding site for nickel(II). As a consequence, the addition of nickel(II) to copper(II)-prion system can significantly modify the distribution of copper(II) among the metal binding sites. Tetra- to octa-peptides have been synthesized and their complex formation was studied by the combined application of potentiometric and various spectroscopic (UV-vis, CD, NMR, EPR) techniques. The sequences of six peptides correspond to those of the specific sites of prion protein around H111 and H96 resdues: MKHM, GTHS and GTHSMKHM. These peptides were synthesized both in the N-terminally free and protected forms. The model heptapeptide AHAAAHG and octapeptide AAHAAAHG were obtained with free termini. The range of metal ions included copper(II), nickel(II) and zinc(II) ions. It was found that histidines of the hepta- and octa-peptides can simultaneously bind both copper(II) and nickel(II) ions and dinuclear mixed metal complexes can exist in slightly alkaline solution.

Keywords: prion protein, peptides, copper(II), nickel(II), zinc(II) stability constants, coordination isomers, potentiometry, UV-Vis and CD spectroscopy

Introduction

Prion diseases are among the most studied forms of neurodegenerative disorders which are caused by the abnormal conformational changes of the normal form of prion protein (PrP^{C}) to the disease-related scrapie isoform (PrP^{Sc}) [1]. The biological functions of prion proteins are not well established yet, but more and more experimental evidence support that they take part in copper(II) homeostasis. Huge number of studies have already been performed on the copper(II) binding affinity of the protein and its various peptide fragments and the most important findings were reviewed by several authors [2-5]. All studies revealed the enhanced copper(II) binding affinity of the protein and the histidyl residues were suggested as the primary metal binding sites. The native human prion protein (HuPrP) contains ten histidyl residues and six of them, four from the octarepeat domain (His61, His69, His77 and His85) and two histidines outside the octarepeat (His96 and His111) were suggested to be involved in metal binding. Our previous studies on the copper(II) complexes of various peptide fragments of prion protein revealed that all peptide can bind as much copper(II) ions as the number of histidyl residues in the peptides [6-9]. It results in the formation of polynuclear species with the multihistidine peptide fragments, while various coordination isomers of the mononuclear species can exist. The order of copper(II) binding affinity of the histidyl sites was described as: His111 > His96 > His(octarepeat). Further studies on the transition metal ion complexes revealed that prion fragments can also effectively bind nickel(II) ions [10-13]. Stability constants of nickel(II) complexes were, however, significantly smaller than those of the corresponding copper(II) species and the nickel(II) binding preference of the various histidyl sites was just the opposite: His96 > His111 >> His(octarepeat). The enhanced metal binding affinity of the histidines outside the octarepat domain is not surprising and can be easily explained by the different size of chelate rings. The imidazole-N (or N_{im}) donor atoms are the primary ligating sites in all cases forming macrochelates in slightly acidic samples. The stability of these macrochelates depends mainly on the number of

histidyl residues and not much affected by the peptide sequence. The 3N and 4N coordinated complexes are formed by increasing pH with the involvement of N_{im} and two or three deprotonated amide nitrogens in metal binding. The deprotonation of amide groups occurs towards the N-terminus for His111 and His96 residues resulting in the formation of 6-membered chelates. In the case of octarepeat, the presence of prolyl residues prevents this type of coordination and the amide deprotonation is possible only towards the C-terminus in the form of 7-membered chelates resulting in the reduced thermodynamic stability of the corresponding metal complexes. The difference in the metal binding affinity of His111 and His96 residues, however, requires further consideration. The coordination environments of both copper(II) and nickel(II) ions are the same in all cases (N_{im}, $3N_{amide}$), but the stability orders always follow the same trends: His111 > His96 for copper(II) and His96 > His111 for nickel(II). These data support that the non-coordinating side chains can also influence the metal binding affinity of peptide molecules. The specific sequences are MetLysHisMet and GlyThrHisSer for His111 and His96 residues, respectively. Now in this work we present the data of systematic studies on the binary and ternary mixed metal complexes of several native and model peptide fragments containing the above-mentioned sequences.

Results

Mixed metal copper(II)-nickel(II) and copper(II)-zinc(II) complexes of multihistidine peptide fragments of prion protein have been studied by the combined application of potentiometric, UV-Vis and CD spectroscopic measurements. Stability constants and spectral parameters of the mixed metal complexes have already been published in our previous publication [14]. The major conclusions on the distribution of metal ions among the available binding sites will be discussed in subsection 2.1. The tetra- and octa-peptides mimicking the sequences around His111 and His96 residues were newly synthesized both in N-terminally free and protected forms. The results of the studies on the metal complexes of these peptides are involved in subsection 2.2. The terminally free model peptides AHAAAHG and AAHAAAHG were also synthesized for the better understanding of the distribution of metal ions among different binding sites. The results of these measurements will be discussed in subsection 2.3.

Mixed Metal Complexes of Peptide Fragments Containing Two or Three Histidyl Residues

Copper(II)-nickel(II) and copper(II)-zinc(II) mixed metal complexes of four peptide fragments containing His85, His96 and His111 residues have been studied by potentiometric and spectroscopic techniques [14]. The ligands included

HuPrP(84-114): Ac-ProHisGlyGlyGlyTrpGlyGlnGlyGlyGlyThrHisSerGlnTrpAsnLysProSerLysProLys-ThrAsnMetLysHisMetAlaGly-NH_2,

HuPrP(91-115): Ac-GlnGlyGlyGlyThrHisSerGlnTrpAsnLysProSerLysProLysThrAsnMetLysHisMet-AlaGlyAla-NH_2

HuPrP(84-114)H85A: Ac-ProAlaGlyGlyGlyTrpGlyGlnGlyGlyGlyThrHisSerGlnTrpAsnLysProSerLys-ProLysThrAsnMetLysHisMetAlaGly-NH_2

HuPrP(84-114)H96A:Ac-ProHisGlyGlyGlyTrpGlyGlnGlyGlyGlyThrAlaSerGlnTrpAsnLysProSerLys-ProLysThrAsnMetLysHisMetAlaGly-NH_2.

Both histidyl residues of the peptides HuPrP(91-115) and HuPrP(84-114)H85A are outside the octarepeat domain and these peptides can easily form dinuclear complexes either with copper(II) or nickel(II) ions. As a consequence, mixed metal complexes are the dominating species in the systems containing both metal ions and the peptide in equimolar concentrations. The significant difference in the CD spectra of the metal complexes bonded at His96 and His111 residues made it possible to determine the ratio of coordination isomers. Fig. 1 shows the CD spectra of the copper(II)-nickel(II)-HuPrP(84-114)H85A system in comparison with the spectra of binary complexes.

It is clear from Fig.1 that the circular dichroism spectra of the $CuNiH_{-6}L$ species of the peptide HuPrP(84-114) H85A can be obtained by the simple superposition of the spectra of complexes with Cu-His111 and Ni-His96 binding modes. These observations support the existence of the same preference of coordination isomers in the mixed metal species as it was obtained for the binary systems.

The peptide HuPrP(84-114)H96A contains also two histidyl residues but one of them is inside (His85), while the other is outside (His111) the octarepeat domain. This peptide can bind two copper(II) ions but only one nickel(II) ion. In the ternary system the formation of the $CuNiH_{-6}L$ mixed metal complex was also detected with the coordination of copper(II) at His85 and nickel(II) at His111 sites. It is evident from these observations that nickel(II) cannot replace but redistribute copper(II) ions among the available metal binding sites.

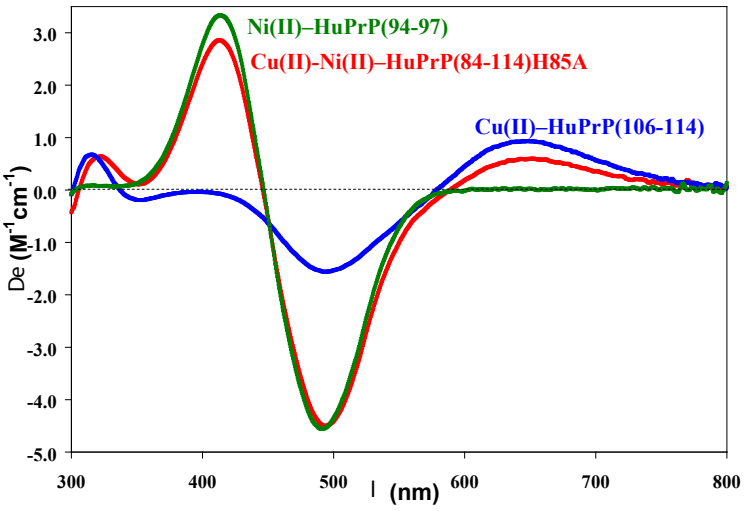

Figure 1: CD spectra of the copper(II)-nickel(II)-HuPrP(84-114)H85A = 1:1:1 system at pH 11.0 as compared to the corresponding binary copper(II) and nickel(II) species.

The results obtained for the mixed metal complexes of the peptide HuPrP(84-114) containing three histidyl residues (His85, His96 and His111) provide further support for the above-mentioned conclusions. In this case, the formation of $CuNiH_{-6}L$ and $Cu_2NiH_{-9}L$ mixed metal complexes was detected, but the species containing one copper(II) and two nickel(II) ions cannot be identified. The previous studies on the copper(II) and nickel(II) complexes of this peptide revealed that HuPrP(84-114) can bind as much as three copper(II) ions but with a preference for binding at His111 and His96 sites [8]. In the case of nickel(II) dinuclear species were obtained with exclusive binding to histidines outside the octarepeat domain. The evaluation of the CD spectra provided an unambiguous proof for the change of copper(II) coordination if one equivalent of nickel(II) ion was added to the copper(II)-HuPrP(84-114) = 2:1 system as it is shown by Fig. 2.

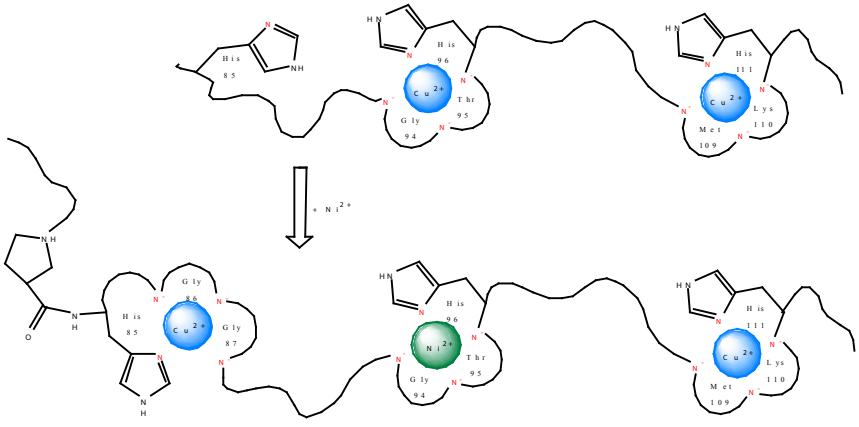

Figure 2: The major metal binding sites of copper(II) and nickel(II) ions in the binary Cu(II)-HuPrP(84-114) = 2:1 and ternary Cu(II)-Ni(II)-HuPrP(84-114) = 2:1:1 systems.

2.2. Copper(II) and Nickel(II) Complexes of Tetra- and Octa-Peptides Containing His96 and His111 Residues

The tetrapeptides MetLysHisMet-NH_2, Ac-MetLysHisMet-NH_2, GlyThrHisSer-NH_2, Ac-GlyTHrHisSer-NH_2 and the octapeptides GlyThrHisSer-MetLysHisMet-NH_2 and Ac-GlyThrHisSer-MetLysHisMet-NH_2 have been synthesized by the use of an automatic solid phase peptide synthesiser and their purity was checked by HPLC and ESI-MS measurements. Copper(II) and nickel(II) complexes of these peptides were investigated by the applications of pH-potentiometric, UV-Vis, CD and EPR spectroscopic measurements. The following conclusions were obtained:

– All peptides with free amino terminus have higher metal binding affinities than those of the corresponding

terminally protected counterparts. This observation can be easily explained by the ATCUN-motif sequence of the peptides (XX-His-X) [15].

– The stability constants of the complexes follow the trends: MetLysHisMet > GlyThrHisSer for copper(II) and the opposite trend was obtained for nickel(II).

– All octapeptides are able to bind two equivalents of copper(II) or nickel(II) ions.

– In the case of the N-terminally free octapeptide the first equivalent of metal ions always saturate the N-terminal binding sites independently on the sequence of the peptide.

– The existence of coordination isomers was identified in the case of the terminally protected octapeptide. The ratio of His111/His96 bonded isomers was around 1 and 0.1 for the copper(II) and nickel(II) complexes, respectively.

– The formation of mixed metal copper(II)-nickel(II) complexes was detected with all octapeptides. In the case of the peptides with free amino terminus the copper(II) ions were always coordinated to the amino terminus and nickel(II) occupied the internal histidyl site. For the terminally protected peptide the same preference of binding sites was observed as it was previously reported for the binary systems: His111 for copper(II) and His96 for nickel(II). This conclusion is best supported by the comparison of circular dichroism spectra of the mononuclear and dinuclear mixed metal complexes depicted in Fig. 3.

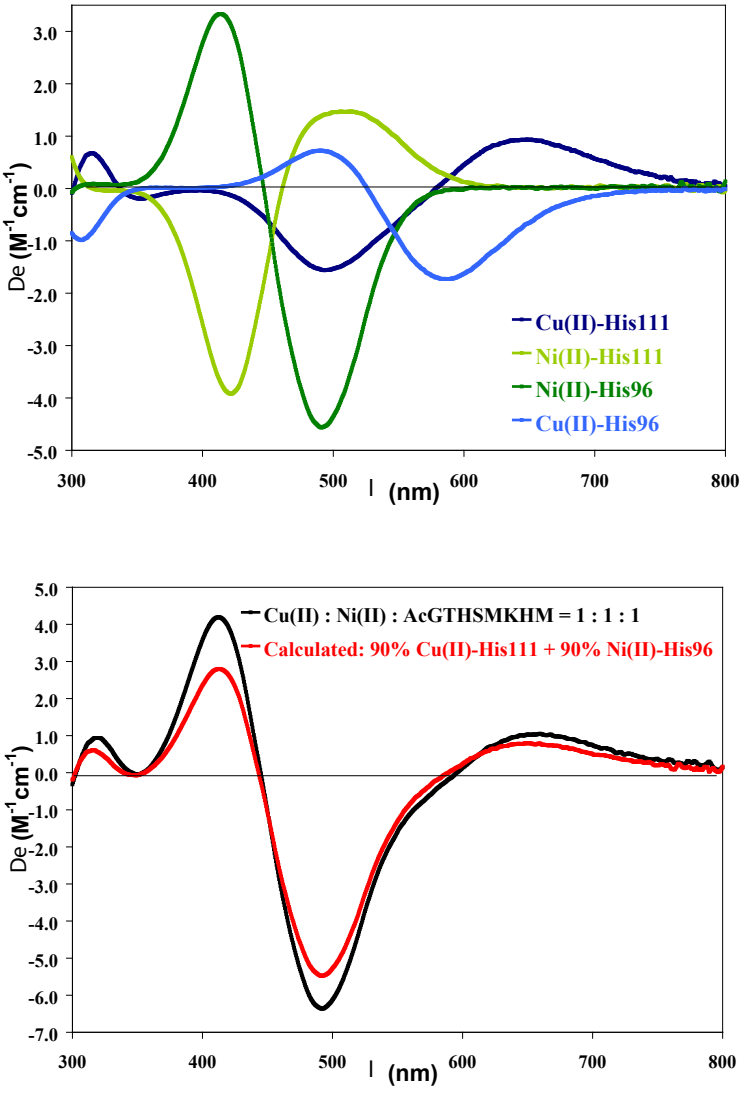

Figure 3: (a) CD Spectra of the mononuclear copper(II) and nickel(II) complexes with His96/His111 coordination sites, (b) measured and calculated CD spectra of the mixed metal complex.

2.3. Metal Complexes of the Terminally Free Hepta- and Octa-Peptides (AHAAAHG and AAHAAAHG)

The terminally free peptides AHAAAHG and AAHAAAHG have been synthesized to compare the copper(II) nickel(II) and zinc(II) binding affinities of these molecules. The histidyl residues close to the C-termini are in the same environments in both ligands and their coordination chemistry should be similar to those of prion peptide fragments. However, there can be a significant difference in the coordination behaviour of the N-termini of the peptides: the tridentate (NH_2,N^-,N_{im}) and tetradentate (NH_2,N^-,N^-,N_{im}) are expected for the hepta- and octa-peptides, respectively. The results of combined potentiometric and spectroscopic measurements provided sufficient proofs for these expectations. The major conclusions are as follows:

– The octapeptide (AAHAAAHG) can effectively bind two equivalents of both copper(II) and nickel(II) ions but its zinc(II) binding affinity is relatively small. The amino terminus is the primary metal binding site with all metal ions. In the mixed metal copper(II)-nickel(II) system copper(II) saturates the amino terminus and nickel(II) occupies the internal histidyl site.

– The most important findings for the heptapeptide (AHAAAHG) is linked to its zinc(II) binding ability via the involvement of deprotonated amide nitrogens in zinc(II) coordination. The mononuclear complexes have an outstanding thermodynamic stability with all metal ions but dinuclear species are also formed with copper(II) and nickel(II). The enhanced stability of the mononuclear complexes was explained by the (NH_2,N^-,N_{im},N_{im}) coordination mode including fused, (5,6)-membered chelates and a macrohelate as it is shown by Fig. 4.

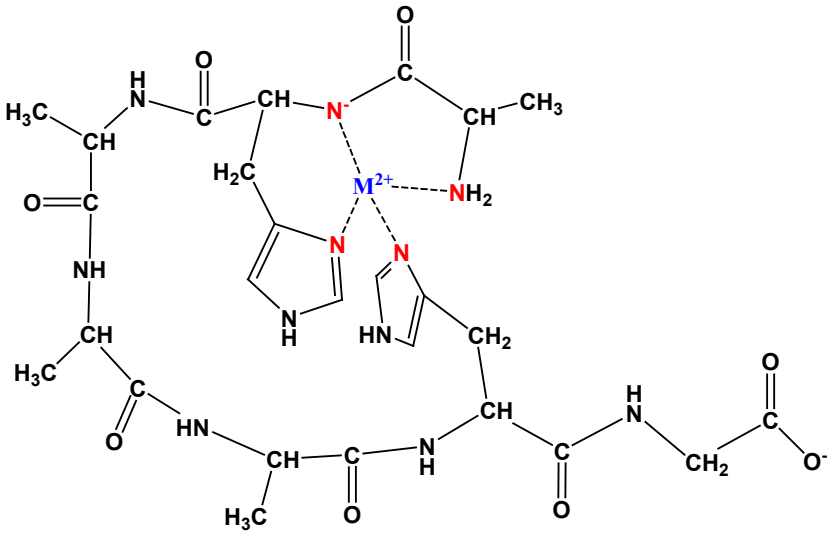

Figure 4: Binding mode of the major species formed with the N-terminally free heptapeptide AHAAAHG (M = copper(II), nickel(II) or zinc(II)).

References

1. Prusiner, S.B. (1991). Science 252, 1515-1522.
2. Millhauser, G.L. (2004). Acc.Chem. Res., 37, 79-85.
3. Brown, D.R., Kozlowski, H. (2004). Dalton Trans., 1907-1917.
4. Kozlowski, H., Janicka-Klos, A., Stanczak, P., Valensin, D., Valensin, G., Kulon , K. (2008) Coor. Chem. Rev., 252, 1069-1078.
5. Arena, G., La Mendola, D., Pappalardo, G., Sóvágó I., Rizzarelli, E., (2012). Coord. Chem. Rev., 256, 2202-2218.
6. Di Natale, G., Grasso, G., Impellizzeri, G., La Mendola D., Micera, G., Mihala, N., Nagy, Z., Ősz, K., Pappalardo, G., Rigó, E., Rizzarelli, E., Sóvágó I. (2005), Inorg. Chem., 44, 7214-7225.
7. Jószai, V., Nagy, Z., Ősz, K., Sanna D., Di Natale, G., La Mendola, D., Pappalardo, G., Rizzarelli E., Sóvágó I. (2006), J. Inorg. Biochem., 100, 1399-1409.
8. Ősz, K., Nagy Z., Pappalardo, G., Di Natale G., Sanna, D., Micera, G., Rizzarelli E. Sóvágó I. (2007), Chem-Eur J., 13, 7129-7143.
9. Di Natale, G., Ősz, K., Nagy, Z., Sanna, D., Micera, G., Pappalardo, G., Sóvágó I., Rizzarelli, E. (2009), Inorg. Chem., 48, 4239-4250.
10. Jones, C.E., Klewpatinond, M., Abdelraheim, S.R.,Brown, D.R., Viles, J.H. (2005), J. Mol. Biol., 346, 1393-1407.

11. Klewpatinond, M., Viles, J.H. (2007), FEBS Letters, 581, 1430-1434.
12. Valensin, D., Gajda K., Gralka, E., Valensin, g., Kamysz, W., Kozlowski, H. (2010), J. Inorg. Biochem., 104, 71-78.
13. Turi, I., Kállay, C., Szikszai, D., Pappalardo, G., Di Natale G., De Bona, P., Rizzarelli, E, Sóvágó I. (2010), J. Inorg. Biochem., 104, 885-891.
14. Jószai V., Turi I., Kállay C., Pappalardo, G., Di Natale G. Rizzarelli, E., Sóvágó I. (2012), J. Inorg. Biochem., 112, 17-24.
15. Sóvágó, I., Kállay, C., Várnagy, K. (2012), 256, 2225-2233.

State of art in chelating agents for the clinical treatment of metal poisoning

Crisponi G.[a*], Nurchi V.M.[a], Lachowicz J.I.[a], Crespo-Alonso M.[a], Toso L.[a], Zoroddu M.A.[b], Peana M.[b]

[a] *University of Cagliari, Department of Chemical and Geological Sciences, Cittadella Universitaria, I-09042 Monserrato (ITALY)*
[b] *University of Sassari, Department of Chemistry and Pharmacy, Via Vienna 2, I-07100 Sassari (ITALY)*
crisponi@unica.it, nurchi@unica.it, jojelcz@gmail.com, m.crespo@unica.it l.toso@unica.it, zoroddu@uniss.it

Abstract

Metal chelators have been largely used since the fifties of last century in the therapy of acute and chronic metal intoxication. In recent years their use has been extended to the treatment of social relevant diseases as cancer, diabetes, and neurodegeneration. This increase of new indications for chelating agents contrasts with the inadequacy of number and kind of existing drugs: the availability of a variety of chelators for a given toxic metal ion gives to the clinicians the possibility of properly modulating the therapy according to the problems of the patient as well as to the severity of intoxication. Till nowadays the considerable effort of the scientific community has in some instance given limited and poor results. This failure can be ascribed to difficulties inherent to the biological, chemical and clinical restraints, and above all to two main causes: the low incidence of some kind of intoxications prevents expensive researches by pharma-industries, and the scarce interaction between chemical and biomedical researchers leads to a wasting of efforts and resources. The present trend of sharing different expertises will lead to achieve the target of ameliorating the pertinent treatment for any metal intoxication.

Keywords: Chelation therapy, Ligands, Metal complexes, Toxic metals, Heavy metals, Speciation

Introduction

Metal ions enter in everyday life: metal compounds are used in medicine, in food chain, in water purification, in cosmetics, in painting, as wood preservatives, and in a many other applications. For this reason the exposure to metal ions is ever increasing, and so their toxic effects to humans. The poisoning action, originated by accidental, occupational/environmental and iatrogenic causes, represents one of the most crucial health and social problems worldwide [1-11]. One of the principal ways to counteract metal toxicity consists in the treatment with metal chelators that transform the toxic metal ion in less dangerous species easily excretable species. The research on this topic is totally insufficient for the limited investments of pharma-industries, due to their poor profitability. Huge investments by health organizations of advanced countries are mandatory for the development of common research project based on different expertises.

Metal ion toxicity

Metal toxicity can be classified in three different groups, according to their sources:

- Acute ingestion of toxic metal ions, accidental, as frequently happens to children, or caused by a voluntary homicidal or suicidal attempt.
- Chronic intoxication, depending on environmental, occupational or iatrogenic causes.
- Metal overload due to genetic diseases.

This first classification is essential in establishing the treatments, spanning from an immediate, short limited in time, massive dose of chelators, to a lifelong treatment for genetic diseases.

Chelation therapy

Aims of chelation therapy are the removal of toxic metal from organism, or the attenuation of its toxicity by transforming it in a less toxic compound or by dislocating it from the site in which the toxic action is exerted. The requisites of a chelating agent, better and better defined in the years, require different considerations on:

- Toxicity of the chelator and of the formed complexes;
- Stability of the complexes in competition with of endogenous ligands;
- Kinetic and mechanism of exchange with endogenous ligands;
- Selectivity toward the target metal ion;
- Metabolism of the chelating agents into the body;
- Absorption and bioavailability;
- Excretion of the formed complexes.

It has to be remembered that complex formation some time presents unwanted effects, as an increase of intestinal absorption when the complex is formed in the gut, or dislocation of complexed metal to more dangerous sites: e.g. transit through the BBB.

Complex stability

The basic requisite for a chelating agent is the stability of its complex, in order that they are completely formed at expenses of endogenous ligand molecules. The stability and the selectivity requisite mainly depend on the hard/soft character both of coordinating groups and metal ions [12-13]. A hard/soft classification of toxic metal ions, and of principal coordinating groups is synthetically presented in Table 1.

Table 1. Hard, intermediate and soft character of metal ions, and of coordinating groups.

Metal		
Hard	**Intermediate**	**Soft**
Li^+,Na^+,K^+,Be^{2+}, Mg^{2+},Ca^{2+},Sr^{2+}, Mn^{2+},Al^{3+},Ga^{3+}, Cr^{3+},Fe^{3+},Sn^{4+}, $(CH_3)_2Sn^{2+}$, UO_2^{2+},VO^{2+}	Fe^{2+},Co^{2+},Ni^{2+}, Cu^{2+},Zn^{2+},Pb^{2+}, Sn^{2+},Sb^{3+},Bi^{3+}	Cu^+,Ag^+,Au^+, Hg^+,Pd^{2+},Cd^{2+}, Pt^{2+},Hg^{2+}, CH_3Hg^+,Pt^{4+}
Coordinating group		
Hard	**Intermediate**	**Soft**
H_2O,OH^-,F^-, $RCOO^-$,Cl^-,RO^-,NH_3, RNH_2	$C_6H_5NH_2$	R_2S, RSH, RS^-

Chelators are classified as bidentate, tridentate and so on according to the number of binding groups on the molecule able to bind at the same time the target metal ion. The denticity of the ligand determines the number and the stoichiometry of formed complexes. As a general rule exadentate chelators, forming only one kind of complex, are generally preferred. Ligands with lower denticity form multiple complexes with speciation pattern depending both on total ligand concentration and on metal/ligand ratio. These lower stoichiometry complexes are sometimes dangerous, since the incomplete coordination does not prevent deleterious reactions, as radical formation through Fenton reaction. The formation stability constant of a complex $M_pL_qH_r$ is related to its formation equilibrium, $pM + qL + rH = M_pL_qH_r$, starting from the completely deprotonated ligand. In reality, when the complex formation is considered *in vivo*, the reacting molecules are the forms of ligand prevailing at pH 7.4 according to its speciation pattern, determined by the protonation constants. Complex formation is therefore a competition between proton and metal ion for the same basic sites on the ligand. For all these reasons (different stoichiometries, proton competition, ..) the comparison of the effectiveness by which different chelating agents bind a metal cannot be made on the basis of the stability constants alone. A recent review by Bazzicalupi et al. [14] thoroughly examines all the comparison methods proposed in literature. We will use here the quantity pM (defined as $-\log[M_f]$ at $[M_T]= 1x10^{-6}$ M and $[L_T] = 1x10^{-5}$ M at pH 7.4, where $[M_f]$ is the concentration of free metal ion and $[M_T]$ and $[L_T]$ are the total concen-

trations of metal and ligand respectively). Structure and denticity of the ligand determine the pre-organization of the complex and the degree of favourable entropic contribution due to the chelate effect [15]. Numerous empirical relationships between a variety of properties of ligands and metals and the stability constants have been proposed, which can be of great utility in the design of the proper chelating agents [15].

Kinetic factors

The behaviour of a chelator depends, besides the thermodynamics of complex formation, on kinetic factors, connected to degradation of the chelating agent, complex formation between the chelator and the free metal ion in the plasma, and exchange reaction between the metal bound to endogenous molecules and the chelating agent. The kinetic of the exchange reaction between the metal ion bound to endogenous molecules and the chelator depends on a variety of factors, among which the structure and the denticity of the chelator. The formation of complexes between the free metal ion in plasma and the ligand is more a theoretic than a real situation, since the circulating toxic metal ion in plasma is mainly bound to endogenous molecules, ranging from macromolecules as transferrin and albumin to low molecular weight ligands as citrate. The general kinetic characteristics of the toxic metal ions determine the kinetic behavior, so slow reactions can be expected for aluminium, chromium and palladium. Sometimes the chelator, because of its solubility and lipophilic properties that prevent cell entrance, acts only on the circulating (not necessarily free) toxic metal ion. Once chelated and excreted the circulating amount, a slow equilibrium will be reconstituted between the intracellular-bound and circulating toxic metal ion, so that the kinetic of this equilibrium will decide the periodicity of chelation treatment.

Metabolism of the chelating agents

Many chelating agents are metabolized in the body to species that loose the chelating properties of the parent molecule. The metabolic reactions can be very different, from the glucuronidation of hydroxypyrydinones, to the acetylation of Trien, or the formation of –S-S- bonds between BAL and SH-containing endogenous molecules. The correct choice of drug administration becomes of vital importance when this kind of metabolic transformation is rapid, as for example the subcutaneous infusion of desferal.

Absorption and bioavailability of the chelating agents

As far as the chemical requisites regarding the absorption and the bioavailability are concerned, Hider pointed out that three key parameters regulate diffusion through biological membranes: molecular size, lipophilicity and net charge [16]. Specifically the cut off molecular weight for drugs to be absorbed in the human intestine is approximately 500 g/mol. Lipophilicity is generally estimated by the water–octanol partition coefficient (*P*). These general properties have been used by Lipinski et al. [17], adopting a four parameter analysis, to predict membrane permeability. Their guidelines state that a poor absorption is likely when:

- molecular weight > 500 g/mol;
- log P>5;
- more than 10 hydrogen bond donors are present in the molecule (expressed as a sum of OH and NH groups);
- more than 10 hydrogen bond acceptors are present in the molecule (expressed as a sum of O and N atoms).

These parameters are also valid for the absorption of the chelating agent into cells, and hold for formed metal complex excretion. In this last situation the formation of a neutral complex is of paramount importance.

Chelating agents

The chelating agents in use for the treatment of metal poisoning belong to few chemical categories:

i) poliaminocarboxylic acids,
ii) ligands characterized by coordinating mercapto groups,
iii) ligands with oxygen coordinating groups, and
iv) dithiocarbamates.

A collection of the most representative chelators is presented in Fig. 1.

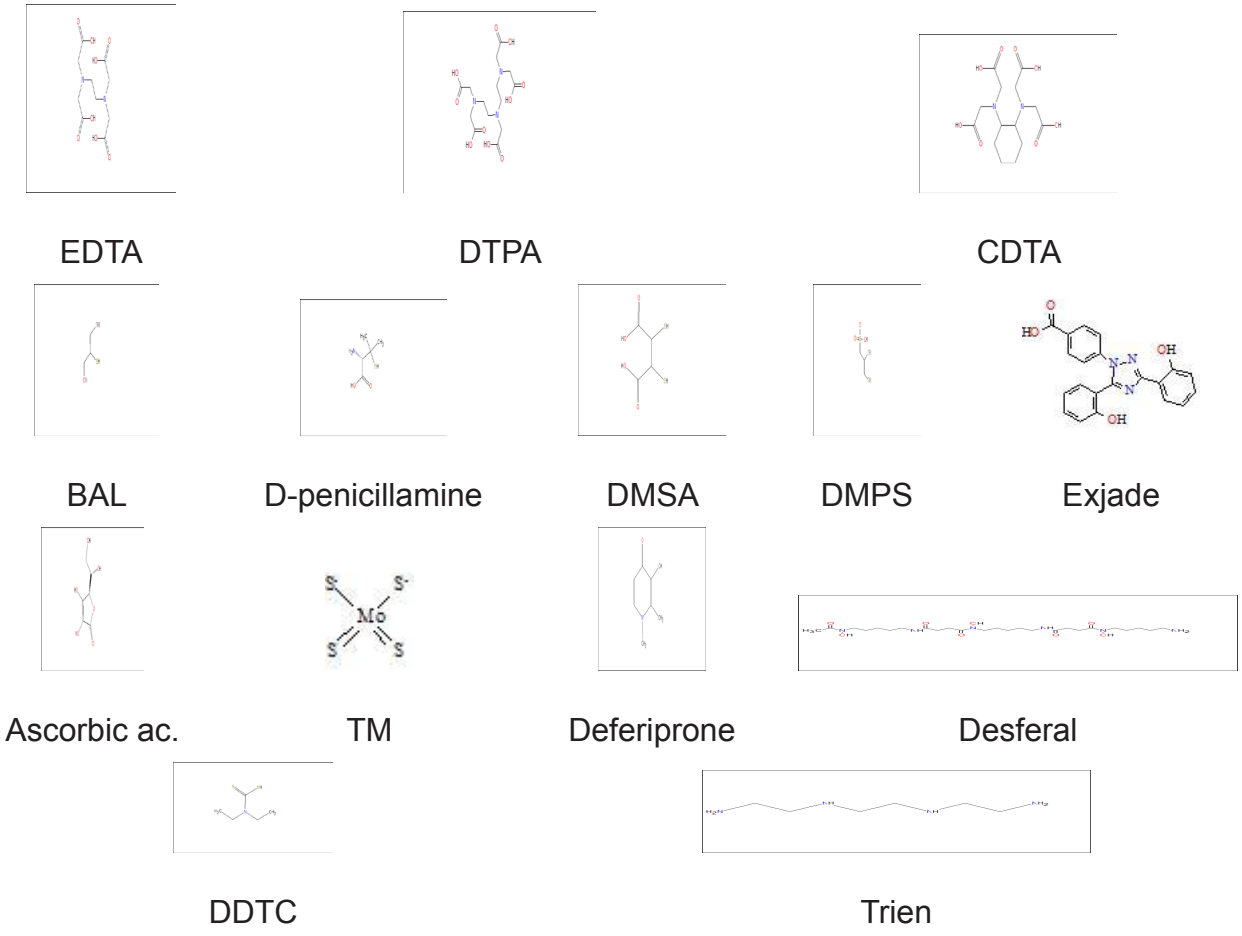

Fig. 1. Representative ligands for toxic metal ions in clinical use for chelation therapy.

The chelating agents in clinical use for each of the most common toxic metal ions are listed in Table 2. For the chelators in use the corresponding pM value is reported, or a symbol is used whenever literature does not present any equilibrium study for it. The stability and the protonation constants used in the pM calculations were obtained from the IUPAC Stability Constant Database [18] that reports all literature data up to 2006. Table 2 gives evidence that more than one half of chelators is used on the basis of biomedical studies (animal or human), while the thermodynamic characterization of the metal-ligand interaction is lacking.

Conclusion

A different scientific approach for new chelators at the drug discovery phase can be proposed: an increasing attention should be given, at earlier discovery stages, to the chemistry-based knowledge of the compounds. Firstly the compounds are designed and in silico screened for the druggability and pharmacokinetic issues. Afterwards, the selected compounds are prepared and then subjected to initial screening involving chemical and toxicological tests to confirm the suitability for further chemistry studies, before embarking on expensive biological screening. These must involve estimations of lipophilicity, water solubility and chelator affinity for the targeted metal ions at physiological pH. The thermodynamic and kinetic parameters, governing metal-chelator interactions, are essential in establishing the level of efficacy and safety of the drug.

	trien	DDTC	exjade	desferal	deferiprone	ascorbic acid	tetrathio molybdate	DMPS	DMSA esters	DMSA	D-penicil.	BAL	CDTA	DTPA	EDTA
Al			□	19.3	16.4										
As											□	□			
Be								□		□					
Bi								□		28.1		□			
Cd		□							□	□				15.8	14.7
Co										□				16.1	14.7
Cu	19.6						[2*]				[2*]				
Fe			23.5	26.6	19.4										
Hg								38.3		□	35.3	40.3			
HgR^+								16.6			15.6				
Mn													14.3	11.1	10.7
Ni		7.9													
Pb		□								11.5	10.0	□			16.2
Pt										7.2					
Sb								□		□		□			
Sn										□		6			
VO^{2+}				□		6		□		□	8.5	□			16.9

Table 2. For each metal ion the chelating agents in use are indicated with the numerical value of pMe whenever reported in literature, or with the symbol [2] when no constants were found.

References

1. Crisponi, G., Nurchi V.M., Crespo-Alonso, M., Toso L. (2012) Chelating agents for metal intoxication. Current Medicinal Chemistry 19, pp. 2794-2815
2. Andersen, O. (1999) Principles and recent developments in chelation treatment of metal intoxication. Chemical Reviews 99, pp. 2683-2710.
3. Blanusa, M., Varnai, V.M.; Piasek, M.; Kostial, K. (2005) Chelators as antidotes of metal toxicity: Therapeutic and experimental aspects. Current Medicinal Chemistry 12, pp. 2771-2794.
4. Baran, E.J. (2010) Chelation therapies: a chemical and biochemical perspective. Current Medicinal Chemistry 17, pp. 3658-3672.
5. Sinicropi, M.S., Amantea, D., Caruso, A., Saturnino, C. (2010) Chemical and biological properties of toxic metals and use of chelating agents for the pharmacological treatment of metal poisoning. Archives of Toxicology 84, pp. 501-520.
6. Crisponi, G.; Remelli, M. (2008) Iron chelating agents for the treatment of iron overload. Coordination Chemistry Reviews 252, pp. 1225–1240.
7. Liu, Z.D., Hider, R.C. (2002) Design of iron chelators with therapeutic application. Coordination Chemistry Reviews 232, pp. 151-171.
8. Crisponi, G., Nurchi, V.M., Fanni, D., Gerosa, C., Nemolato, S., Faa, G. (2010) Copper-related diseases: from chemistry to molecular pathology. Coordination Chemistry Reviews 254, pp. 876-889.
9. Crisponi, G., Nurchi, V.M., Bertolasi, V., Remelli, M., Faa, G. (2012) Chelating agents for human diseases related to aluminium overload. Coordination Chemistry Reviews 256, pp. 89-104.
10. Santos, M.A. (2002) Hydroxypyridinone complexes with aluminium. In vitro/vivo studies and perspectives. Coordination Chemistry Reviews 228, pp. 187-203.
11. Berthon, G. (2002) Aluminium speciation in relation to aluminium bio-availability, metabolism and toxicity. Coordination Chemistry Reviews 228, pp. 319-341.
12. Pearson, R.G. (2005) Chemical hardness and density functional theory. Journal of Chemical Sciences 117, pp. 369-377.
13. Pearson, R.G. (1963) Hard and Soft Acids and Bases. Journal American Chemical Society 85(22), pp. 3533-3539.
14. Bazzicalupi, C., Bianchi, A., Giorgi, C., Clares, M.P., García-Espana, E. (2012) Addressing selectivity criteria in binding equilibria. Coordination Chemistry Reviews 256, pp. 13-27.
15. Hancock, R.D., Martell, A.E. (1989) Ligand design for the selective complexation of metal ions in aqueous solution. Chemical Reviews 89, pp. 1875-1914.
16. Hider, R.C., Liu, Z.D. (2003) Emerging understanding of the advantage of small molecules such as hydroxypyridinones in the treatment of iron overload. Current Medicinal Chemistry 10, pp. 1051-1064.
17. Lipinski, C.A., Lombardo, F., Dominy, B.W., Feeney, P.J. (1997) Experimental and computational approaches to estimate solubility and permeability in drug discovery and development settings. Advanced Drug Delivery Reviews 23, pp. 3-25
18. Pettit L.D., Powell, K.J. (2006) The IUPAC Stability Constants Database, Academic Software and IUPAC, Otley, U.K.

Stereospecific interligand interactions affecting base-specific and high-order structure-specific metal bonding to nucleic acid constituents and polynucleotides

Aoki K.

Toyohashi University of Technology, Department of Environmental and Life Sciences, Toyohashi 441-8580 (Japan)
aoki003@edu.imc.tut.ac.jp

Abstract

We have demonstrated the importance of stereospecific interligand interactions as a factor that could affect base- and site-specific metal bonding to nucleic acid constituents, based on X-ray studies of the rationally designed metal complexes that could specifically recognize adenine or guanine bases among the five common bases. High-order structure-specific metal bonding to polynucleotides is also briefly discussed in terms of stereospecific interligand interactions.

Keywords: Base-specific metal bonding, crystal structures, high-order structure-specific metal bonding, interligand interactions, nucleic acid constituents, polynucleotides.

Introduction

Metal ion interactions with nucleic acids and their constituents have received much attention since the mid-1960s because of the involvement of metal ions and their biological significance in nucleic acid processes, resulting in a large body of data involving thermodynamic and kinetic properties, metal binding sites and modes, and structures formed [1-6], but there has been a continued demand for the elucidation of factors that govern the metal binding sites on nucleobases, in order to fully document structural principles with which we can predict the sites on nucleobases to which metal ions bind. Marzilli and Kistenmacher demonstrated, as early as 1977, that stereospecific interligand interactions involving hydrogen bonding, electrostatic repulsion, and steric constraints could work as such a factor [7]. According to this concept, we have attempted to make the rationale design of metal complexes that could specifically recognize the individual of five common bases (adenine, guanine, cytosine, thymine, or uracil). It has now been well documented that the metal ion binds to nucleobases preferably through the ring nitrogens, N7 and N1 for adenine, N7 for guanine, and N3 for cytosine, and occasionally through the exocyclic substituents, O6 of guanine, O2 of cytosine, and O2 and O4 for thymine or uracil, under physiological conditions. Our concrete strategy for the design of metal complexes that could perform the base-specific metal bonding is the followings: when the metal centre is highly crowded, interligand steric constraints could occur and thus we can expect that (i) when the ligands (other than the nucleobase) possess the functional groups that could work as H-bonding acceptor only, the metal ion could bind adenine-specifically to N7 with the formation of an intramolecular interligand H-bond with the N6 amino substituent of adenine but neither to N7 of guanine due to interligand electrostatic repulsion with the O6 keto substituent nor to N3 of cytosine due to interligand electrostatic repulsion with the O2 keto substituent, and (ii) when the ligands possess the functional groups that could work as H-bonding donor only, the metal ion could bind guanine-specifically to N7 with the formation of an intramolecular interligand H-bond with the O6 substituent of guanine but neither to N7 of adenine due to interligand steric constraints with the N6 substituent nor to N3 of cytosine due to interligand steric constraints with the N4 substituent.

We present here two adenine-specific and two guanine-specific metal bonding systems. We have not succeeded in designing cytosine-specific or thymine (or uracil)-specific metal bonding systems but we mention here on factors

that could affect metal binding sites and modes for cytosine. An additional discussion in terms of interligand interactions is maid on high-order structure-specific metal bonding to polynucleotides.

Base- and Site-Specific Metal Bonding to Nucleic Acid Constituents

2.1 Adenine-specific metal bonding

2.1.1 $[Rh_2(OAc)_4]$ complex system [8.9]

Treatment of $[Rh_2(OAc)_4]$ with adenine, 9-methyladenine, adenosine, 9-ethylguanine, guanosine, inosine, cytosine, uracil, or thymine in methanolic aqueous solution at room temperature, where the AcO^- ligand functions as H-bonding receptor only, gave *specifically* and *quantitatively* pink complexes of adenine or its derivatives (= L), $[Rh_2(OAc)_4(L)]$ but no compound for others. In addition, a competitive reaction between $[Rh_2(OAc)_4]$ and four nucleobases (9-methyladenine, 9-ethylguanine, 1-methylcytosine, and uracil) immediately and *quantitatively* gave pinc precipitates of a single product formed with 9-methyladenine. On the other hand, treatment of $[Rh_2(HNOCCF_3)_4]$ with these nucleobases or nucleosides (= L), where the CF_3CONH^- ligand acts as both H-bonding donor and acceptor, gave *non-specifically* pink or red complexes of adenine derivatives $[Rh_2(HNOCCF_3)_4(L)]$, $[Rh_2(HNOCCF_3)_4(L)_2]$ for guanine derivatives including inosine, and $[Rh_2(HNOCCF_3)_4(L)]$ for cytosine or $[Rh_2(HNOCCF_3)_4(L)_2]$ for 1-methylcytosine but no compound for uracil. Crystal structures of all of these complexes were determined by X-ray diffraction, except for $[Rh_2(OAc \text{ or } HNOCCF_3)_4(L)]$ complexes of adenine derivatives, which were unsuitable for X-ray analysis because of their poor-crystallinity most probably due to the formation of the polymeric structure with the adenine-bridge through axial metal–N7 and –N1 bondings. In consistent with this speculation, when N6-methyl-adenosine (= L) was reacted with $[Rh_2(HNOCCF_3)_4]$, a complex $[Rh_2(HNOCCF_3)_4(L)_2]$ (**1**) was obtained and successfully characterized by X-ray analysis [10]: the complex forms a discrete structure with two nucleoside molecules coordinating to both the axial-positions of the $[Rh_2(HNOCCF_3)_4]$ nucleus each through N7 with the formation of intramolecular interligand N6(adenine)–H···O(amidato) hydrogen bonds, as shown in Figure 1. The methyl group attached to the N6 substituent prevents the Rh bonding to N1 because steric clashes might occur with acetamidato ligands when the metal ion binds to N1, providing a good example showing that interligand interactions (steric constraints in this case) affect the metal binding site.

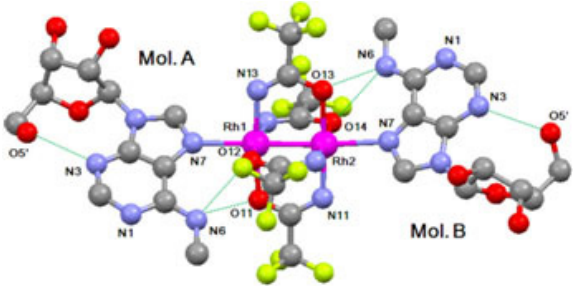

Figure 1. Crystal structure of $[Rh_2(HNOCCF_3)_4(N6\text{-methyladenosine})_2]$ (**1**) [10]. Broken lines denote hydrogen bonds.

The crystal structure of $[Rh_2(HNOCCF_3)_4(guanosine)_2]$ (**2**) [9] is shown in Figure 2, where the dirhodium core is occupied at either axial-side by two guanine moieties each through N7 with the formation of intramolecular interligand N(amidato)–H···O6(guanine) hydrogen bonds.

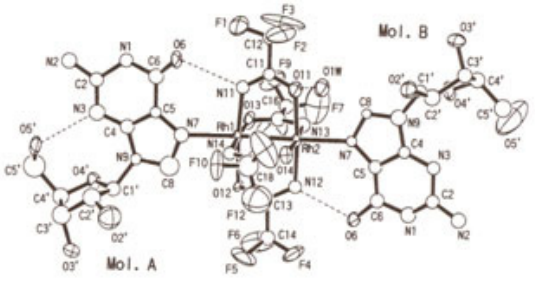

Figure 2. Crystal structure of $[Rh_2(HNOCCF_3)_4(guanosine)_2]$ (**2**) [9].Broken lines denote H-bonds.

Figure 3 shows the crystal structure of $[Rh_2(HNOCCF_3)_4(1\text{-methylcytosine})_2]$ (**3**) [8], where the dirhodium core is occupied at either axial-side by two 1-methylcytosine moieties each through N3 with the formation of two intramolecular interligand hydrogen bonds, one N4(cytosine)–H···O(amidato) and the other N(amidato)–H···O2(cytosine) hydrogen bonds.

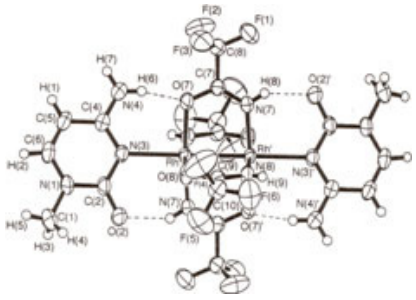

Figure 3. Crystal structure of $[Rh_2(HNOCCF_3)_4(1\text{-methylcytosine})_2]$ (**3**) [8]. Broken lines denote H-bonds.

These X-ray results show that for adenine, the axial-bonding of the adenine moiety to the $[Rh_2(L)_4]$ core through N7 and/or N1 is possible when the ligand L possesses the functional group that could act as H-bonding acceptor to form a H-bond with the N6 amino group of adenine; for guanine, the axial-bonding to $[Rh_2(L)_4]$ through N7 is possible when the ligand (L) involves the functional group that could act as H-bonding donor to form a H-bond with the O6 keto group of guanine but it is impossible when the ligand functions as H-bonding acceptor only (in this case, L = AcO^-), since electrostatic O(acetato)···O6(guanine) repulsion may occur when the metal ion binds to N7; for cytosine, the axial-bonding to $[Rh_2(L)_4]$ through N3 is possible when the ligand involves two functional groups that could act as both H-bonding acceptor and donor (in this case, L = CF_3CONH^-) to form an N4(cytosine)–H···O(amidato) and an N(amidato)–H···O2(cytosine) H-bonds, while no complex formation of $[Rh_2(OAc)_4]$ with cytosine may be due to O(acetato)···O2(cytosine) electrostatic repulsion when the metal ion binds to N3; for thymine or uracil, no complex formation with $[Rh_2(OAc)_4]$ or $[Rh_2(HNOCCF_3)_4]$ might be due to the attachment of a proton at N3 under neutral conditions.

In summary, $[Rh_2(OOCR)_4]$ could act as adenine-specific reagents while $[Rh_2(HNOCR)_4]$ could exhibit no base-specificity in their reactions with nucleobases. We can predict that $[Rh_2(HNHNCR)_4]$, where the amidinato ligand functions as H-bonding donor only, could act as guanine-specific reagents.

2.1.2 Tripodal nitrilotriacetato (nta) ligand-system [11]

Treatment of $Ni(OAc)_2$ and *nta* with adenine, 9-ethylguanine, cytosine, or uracil, where *nta* functions as H-bonding receptor only, gave an adenine complex $[Ni(nta)(adeninium)(H_2O)]_2$ (**4**) and two cytosine salts of $[Ni(nta)(H_2O)_2]^-$ anion but no compound for 9-ethlguanine and uracil. Figure 4 shows the crystal structure of **4**, where the *nta*-capped octahedral Ni^{2+} ion binds to the adeninium ligand through N7 with the formation of interligand N(adenine)–H···O(*nta*) H-bonds. Results could be rationalized in terms of interligand interactions discussed above in *2.1.1*.

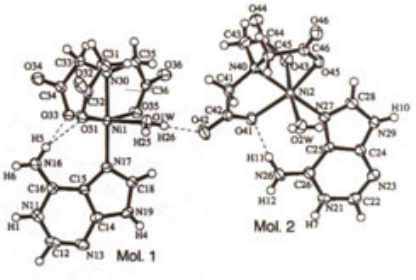

Figure 4. Crystal structure of $[Ni(\mathbf{nta})(adeninium)(H_2O)]_2$ (**4**) [11].
There exist two crystallographically independent but chemically equivalent molecules (Mol. 1 and Mol. 2). Broken lines denote H-bonds.

2.2 Guanine-specific metal bonding

2.2.1 Tripodal tris(2-aminoethyl)amine (tren) ligand-system [12,13]

Treatment of $Cu(ClO_4)_2$ or $Ni(ClO_4)_2$ and *tren* with 9-methyladenine, 9-ethylguanine, cytosine, or uracil, where t*ren* acts as H-bonding donor only, gave 9-ethylguanine complexes $[Ni(tren)(9\text{-ethylguanine–}0.5H)(H_2O)]_2\cdot(ClO_4)_{2.5}\cdot(ClO_3)_{0.5}$

(**5**) under pH 6–7 [12] or [Cu(*tren*)(9-ethylguanine)]·$(ClO_4)_2$ (**6**) under pH 8–9 [13] and a cytosine complex [{Cu(*tren*)}$_2$(cytosinato)]·$(ClO_4)_3$·0.5(H_2O) (**7**) under pH 8–9 [14] but no compound for 9-methyladenine and uracil [12]. Figure 5 shows the crystal structure of **6**, where the *tren*-capped Cu^{2+} ion binds the guanine base through N7 with the formation of an interligand N(*tren*)–H···O6(guanine) H-bond.

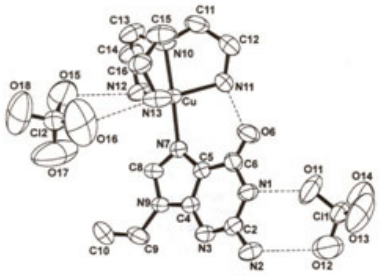

Figure 5. Crystal structure of [Cu(**tren**)(9-ethylguanine)]·$(ClO_4)_2$ (**6**) [13]. Broken lines denote H-bonds.

2.2.2 *Tetradentate 1,4,7,10-tetraazacyclodecane (cyclen) ligand-system [15]*

Treatment of $Cu(ClO_4)_2$ and *cyclen* with adenine, xanthine (as a guanine derivative), cytosine, or uracil under pH 8–9, where *cyclen* acts as H-bonding donor only, gave an adenine complex [Cu(*cyclen*)(adeninato)]·$(ClO_4)_4$·$2H_2O$ (**8**) and a xanthine complex [Cu(*cyclen*)(xanthinato)]·ClO_4·-4.5H_2O (**9**) but no compound for cytosine and uracil. In the adenine complex **8**, the *cyclen*-capped square-pyramidal Cu^{2+} ion binds to the adenine base through the deprotonated N9 site but not through N7 most possibly due to N(*cyclen*)–H···H–N6(adenine) steric constraints when the metal ion binds to N7. In the crystal structure of **9**, the *cyclen*-capped Cu^{2+} ion binds to the xanthine base through N7 with the formation of an interligand N(*cyclen*)–H···O6(xanthine) H-bond.

In summary, *tren*- or *cyclen*-capped metal ions, where *tren* and *cyclen* ligands function as H-bonding donor only, could act as guanine-specific reagents. This could be rationalized in terms of intramolecular interligand interactions discussed in *2.1.1*.

2.3 *Factors affecting metal binding sites and modes for cytosine*

Cytosine is a good target for evaluating interligand steric effects, since N3 of cytosine, the most preferable metal binding site, is sterically hindered by the two flanking amino and keto substituents. As early as 1979, Gellert and Bau pointed out a correlation between the coordination number and the metal binding site on nucleobases [16]: for cytosine, the metal bonding to N3 might prefer a lower four- or five-fold coordination number and thus, it was suggested that an octahedral Mn^{2+} ion binds to cytosine through the exocyclic O2 but not N3 in the crystal structure of $[Mn(5'\text{-CMP})(H_2O)]_n$ [17]. We present here two ways in which the metal ion with the more than six-fold coordination number binds to N3. One way is, as noted in *2.1.1*, through the formation of two simultaneous interligand H-bonds involving the O2 and N4 substituents, where the ligands other than the cytosine ligand have to have two functional groups that act as both H-bonding donor and acceptor (see Figure 3). The other way is through the four-membered N3,O2- or N3,N4(deprotonated)-chelation, as observed, for example, in the crystal structure of [{Cu(*tren*)}$_2$(cytosinato)]·$(ClO_4)_3$·0.5(H_2O) (**7**) [14] (Figure 6) for the former chelation or in [$(Cp)_2$Mo(1-methylcytosinato)]·PF_6 [18] for the latter.

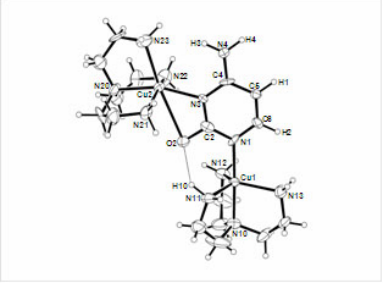

Figure 6. Crystal structure of [{Cu(**tren**)}$_2$(cytosinato)]$^{3+}$ (**7**) [14]. A broken line denotes a H-bond.

High-Order Structure-Specific Metal Bonding to Polynucleotides

A relatively large number of X-ray data on metal interactions with oligonucleotide duplexes (fragments of A-RNA and A/B/Z-DNA) have been accumlated [1,19] and now certain general observations emerge: (i) Metal cations, usually hydrated, preferentially bind to phosphate groups, either directly or mediated by water ligands by forming H-bonds, and serve to partially neutralize negative charges of phosphates. (ii) In the minor groove in A·T-rich regions in B-DNA, monovalent cations are directly bound to the base moieties by replacing water molecules that constitute a spine of hydration. (iii) *Polyhedral* metal ions, which are usually hydrated, bind to the *interior guanines* through *outer*sphere contacts in the *major* groove in *A/B*-type *right*-handed duplexes while they bind to the *interior guanines* through *inner*sphere contacts in *Z*-type *left*-handed duplexes. The point (iii) might be explained in terms of interligand interactions: for A/B-type duplexes, there would be steric clashes of the octahedrally hydrated metals bound to N7 of guanine with the previous (the 5'-side) base in the sequence, preventing the metal ion from directly binding to the base. On the other hand, for Z-DNA with a convex surface exposing the edge of base pairs directly to the solvent and a narrow and deep minor groove, polyhedral metal ions have much less access to the minor groove, whereas the lack of steric restriction on the convex surface makes it possible for any metal ion to attack the functional groups of bases, exclusively N7 of guanine. Thus, in principle, sterically highly-hindered metal ions could distinguish *single*-stranded structure or *double*-stranded *left*-handed helical structure from *double*-stranded *right*-handed one.

Hence we can expect that our designed metal complexes here could exhibit two functions, one as base(adenine or guanine)-specific reagents and the other as high-order structure(single-stranded or double-stranded left-haned duplex)-specific metal-bonding reagents.

Conclusions

We have shown that interligand interactions are a major factor that could affect the base- and site-specific metal bonding to nucleobases, and high-order structure-specific metal bonding to polynucleotides as well, where sterically highly-hindered coordination environment about the metal center is definitely important for the metal ion to generate its base-specific reactivity, since the steric fitting or hindrance due to attractive or repulsive interactions work effectively only under this steric requirement. We emphasize the wide validity of an approach in which metal ion–nucleic acid interactions could be better understood in terms of interligand interactions.

We wish to thank the support of this work by the Grand-in-Aid for Scientific Research (No. 19590038 to K.A.) from the Ministry of Education, Culture, Sport, Science and Technology, Japan. We also wish to acknowledge our co-workers, Dr. Md Abdus Salam, Dr. Hou Qun Yuan, Ikuhide Fujisawa, Chie Munakata, Takanori Kikuchi, Nilesh Anad Prasad, and Md. Shahidur Rahman, and others who have contributed so much to the success of this endeavor.

References

[1] Aoki, K. (1996). Metal Binding Effects on Nucleic Acid Structures in Comprehensive Supramolecular Chemistry, Vol. 5, Ed. J.-M. Lehn, Pergamon Press, Oxford, pp. 249-294.

[2] Metal Ions in Biological Systems, Vol. 32, Eds Sigel, A.; Sigel, H., Dekker, New York, 1996.

[3] Nucleic Acid-Metal Ion Interactions, Ed Hud, N. V., Royal Society of Chemistry Publishing, Cambridge, UK, 2009.

[4] Metal Complex-DNA Interactions, Eds Hadjiliadis, N.; Sletten, E., John Wiley & Sons, Chichester, UK, 2009.

[5] Metal Ions in Life Sciences, Vol. 9, Eds Sigel, A.; Sigel, H.; Sigel, P. K. O., Royal Society of Chemistry, Cambridge, UK, 2011.

[6] Metal Ions in Life Sciences, Vol. 10, Eds Sigel, A.; Sigel, H.; Sigel, P. K. O., Springer, Dordrecht, Heidelberg, London, New York, 2012.

[7] Marzilli, L. G.; Kistenmacher, T. J. (1977). Stereoselectivity in the Binding of Transition-Metal Chelate Complexes to Nucleic Acid Constituents: Bonding and Nonbonding Effects. Acc. Chem. Res. 10, 146-152.

[8] Aoki, K.; Salam, M. A. (2001). Interligand Interactions Affecting Specific Metal Bonding to Nucleic Acid Bases: The Tetrakis(μ-trifluoroacetamidato)dirhodium(II)–Cytosine System. Crystal Structures of $[Rh_2(HNOCCF_3)_4(cytosine)]$, and $[Rh_2(HNOCCF_3)_4](1\text{-methylcytosine})_2]\cdot 2H_2O$. Inorg. Chim. Acta 316, 50-58.

[9] Aoki, K.; Salam, M. A. (2002). Interligand Interactions Affecting Specific Metal Bonding to Nucleic Acid Bases. A Case of $[Rh_2(OAc)_4]$, $[Rh_2(HNOCCF_3)_4]$, and $[Rh_2(OAc)_2(HNOCCF_3)_2]$ toward Purine Nucleobases and Nucleosides. Inorg. Chim. Acta 339, 427-437.

[10] Salam, M. A.; Aoki, K., unpublished work.

[11] Salam, M. A.; Aoki, K. (2000). Interligand Interactions Affecting Specific Metal Bonding to Nucleic Acid Bases: The Tripodal Nitrilotriacetato (nta) Ligand System. Crystal Structures of [(nta)(adeninium)(aqua)nickel (II)] Hydrate, [(nta)(diaqua)nickel(II)]·(cytosinium) Hydrate, and [(nta)(diaqua)nickel(II)]·(cytosinium)·(cytosine) Hydrate. Inorg. Chim. Acta 311, 15-24.

[12] Salam, M. A.; Aoki, K. (2001). Metal Ion Interactions with Nucleobases in the Tripodal Tris(2-aminoethyl)amine (tren) Ligand-System. Crystal Structures of [Cu(tren)(adeninato)]·ClO_4, [Ni(tren)(9-ethylguanine–0.5H)$(H_2O)]_2$·$(ClO_4)_{2.5}$·$(ClO_3)_{0.5}$ and [{Cu(tren)}$_2$(hypoxanthinato)]·$(ClO_4)_3$. Inorg. Chim. Acta 314, 71-82.

[13] Aoki, K.; Salam, M. A.; Munakata, C.; Fujisawa, I. (2007). Metal Ion Interactions with Nucleic Acid Bases in the Tripodal Tris(2-aminoethyl)amine (tren) Ligand-System: Crystal Structures of [Ni(tren)(adeninato)(ClO_4)]·adenine, [Cu(tren)(9-ethylguanine)]·$(ClO_4)_2$, [{Ni(tren)(H_2O)}$_2$(hypoxanthinato)]·$(ClO_4)_3$·1.5H_2O, [Ni(tren)(hypoxanthinato)(H_2O)]·ClO_4·2H_2O, and [{Ni(tren)(H_2O)}$_2$(hypoxanthinato)]$_2$·$(NO_3)_6$·4.5H_2O. Inorg. Chim. Acta 360, 3658-3670.

[14] Rahman, M. S.; Aoki, K., unpublished work.

[15] Rahman, M. S.; Yuan, H. Q.; Kikuchi, T.; Fujisawa, I.; Aoki, K. (2010). Metal Ion Interactions with Nucleobases in the Tetradentate 1,4,7,10-Tetraazacyclododecane (cyclen)-Ligand System. Crystal Structures of [Cu(cyclen)(adeninato)]·ClO_4·2H_2O, [{Cu(cyclen)}$_2$(hypoxanthinato)]·$(ClO_4)_3$, [Cu(cyclen)(theophyllinato)]$_3$·$(ClO_4)_3$·2H_2O, and [Cu(cyclen)(xanthinato)]·(0.7ClO_4)·(0.3ClO_4)·3H_2O·(0.5H_2O)$_3$. J. Mol. Struct. 966, 92-101.

[16] Gellert, R. W.; Bau, R. (1979). X-Ray Structural Studies of Metal–Nucleoside and Metal–Nucleotide Complexes. Metal Ions Biol. Syst. 8, 1-55.

[17] Aoki, K. (1976). X-Ray Crystal Structure of the 1:1 Manganese–Cytosine 5'-Phosphate Complex: Metal Bonding to Both O(2) of the Base and Phosphate. J. Chem. Soc., Chem. Commun., 748-749.

[18] Kuo, L. Y.; Kanatzidis, M. G.; Sabat, M.; Tipton, A. L.; Marks, T. J. (1991). Metalocene Antitumor Agents. Solution and Solid-State Molybdenocene Coordination Chemistry of DNA Constituents. J. Am. Chem. Soc. 113, 9027-9045.

[19] Aoki, K.; Murayama, K. (2012). Nucleic Acid-Metal Ion Interactions in the Solid State. Met. Ions Life Sci. 10, 43-102.

Marinobacter hydrocarbonoclasticus **is an aerobic denitrifier**

Pauleta S.R.[1], Ramos S.[1], Pietsch M.[1], Carreira C.[1], Dell'Acqua S.[2], Moura I.[1]

[1] REQUIMTE/CQFB, Departamento de Química, Faculdade de Ciências e Tecnologia, Universidade Nova de Lisboa, 2829-516 Caparica, Portugal. [2]Dipartimento di Chimica, Università di Pavia, Via Taramelli 12, 27100 Pavia, Italy. Email: srp@fct.unl.pt, isabelmoura@fct.unl.pt

Summary

Marinobacter hydrocarbonoclasticus is a marine bacterium widespread in the Mediterranean sea and Atlantic Ocean, and growing at temperate temperatures. This bacterium can perform complete denitrification, reducing nitrate to molecular nitrogen under anaerobic conditions. Here the nitrite concentration, pH and nitrous oxide reductase activity was monitored during bacterial growth, showing that this bacterium can also perform complete denitrification under low oxygen tension, using lactate as carbon source, in the presence of nitrate as alternative electron acceptor. Nitrous oxide reductase activity was observed after 7 h of growth under low oxygen tensions, and is maintained constant after 48h. Nitrite concentration reaches its maximum at mid-exponential phase and in the stationary phase, at lower oxygen tensions is almost non-existent.

Introduction

Bacterial denitrificaton is the dissimilatory conversion of nitrate, NO_3^-, in four reductive steps trough nitrite, NO_2^-, nitric oxide, NO, and nitrous oxide, N_2O yielding the inert and stable end product dinitrogen, N_2 (Zumft 1997). In anaerobic conditions, nitrate is an energetically highly favorable electron acceptor and denitrification is commonly the dominant metabolic process in microoxic or anoxic environments. Each step is catalyzed by a different enzyme: nitrate reductase (NAR), nitrite reductase (NIR), nitric oxide reductase (NOR) and nitrous oxide reductase (N_2OR) (Tavares et al. 2006).

The last step of denitrification process, the reduction of nitrous oxide to molecular nitrogen, requires two protons and two electrons, according to Equation 1 (Zumft et al. 2007):

$$N_2O + 2\ H^+ + 2\ e^- \rightarrow N_2 + H_2O \quad \text{(Eq. 1)}$$

$$E^{o\prime}\ (\text{pH } 7.0) = 1.35\ \text{V};\ \Delta G' = -\ 339.5\ \text{kJ/mol}$$

The enzyme nitrous oxide reductase overcomes the kinetic barrier of this reaction by activating the N_2O molecule, which is also a poor transition metal ligand, due to its weak σ-donating and π-accepting properties. The three-dimensional structure of N_2OR, available from different bacterial sources (*Marinobacter hydrocarbonoclasticus* (Brown et al. 2000), *Paracoccus denitrificans* (Brown et al. 2000), *Achromobacter cycloclastes* (Paraskevopoulos et al. 2006) and *Pseudomonas stutzeri* (Pomowski et al. 2011), shows that is a functional homodimeric enzyme containing two different multicopper sites: the electron-transfer centre CuA and the catalytic centre CuZ.

Recent studies from our group show that *Marinobacter hydrocarbonoclasticus* can perform both the aerobic and anaerobic denitrification depending on the bacterial growth conditions (Dell'acqua et al. 2012) and so can be classified as an aerobic denitrifier, similarly to *Paracoccus denitrificans* and *Pseudomonas stutzeri* (Baker et al. 1998; Lalucat et al. 2006). Previously, we have reported the isolation and biochemical properties of the enzyme isolated under this conditions. Here, we report the growth kinetics and also the profile of nitrous oxide reductase activity during the growth using either lactate or acetate as carbon source.

Materials and Methods

Cell growth. Marinobacter hydrocarbonoclasticus cells were grown in synthetic sea water medium consisting in 0.2 M NaCl, 0.05 M $MgSO_4.7H_2O$, 0.01 M KCl, 0.05 M Tris-base, 0.056 M NH_4Cl, 0.1% (w/v) yeast extract, 0.014 M sodium lactate, 0.44 mM K_2HPO_4, 0.01 M $CaCl_2.2H_2O$ and 7.2 μM $FeSO_4.7H_2O$, supplemented with 10 mM sodium nitrate. The medium was further supplemented with a modified Starkey oligoelement solution (1 mL/L of culture) (Starkey 1938). Agar plates were prepared by adding 1% (w/v) agar to the medium. The plates were grown for 24 h up to 120 h at 30ºC. Liquid cultures were grown aerobically at 30ºC in an orbital shaker at 210 rpm, 100 rpm or 50 rpm. The growths were performed in three steps: a 5 mL pre-culture was first prepared from the agar plate, which was then used to inoculate 50 mL of medium; finally 25 mL of the previous growth were used to inoculate a third set of flasks containing 0.5 L of medium. Growing times varied from 24 up to 48 h for the final growths. Cells were grown in duplicate and harvested in the stationary phase, after 48 h. The pH and optical density (at 600 nm) was monitored during the last stage of the growth by removing a 1 ml aliquot in one hour intervals. These same aliquots were stored at -80ºC and used to quantify the nitrite and nitrous oxide reductase activity.

Nitrite quantification. Nitrite was quantified using a colorimetric method, in which nitrite ion reacts with sulfanilamide / N-(1-naphthyl)ethylenediamine dihydrochloride, in acidic medium (Griess 1879).

Nitrous oxide reductase activity. N_2O reductase was measured inside a glove box, using reduced methyl viologen (0.1 mM), as electron donor, 100 mM Tris-HCl pH 7.6 and the reaction was started by the addition of 1.0 mM nitrous oxide, and followed at 600 nm (Dell'acqua et al. 2008). The initial velocity was determined from the linearization the initial part of the curve. The activity is reported as μmol N_2O reduced/minute x mg of total protein. Protein content was determined using the BCA assay kit (Sigma), using bovine serum albumin as standard protein.

Results

The bioinformatic analysis of the DNA region involving the gene encoding nitrous oxide reductase in *Marinobacter hydrocarbonoclasticus*, *nosZ*, indicates the presence of three transcriptional units, *nosR*, *nosZ* and *nosDFYL*. In addition, it was identified a ORF upstream of *nosR* (Figure 1) that has a high sequence homology to DNR from *Pseudomonas aeruginosa* (Giardina et al. 2009). DNR is a transcriptional regulator of the same family as FNR (fumarate and nitrate reduction regulator), which is proposed to be involved in the activation of the genes encoding nitrite and nitric oxide reductases in *Pseudomonas aeruginosa*. This transcription regulator is proposed to non-covalently bind a heme group and responds to N-oxides.

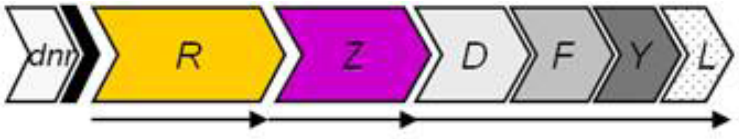

Figure 1 - Representation of *nos* gene cluster from *Marinobacter hydrocarbonoclasticus*.

The presence of *dnr* upstream the *nos* gene cluster points out to its involvement in the transcriptional regulation of those genes in *Marinobacter*. Moreover, like for other denitrifiers, the expression of *nos* genes is expected to also be regulated by the oxygen concentration, possibly through FNR, which in *Marinobacter hydrocarbonoclasticus* has not yet been identified.

We have studied the effect of oxygen tension in the denitrification pathway of *Marinobacter hydrocarbonoclasticus*, by changing the agitation speed (210 rpm and 100 rpm). In Figure 2, it is shown the profile of the optical density and pH during the growth of *Marinobacter hydrocarbonoclasticus* in the presence of nitrate as alternative electron donor, and sodium lactate as carbon source. The pH increases from 7.2 to 7.75 or 8.0, for the growth under low and higher orbital speeds, respectively, due to the consumption of protons in the denitrification pathway. This increase in pH may also be the cause for the cessation of growth of *Marinobacter* (optimum pH near neutral) (Marquez et al. 2005). The doubling time of *Marinobacter* under this conditions was determined to be 200 min versus 340 min, at low and high agitation speeds, respectively. The higher growth rates observed in the growth performed at 210 rpm can be attributed to the higher oxygen dissolved in the growth media.

The concentration of nitrite and nitrous oxide reductase activity were also monitored in these two growth conditions (Figure 3).

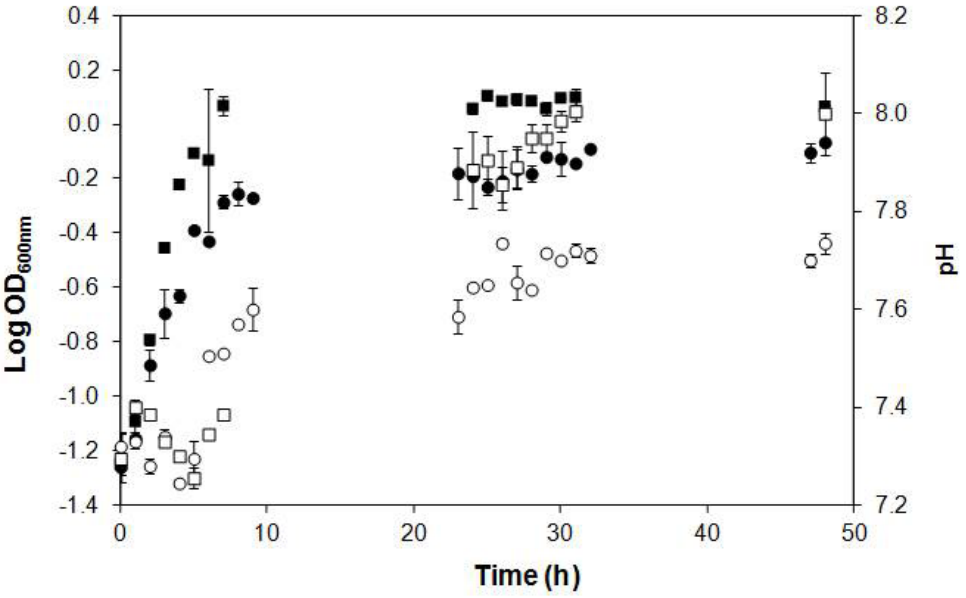

Figure 2 - Growth curve and pH profile of *Marinobacter hydrocarbonoclasticus* grown aerobically with an orbital speed of 210 rpm (squares) and 100 rpm (circles). Legend: ■ $logOD_{600nm}$ (210 rpm), □ pH (210 rpm), ● $logOD_{600nm}$ (100 rpm) and ○ pH (100 rpm).

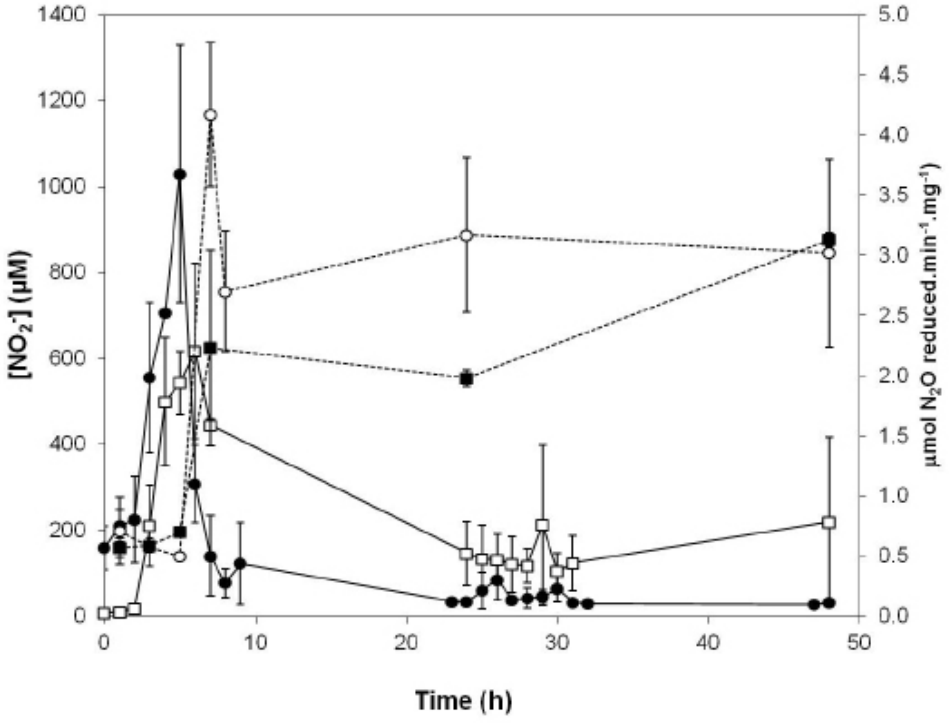

Figure 3 - Nitrite concentration profile and nitrous oxide reductase activity (in µmol N_2O reduced/min/mg protein) during *Marinobacter hydrocarbonoclasticus* grown aerobically with an orbital speed of 210 rpm and 100 rpm. Legend: □ $[NO_2^-]$ (210 rpm), ■ N_2O reduced (210 rpm), ● $[NO_2^-]$ (100 rpm) and ○ N_2O reduced (100 rpm).

Conclusions

Marinobacter hydrocarbonoclasticus is a marine bacterium capable of performing the complete denitrification under aerobic or microaerobic conditions, in the presence of nitrate as an alternative electron acceptor. The

microaerobic conditions were established by lowering the agitation speed of the growth in liquid medium. The results show that under these conditions, *Marinobacter* reaches the stationary phase 7 hours, and that the nitrite concentration is maximum at mid-exponential phase, which most probably induces the transcription of the enzyme cytochrome cd_1 nitrite reductase. The activity and/or amount of this enzyme is maximum in the cells grown under lower agitation speeds, as the concentration of nitrite present in the medium decreases fasters and is practically inexistent at the end of the growth. This result agrees with the fact that the expression of the gene coding for this enzyme may be induced by low oxygen tensions and nitrate (through DnrD), as observed in *Pseudomonas stutzeri* (Vollack et al. 1999).

The activity of the last enzyme of the denitrification pathway, nitrous oxide reductase, was observed after 7h, indicating that as reported by other authors the transcription of this gene might be induced by NO (Bergaust et al. 2012), the product of nitrite reductase, and strengthens the possibility that in *Marinobacter hydrocarbonoclasticus nos* gene cluster is also regulated by DNR, encoded by the gene located upstream this cluster (Figure 1).

References

BAKER SC, et al. Molecular genetics of the genus Paracoccus: metabolically versatile bacteria with bioenergetic flexibility. Microbiol Mol Biol Rev 62(4): 1046-1078, (1998).

BERGAUST L, et al. Expression of nitrous oxide reductase in Paracoccus denitrificans is regulated by oxygen and nitric oxide through FnrP and NNR. Microbiology 158(Pt 3): 826-834, (2012).

BROWN K, et al. Revisiting the catalytic CuZ cluster of nitrous oxide (N2O) reductase. Evidence of a bridging inorganic sulfur. J. Biol. Chem. 275(52): 41133-41136, (2000).

BROWN K, et al. A novel type of catalytic copper cluster in nitrous oxide reductase. Nat. Struct. Biol. 7(3): 191-195, (2000).

DELL'ACQUA S, et al. Electron transfer complex between nitrous oxide reductase and cytochrome c552 from Pseudomonas nautica: kinetic, nuclear magnetic resonance, and docking studies. Biochemistry 47(41): 10852-10862, (2008).

DELL'ACQUA S, et al. Biochemical characterization of the purple form of Marinobacter hydrocarbonoclasticus nitrous oxide reductase. Philos Trans R Soc Lond B Biol Sci 367(1593): 1204-1212, (2012).

GIARDINA G, et al. A dramatic conformational rearrangement is necessary for the activation of DNR from Pseudomonas aeruginosa. Crystal structure of wild-type DNR. Proteins 77(1): 174-180, (2009).

GRIESS P. Bemerkungen zu der Abhandlung der HH. Weselsky und Benedikt „Ueber einige Azoverbindungen". Berichte der deutschen chemischen Gesellschaft 12(1): 426-428, (1879).

LALUCAT J, et al. Biology of Pseudomonas stutzeri. Microbiol Mol Biol Rev 70(2): 510-547, (2006).

MARQUEZ MC, et al. Marinobacter hydrocarbonoclasticus Gauthier et al. 1992 and Marinobacter aquaeolei Nguyen et al. 1999 are heterotypic synonyms. Int J Syst Evol Microbiol 55(Pt 3): 1349-1351, (2005).

PARASKEVOPOULOS K, et al. Insight into catalysis of nitrous oxide reductase from high-resolution structures of resting and inhibitor-bound enzyme from Achromobacter cycloclastes. J. Mol. Biol. 362(1): 55-65, (2006).

POMOWSKI A, et al. N2O binding at a [4Cu:2S] copper-sulphur cluster in nitrous oxide reductase. Nature 477(7363): 234-237, (2011).

STARKEY RL. A study of spore formation and other morphological characteristics of vibrio desulfuricans. Archives of Microbiology 9: 268-304, (1938).

TAVARES P, et al. Metalloenzymes of the denitrification pathway. J Inorg Biochem 100(12): 2087-2100, (2006).

VOLLACK KU, et al. Multiple transcription factors of the FNR family in denitrifying Pseudomonas stutzeri: characterization of four fnr-like genes, regulatory responses and cognate metabolic processes. Mol Microbiol 31(6): 1681-1694, (1999).

ZUMFT WG. Cell biology and molecular basis of denitrification. Microbiol. Mol. Biol. Rev. 61(4): 533-616, (1997).

ZUMFT WG, et al. Respiratory transformation of nitrous oxide (N2O) to dinitrogen by Bacteria and Archaea. Adv. Microb. Physiol. 52: 107-227, (2007).

Hydroxypyrones, an intriguing family of chelating agents for Fe(III) and Al(III)

Toso L.[1], Nurchi V.M.[1], Crisponi G.[1], Crespo-Alonso M.[1], Lachowicz J.I.[1], Marques S.M.[2], Santos M.A.[2], Niclós-Gutiérrez J.[3], Domínguez-Martín A.[3], González-Pérez J.M.[3], Zoroddu M.A.[4], Peana M.[4]

[1] Department of Chemical and Geological Sciences, Cittadella Universitaria, I-09042 Monserrato Cagliari (Italy)
[2] Centro Quimica Estrutural, Instituto Superior Tecnico-UTL, Av. Rovisco Pais, 1049-001 Lisboa (Portugal)
[3] Department of Inorganic Chemistry, Faculty of Pharmacy, Campus Cartuja, University of Granada, E-18071 Granada (Spain)
[4] Department of Chemistry and Pharmacy, Via Vienna 2, 07100 Sassari (Italy)
l.toso@unica.it, nurchi@unica.it, crisponi@unica.it, m.crespo@unica.it, jojelcz@gmail.com, smar@ist.utl.pt, masantos@ist.utl.pt, jniclos@ugr.es, adominguez@ugr.es, jmgp@ugr.es, zoroddu@uniss.it, peana@uniss.it

Abstract

With the aim to design new chelators for the clinical treatment of different diseases depending on overload of trivalent metal ions Fe(III) and Al(III), we presented the equilibria between these two metal ions and kojic acid, and three its derivatives. Potentiometric and spectrophotometric techniques for iron, and potentiometry and ^{1}H NMR for aluminium were used, supported by X-ray, electrospray ionization-mass spectrometry (ESI-MS), calorimetry and quantum chemical calculations. Evidence was given of the formation of ML, ML_2, and ML_3 complexes of both metal ions with kojic acid, confirmed by the X-ray structure of the FeL_3 complex, and of variously protonated M_2L_2 and MeL_2 complexes for all the three derivatives. The extremely good pFe value for these ligands gives confidence to, and opens perspectives for, the search of new kojic acid derivatives. In this paper we present the synthesis of four new derivatives characterized by a longer linker, and the study of their acid-base properties based on potentiometric, spectrophotometric and ^{1}H NMR measurements.

Keywords: Kojic acid, hydroxypyrone, iron, aluminium, chelating agent, potentiometry, spectrophotometry, ^{1}H NMR.

Introduction

The use of chelating agents for iron and aluminium has found increasing attention in the last thirty years [1-4]. Desferal, deferiprone and deferasirox, the chelating agents nowadays in use to treat iron overload in beta-thalassemic patients, are based on hydroxamic groups, hydroxyl-substituted pyridinones or aromatic ring systems; all these three chelating agents present various drawbacks, so there is an urgent need for more efficient chelators. In order to design new coordinating molecules we presented the equilibria of kojic acid and some its derivatives [5-6]. Kojic acid (5-hydroxy-2-(hydroxymethyl)-4-pyrone) is a natural derivative of 4-pyrone, produced by certain species of moulds. It is characterized by antibacterial and antifungal activity; it also inhibits the rate of formation of pigmented products in animal and vegetable tissues and takes part in the processes of oxygen absorption. Kojic acid is widely used in foods and cosmetics to preserve or enhance the colours; when used on cut fruit, it prevents oxidative browning; in seafood it preserves pink and red colours. Kojic acid is a good chelating agent for hard metals such as Fe^{III} and Al^{III} as well as its dimer, 6-[5-hydroxy-2-hydroxymethyl-pyran-4-one]-5-hydroxy-2-hydroxymethyl-pyran-4-one. In a first work [5], evidence was given of the formation of ML, ML_2, and ML_3 complexes of both metal ions with kojic acid, confirmed by the X-ray structure of a FeL_3 complex. In addition, various protonated M_2L_2 and ML_2 complexes of the former dimer have been observed. On the basis of pFe value (23.1), and

of its ability to scavenge iron from inside cells, we extended the investigation to related compounds 2 and 3 (see Fig. 1), in which vanillin and *o*-vanillin substituents were placed on the linker that joins the two kojic units [6]. The found pFe values (18.9 for ligand 2 and 22.2 for ligand 3), despite lower than that for desferal (26.6), but surely comparable with that of deferiprone (20.7), are very confident. A huge advantage of these molecules is that they are easy and cheap to produce (the starting materials, kojic acid and vanillin, are not expensive). Hence, they deserved further examination to determine their toxicity and their capacity to remove iron and/or aluminium from intra-cellular sites in living organisms.

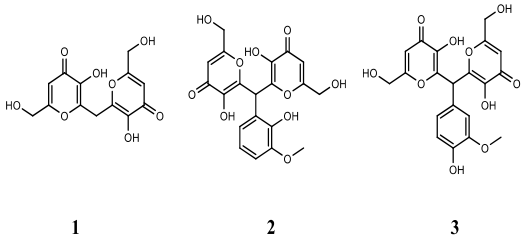

Fig. 1. Chemical structures of the studied kojic acid derivatives.

In M_2L_2 complexes formed with ligands 1-3, each metal ion is coordinated by two CO-C(OH)-chelating moieties, one from each coordinating molecule. Actually, the length of the linker between the two kojic units prevents the coordination of both kojic units to the same metal. Therefore, aimed at obtaining more efficient kojic acid derivatives, we have designed and synthesized a new set of bis-kojic ligands: 4, 5, and 6, whose linkers are differentiated both in terms of type and length. The compound 7 was also synthesized, it can be useful in determining the acid properties of the nitrogen atom in the linker. The protonation equilibria studied by potentiometry, UV-Vis spectrophotometry and ^{1}H NMR spectroscopy will be described and discussed.

Experimental

1.1. Reagents

HCl, KCl, KOH, D_2O, ethanol, DCl, and NaOD were Aldrich products, 5-hydroxy-2-hydroxymethyl-pyran-4-one (kojic acid) was Fluka products. Carbonate free potassium hydroxide solutions were prepared according to Albert and Serjeant [7].

1.1.1. Synthesis

The synthesis of the new derivates, [4: 6,6'-(methylazanediyl)bis(methylene) bis(5-hydroxy-2-(hydroxymethyl)-4H-pyran-4-one)], [5: 6,6'-(benzylazanediyl) bis(methylene) bis(5-hydroxy-2-(hydroxymethyl) -4H-pyran-4-one)], [6: 6,6'-(piperazine-1,4-diylbis (methylene)) bis(5-hydroxy-2-(hydroxymethyl)-4H-pyran-4-one)], [7; 6,6'-(methylazanediyl)bis (methylene)bis(5-hydroxy-2-(hydroxymethyl)-4H-pyran-4-one)] are depicted in Fig. 2.

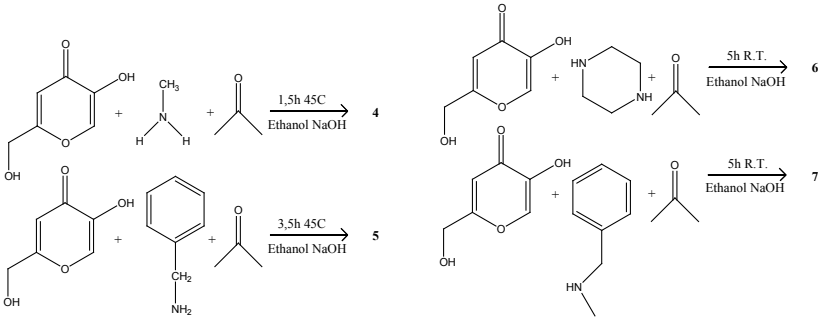

Fig. 2. Scheme of the synthesis of the new compounds.

1.2. Spectrophotometric-potentiometric measurements

Protonation and complex formation equilibria were studied in a thermostatted glass cell equipped with a magnetic stirrer, a Metrohm LL UNITRODE glass electrode connected to a Metrohm 691 pH-meter, a microburette delivery tube connected to a Dosimat 665 Metrohm titrator, an inlet-outlet tube for Argon and a fibre optic dip probe connected to a Varian Cary 50 UV-vis spectrophotometer. Accuracy and precision of the fibre-optic measurements have been discussed previously [8]. Protonation constants were determined from titration data in which potentiometric and spectrophotometric data were obtained simultaneously. Solutions were titrated with 0.1M KOH at 25.0 °C, and 0.1 M KCl ionic strength. The glass electrode was daily calibrated in terms of hydrogen ion concentration by titrating HCl with KOH under the same experimental conditions. Calibration was performed using the Gran procedure [9]. Potentiometric and spectrophotometric data were processed with Hyperquad program [10]. Spectra of pure ligands were recorded in the 200-400 nm spectral range with 0.2 cm path length.

1.3. NMR measurements

^{1}H NMR measurements were made on D_2O solutions at 25 °C with a Bruker Avance 300 MHz (7.05 T) spectrometer operating at 300.131 MHz. A standard BVT 3000 variable temperature control unit with an accuracy of ± 0.5 °C was used. The NMR spectra of free ligand were recorded at different pD values. The pD was adjusted by adding DCl or NaOD and calculated as $pD = pH_{[pHmeter\ reading]} + 0.4$. Chemical shifts were referenced to residual solvent signal (4.800 ppm).

Results and discussion

The protonation equilibria of ligands 4-7 were studied by simultaneous spectrophotometric and potentiometric measurements. The protonation constants calculated using Hyperquad program are reported in Table 1.

Table 1. Protonation constants (logK).

Ligand	LH	LH_2	LH_3	LH_4
4	9.07	7.52	4.59	/
5	9.18	7.48	3.25	/
6	8.36	7.78	5.7	3.36
7	8.58	5.99	/	/

The four ligands are characterized by the protonation constants of the phenolic groups of kojic units, and of nitrogen atoms in the linker. In order to attribute the constants to the protonation of these different groups, we collected the UV spectra; those of 4 and 7 are presented in Fig. 3.

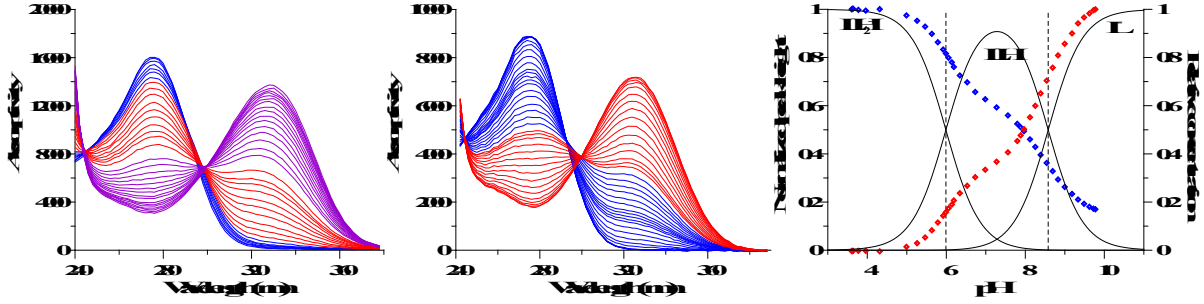

Fig 3. Absorptivity spectra for the titration of 4 (2 X 10^{-4} M), and 7 (3 X 10^{-4} M) collected with a 1 cm optical path length. Speciation plot of 7 with superimposed peak heights

As principal spectral features of kojic acid, L^- and HL species present bands at 315 nm (ε = 5900 $M^{-1}cm^{-1}$) and 270 nm (ε = 8700 $M^{-1}cm^{-1}$) with sharp isosbestic points at 242 nm and 290 nm [3]. The protonation of linker nitrogen instead should imply no, or very limited, spectral variation. The spectra, mainly those relative to the simplest

7 ligand, are extremely intriguing and a microspeciation scheme has to be invoked to explain them. The heights of ligand 7 bands, overlapping the speciation plot, clearly show that spectral variation connected to phenolic group is almost equally splitted between the two protonation steps, as expected on the basis of microspeciation with almost comparable K_{11} and K_{12} values. The ^{1}H NMR results further confirm the protonation constants of these ligands.

Acnkowledgment: GC and JIL acknowledge Regione Sardegna for the financial support CRP-27564 to the project "Integrated approach in the design of chelators for the treatment of metal overload diseases".

References

[1] Crisponi, G., Remelli, M. (2008) Iron chelating agents for the treatment of iron overload. Coordination Chemistry Reviews 252, pp. 1225-1250

[2] Santos, M.A., Marques, S.M., Chaves, S. (2012) Hydroxypyridinones as "privileged" chelating structures for the design of medicinal drugs. Coordination Chemistry Reviews 256, pp. 240-259

[3] Crisponi, G., Nurchi, V.M., Bertolasi, V., Remelli, M., Faa, G. (2012) Chelating agents for human diseases related to aluminium overload. Coordination Chemistry Reviews 256, pp. 89-104.

[4] Crisponi, G., Nurchi, V.M., Faa, G., Remelli M. (2011) Human diseases related to aluminium overload. Monatshefte fur Chemie 142, pp. 331–340

[5] Nurchi, V.M., Crisponi, G., Lachowicz, J.I., Murgia, S., Pivetta, T., Remelli, M., Rescigno, A., Niclós-Gutíerrez, J., González-Pérez, J.M., Domínguez-Martín, A., Castiñeiras, A., Szewczuk, Z. (2010) Iron(III) and aluminum(III) complexes with hydroxypyrone ligands aimed to design kojic acid derivatives with new perspectives. Journal of Inorganic Biochemistry 104, pp. 560-569

[6] Nurchi, V.M., Lachowicz, J.I., Crisponi, G., Murgia, S., Arca, M., Pintus, A., Gans, P., Niclós-Gutiérrez, J., Dominguez-Martin, A., Castineiras, A., Remelli, M., Szewczuk, Z., Lis, T. (2011) Kojic acid derivatives as powerful chelators for iron(III) and aluminium(III). Dalton Trans 103, pp. 227-236.

[7] Albert, A., Serjeant, E.P. in The determination of ionization constants: a laboratory manual (Eds: Chapman and Hall), London 1984, Ch. 2

[8] Crisponi, G., Caredda, A., Cristiani, F., Diaz, A., Nurchi, V.M., Pinna, R., Pivetta, T., Silvagni, R. (2004) Evaluation of a fibre optic device in solution equilibria studies. Application to 3-hydroxybenzoic acid ionization. Annali di Chimica 94, pp. 147-153

[9] Gran, G. (1952) Determination of the equivalence point in potentiometric titrations. Part II. Analyst 77, pp. 661-671

[10] Gans, P., Sabatini, A., Vacca, A. (1996) Investigation of equilibria in solution. Determination of equilibrium constants with the Hyperquad suite of programs. Talanta 43, pp. 1739-1753

Author Index